Computersimulations of ferromagnetic - antiferromagnetic multilayers

Vom Fachbereich Physik
der Universität Duisburg-Essen
(Standort Duisburg)
zur Erlangung des akademischen Grades eines
Doktors der Naturwissenschaften
genehmigte Dissertation

von
Björn Beckmann
aus Dinslaken

Referent: Prof. em. Dr. Klaus D. Usadel
Korreferent: Prof. Dr. Hans Werner Diehl

Tag der mündlichen Prüfung: 10. Januar 2008

Zusammenfassung

Gegenstand dieser Arbeit sind austauschgekoppelte ferromagnetische-antiferromagnetische Schichtsysteme, die im Rahmen des Domänenzustandsmodells für *Exchange Bias* anhand von Monte-Carlo Simulationen untersucht werden.

Zunächst werden Systeme, in denen der Antiferromagnet entweder durch eine uniaxiale Anisotropie gekennzeichnet ist oder bei denen sich dieser durch zwei senkrecht zueinander ausgerichtete leichte Achsen auszeichnet, hinsichtlich ihres Ummagnetisierungsverhaltens untersucht. In beiden Fällen führt eine systematische Variation des Winkels zwischen äußerem Feld und einer der leichten Achsen des Antiferromagneten zu einer Vielzahl unterschiedlicher Ummagnetisierungsmechanismen, wobei im Falle des Systems mit zwei leichten Achsen im Antiferromagneten auch eine ausgeprägte Abhängigkeit von der Richtung des Feldes während des Kühlens beobachtet werden kann. Bei der Charakterisierung der Ummagnetisierungsmoden des Ferromagneten sind die Magnetisierungspfade innerhalb der Filmebene von zentraler Bedeutung. Zudem erlaubt die Untersuchung der Spinstrukturen einen tieferen Einblick in die Mechanismen, die bei der Ummagnetisierung eine wesentliche Rolle spielen. Es wird gezeigt, daß experimentell beobachtete Asymmetrien in entsprechenden Multilagensystemen im Rahmen des Domänenzustandsmodells verstanden werden können.

In einem weiteren Teil der Arbeit wird gezeigt, daß ein System bestehend aus einem Ferromagneten austauschgekoppelt mit einem Antiferromagneten, bei dem nicht die magnetischen Momente sondern deren Austauschkopplung zufällig auf Null gesetzt werden, alle wesentlichen Eigenschaften aufweist, wie sie auch im Falle des Systems mit einem verdünnten Antiferromagneten beobachtet werden. Dies untermauert die Annahme, daß die strukturelle Unordnung im Antiferromagneten entscheidend für das Auftreten des *Exchange Bias* Effektes ist und die Art und Weise, wie diese sich manifestiert, nur eine untergeordnete Rolle spielt.

Schließlich wird ein Ausblick auf nanostrukturierte Systeme gegeben. Darin wird das Verhalten des *Exchange Bias* Effektes hinsichtlich variierender Systemgrößen untersucht, wobei zum einen lediglich die laterale Größe des Ferromagneten geändert wird, zum anderen eine solche systematische Variation sowohl beim Ferromagneten als auch beim Antiferromagneten vorgenommen wird. In beiden Fällen lassen sich Zusammenhängen zwischen der Domänenstruktur im Antiferromagneten und der Größe der austauschgekoppelten ferromagnetischen Strukturen erkennen, wobei jedoch das superparamagnetische Verhalten bei sehr kleinen Systemgrößen weitere Untersuchungen erforderlich macht.

Abstract

Compound systems consisting of exchange coupled ferromagnetic-antiferromagnetic multilayers are examined within the framework of the domain state model for exchange bias by means of Monte-Carlo simulations.

Initially, systems with uniaxial anisotropies as well as systems where the antiferromagnet shows a twinned structure, with two easy axes then perpendicular to each other, are investigated in order to explore the reversal mechanisms during hysteresis.

In both cases, a systematic variation of the angle between the field axis and one of the easy axes of the antiferromagnet reveals a rich variety of different reversal modes. For the latter one, a distinctive dependence on the direction of the cooling field is observed as well. For the characterization of the different kinds of reversal modes, the analysis of the in-plane magnetization paths of the ferromagnetic layer plays an important role. Also, the investigation of its corresponding spin structures allows for a deeper insight into the reversal mechanism. It is shown that experimentally observed asymmetries of the reversal modes in corresponding multilayer systems can be explained within the context of the domain state model.

Another part of this work deals with a more general aspect of the domain state model itself, where it is shown that a bond-diluted antiferromagnet exchange coupled to a ferromagnetic layer displays the same characteristic features as the model where a site-diluted antiferromagnet is utilized. This supports the idea that it is structural disorder which is crucial for exchange bias to occur in such multilayers and the kind of disorder introduced plays only a secondary role.

Finally, an outlook of nanostructured systems is given. The dependence of the exchange bias effect on the variation of the system size is investigated, where in the first setup the lateral dimension of the ferromagnet is varied, while in the second one the size of both the ferromagnet and the antiferromagnet is subject to such a variation. In both cases, a connection between the domain structure of the antiferromagnet and lateral size of the ferromagnet structure seems to be apparent. However, approaching very small systems sizes the superparamagnetic behavior demands for further investigations.

Contents

List of Figures

1 Introduction

The scope of the presented work touches three areas of physics, all of which are both highly interesting and up to date: the areas of computer simulations, magnetism, and, finally, multilayer systems.

Computer simulations have become a third branch of physics which deserves to be mentioned along with the two traditional ones - the long and well established fields of experimental and theoretical physics. Originally, the computer only served as a means for assisting in theoretical physics, e. g. solving sets of differential equations being too complex to be solved analytically. Nowadays, though, it is rather common to design a model for a certain physical problem, which is intended to be treated solely within computer simulations.

Yet, it has to be mentioned that the capabilities of computer simulations are also limited. One has to keep in mind that in general the results are by no means exact. Just considering that time and space in computer simulations are discretized quantities gives rise to such limitations. Also, there are many problems for which it is in principle possible to state the connected algorithm and implement them. But with the current computational power the time scale for finding a solution would be exponentially long. As a consequence, one often switches over from deterministic to probabilistic methods, for the latter one of the most prominent example is the Monte-Carlo simulation.

Besides the ever increasing computational power the technological advances in magnetism play a key role in the world of information technology. According to a study of the University of Berkeley [Lyman and Hal, 2003], in 2003 the inconceivable amount of 5187 Petabyte[1] of data was stored on magnetic media, among others including video tapes, zip disks, and, of course, hard disks. The annual growth rate for the produced data to be stored on magnetic media was said to approach almost 60%. The only way to surmount this huge amount of data is to work towards the miniaturization of magnetic memory devices. Therefore, it is crucial to know about the underlying physics of the ever decreasing length scales of such devices, in order to be able to influence their physical properties.

However, when shrinking these devices one constraint is given by the super-

[1] 1 Petabyte=10^3 Terabyte=10^6 Gigabyte

paramagnetic limit [Chantrell and O'Grady, 1994]. This limit gives the minimal size of a magnetic particle at which it is thermally stable and thus suitable to carry information in terms of a so called bit. As soon as the size of such a particle falls below this limit, thermal fluctuations can lead to a flipping between formerly two stable states, which were given by, e. g., the shape or crystallographic anisotropies; measuring over a period of time leads to a vanishing signal. Thus, the information stored is lost. For a spherical particle with an anisotropy constant of the order of 10^{-5}J/m, the critical radius is approximately 7.3 nm [O'Handley, 2000] in order to be thermally stable for a period over one year. Just reducing this radius to 6 nm has the effect that the particle is stable for just a couple seconds.

Therefore, when pushing down this limit to smaller and smaller sizes, one has to find a compromise between soft and hard magnetic materials. The larger the material's anisotropy is, i. e., it is magnetically hard, the smaller its superparamagnetic limit. The trade-off is to have to utilize larger magnetic fields in read-/write-heads in order to switch the particle's magnetic state or to have an increased switching time. Both are undesirable effects when it comes to writing information to a data recording medium.

On the way towards miniaturization, heterostructures are of extreme importance. Here, materials with different physical properties are in contact at least through one interface. As a consequence of the ever decreasing dimensions of the involved structures, the exchange couplings at the interface differ significantly from those observed in homogeneous materials. It is most important to understand the underlying physics, in order to be able to deliberately tune the material's properties. Also, one could even design compound systems with entirely new physical features.

The effects of such heterostructures can be observed, for instance, in the phenomena of the giant [Binasch et al., 1989] or the tunnel magnetoresistance [Moodera et al., 1995]. In both cases, the magnetoresistance effect is the basis. It describes the relative change of electric conductivity of a material when applying an external field. At room temperature, for magnetic fields of approximately 2 Tesla the electric resistance can be increased by up to 50% when Fe-layers are seperated by thin non-ferromagnetic Cr-layers. Spin-dependent scattering of the electrons in the conduction band accounts for this effect. If these Cr-layers are replaced by non-conducting layers, spin-dependent tunnel currents through the insulator lead to the so-called tunnel magnetoresistance. Its sensitivity with

respect to external magnetic fields is considerably higher than for the plain magnetoresistance, because now field changes within the range of 10^{-2} Tesla cause a change of resistance of up to 40%.

The discovery of the giant magnetoresistance effect quickly led to the development of new technological devices in the area of magnetic recording, spin valves sensors certainly being the most important ones. Spin valves are layered thin films consisting of two ferromagnetic layers which are separated by a non-magnetic spacer layer. When keeping the magnetization of one of the ferromagnetic layers fixed in a specific direction while the magnetization of the other can freely align with an external field, then the changes of the resistance of the spin valve are easily detected due to the giant magnetoresistance effect. The reason for this is that if the free ferromagnetic layer is aligned with an external field such that both ferromagnetic layers of the device are aligned parallel, its resistance is minimal, while it is maximal in the case of anti-parallel alignment.

A direct application of these spin valves is found in read heads of nearly ever hard disk where they have become the de-facto standard. Therefore, in order to increase the sensitivity of spin valve sensors, and thus, increasing data storage density and efficiency, there is a major interest to explore the physics of the effects which are utilized in such devices. One question regarding this matter is connected to the pinning of one of the ferromagnetic layers. For this the above mentioned exchange bias effect is utilized.

This effect is another example for a heterostructure, this time consisting of exchange coupled multilayers of ferromagnetic and antiferromagnetic materials. When cooled below the antiferromagnet's ordering temperature in an external field, these compound materials may display a shift of the hysteresis curve along the field axis. This effect is commonly referred to as *exchange bias*, and its unidirectional anisotropy may help to control the magnetization of different devices such as so called spin-valves.

The underlying details of this exchange coupling and its microscopic origin have long been under debate, for which many competing models and theories give proof of. Yet, it is of utmost importance to find answers to the open questions connected to the exchange bias effect, simply, to have the ability to optimize those devices making use of it. Beyond the first attempt by Meiklejohn and Bean [1956] who discovered this effect over fifty years ago, several models have addressed a wide range of features connected to it more or less successfully.

Most important was not to give a quantitative description of this effect but

rather a qualitative one allowing for a concise view of the underlying physics. One approach was to attribute the exchange bias effect to the formation of domain walls in the antiferromagnet as argued by Malozemoff [1987, 1988]. Domain walls perpendicular to the ferromagnetic/antiferromagnetic interface were supposed to be due to interface roughness, and they presumably formed during the field cooling process. Thus, when exposed to an external field, a small net magnetization would be carried at the interface leading to the shift of the hysteresis curve. However, the major drawback of this model is that the formation of domain walls is energetically not favorable when only interfacial roughness is considered to be the origin of such.

A more recent model which also assumes domain walls perpendicular to the ferromagnetic/antiferromagnetic interface is the so called domain state model [Miltényi et al., 2000] which successfully explains many experimental observations. Along with a corresponding theoretical model [Nowak et al., 2002b], it could be shown that by magnetically diluting the volume of the antiferromagnet – the antiferromagnetic material was partly replaced by a non-magnetic material ($Co_{1-x}Mg_xO$), or defects were built in ($Co_{1-x}O$) – one can deliberately tune main properties of such a multilayer system. The idea behind it is that domain walls can preferentially pass through nonmagnetic sites such that the energy which is necessary to create such a wall is reduced considerably.

The presence of the domain structure in the antiferromagnet, which forms during a field cooling process, plays the key role in order for the exchange bias effect to occur. This idea is supported by a direct spectroscopic observation of such a structure [Nolting et al., 2000; Ohldag et al., 2001], and the importance of dilution has been stressed in several experiments [Shi et al., 2002; Mewes et al., 2000; Mougin et al., 2001; Misra et al., 2003].

Many key properties of the exchange bias effect can be explained within the domain state model, among which are the dependence on dilution, the dependence on the thickness of the antiferromagnetic layer, positive exchange bias, temperature dependence, and the training effect. One aspect missing so far is the investigation of the experimentally observed asymmetries which manifests itself either directly as an asymmetric shape of the hysteresis loop or – in more detail – by different reversal modes on each side of the hysteresis loop which can be observed, e. g., by means of neutron scattering techniques [Fitzsimmons et al., 2000; Radu et al., 2003].

Another aspect touches a more general issue regarding the domain state

model. Despite successfully explaining many features connected to the exchange bias effect, one common objection is that in experimental setups the antiferromagnetic sample is not diluted intentionally. Nevertheless, such systems may also display all the characteristic properties of exchange bias systems. It is therefore important to show that by magnetically diluting structural disorder is introduced into the antiferromagnet which is crucial for exchange bias to occur, and that this is only one way to do so.

Hence, these open issues will be of major concern for this present work as an understanding of these effects will also add to a more complete picture of exchange bias effect within the domain state model.

The presented work is structured as follows. After giving an overview of the theoretical approaches for describing the exchange bias effect, and after giving an insight into the manifold systems where asymmetric reversal modes are observed, a detailed introduction to the domain state model for exchange bias will be given in the following. It will be the basis for the investigation not only for the asymmetric reversal modes but also for exploring the effects of nanostructures in exchange bias systems. Furthermore, the idea of introducing structural defects into the antiferromagnet by magnetically dilution will be revisited in a model where random bonds represent these structural defects. Finally, an outlook will be given where the behavior of nanostructured exchange bias systems will be investigated.

2 Exchange bias – An overview

Exchange coupled multilayer systems, as studied in the presented work, fall into the category of magnetism where the coupling of two different magnetic materials introduces a new anisotropy within this compound system. One example for such a compound material are exchange coupled ferromagnetic-antiferromagnetic multilayers which – under certain conditions – display a shift of the hysteresis curve, called exchange bias. To begin with, the phenomenology of this effect will be explained, followed by a discussion of some of the models trying to describe one or the other aspect of exchange bias. For a detailed overview over the experiments dealing with exchange bias systems, the reader is referred to the work of Nogués and Schuller [1999].

2.1 Terminology

The exchange bias effect has been known since the year 1956 when W. H. Meiklejohn and C. P. Bean discovered a unidirectional anisotropy in an experiment with one of their samples consisting of cobalt and its natural oxide, i. e., a ferromagnetic and antiferromagnetic material [Meiklejohn and Bean, 1956, 1957]. For this to occur, the sample had to be cooled below the Néel temperature of the cobalt oxide. The unidirectional anisotropy was observed during torque measurements when the sample was exposed to an external magnetic field. The angular dependence turned out to be proportional to $\sin(\theta)$ instead of an expected $\sin(2\theta)$ for the uniaxial anisotropy of pure cobalt. Also, a shifted hysteresis curve as shown in Fig. 2.1 was another striking characteristic feature. If the sample was cooled in an external field B_{FC} from above to below the ordering temperature of the antiferromagnet[1], the resulting hysteresis curve was shifted opposite to this external field along the field axis. I. e., the field which is needed to reverse the sample's magnetization is larger than the one needed to restore the original magnetization. The shift of the hysteresis curve away from its origin is called the exchange bias field B_{EB}. Quantitatively, this field B_{EB}

[1] This procedure where the multilayer system is cooled in an external field below the Néel temperature of the antiferromagnet will be referred to as field cooling process.

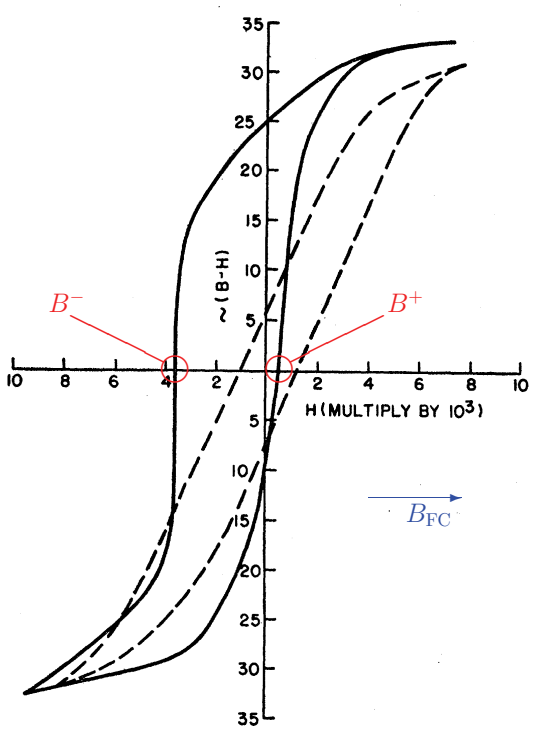

Figure 2.1: Shifted hysteresis curve as discovered by Meiklejohn and Bean. The red circles indicate the coercive fields B^- and B^+. The blue arrow gives the direction of the cooling field B_{FC} ([Meiklejohn and Bean, 1956]).

is calculated by $B_{\mathrm{EB}} = (B^+ + B^-)/2$, where B^- and B^+ are the field values at which the hysteresis curve intersects the field axis (see Fig. 2.1). Connected to the exchange bias field is the coercivity B_{C} which describes the width of the hysteresis loop, and it is defined by $B_{\mathrm{C}} = (B^+ - B^-)/2$.

The answer to the question why exchange bias occurs is certainly connected to the question as to where some interface magnetization within the antiferromagnet is coming from, and how its stability during reversal can be explained. In the course of discussing different theoretical approaches two competing views regarding the interface structure of the antiferromagnet will be utilized, which are the so-called compensated and uncompensated interface. Therefore, these structures will be discussed here together with the explanation of a perfect and

rough interface for each of these.

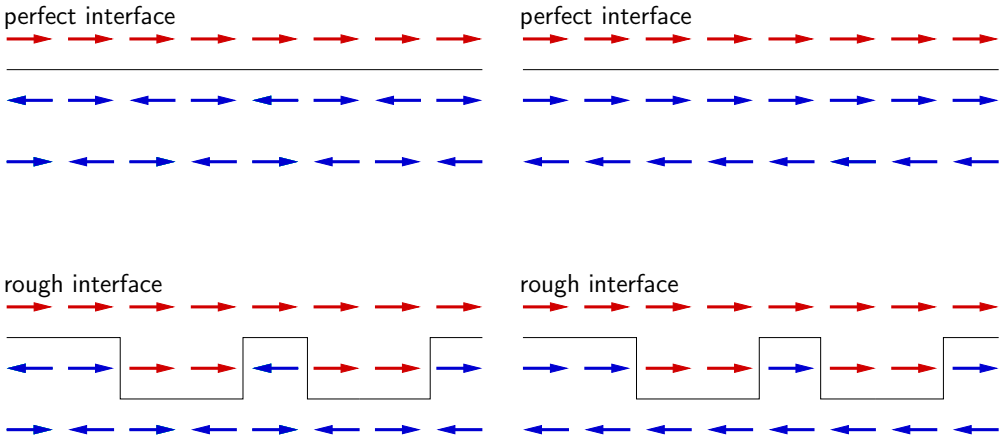

(a) Compensated spin structures. **(b)** Uncompensated spin structures

Figure 2.2: Perfect (top) and rough (bottom) interfaces for compensated (left) and uncompensated (right) antiferromagnetic spin structures (bottom layers, blue arrows) in contact with a ferromagnetic layer (top layer, red arrows); see text for a detailed description.

In Fig. 2.2 both perfect and rough interfaces are shown for the case of compensated and uncompensated antiferromagnetic spin structures. In the case of a compensated structure and a perfect interface, adjacent spins across the interface are aligned antiparallel, whereas in the case of a fully uncompensated structure, spins are aligned parallel within the interface layer, and change of sign occurs across adjacent antiferromagnetic layers. For rough interfaces, the only difference is that spins of the ferromagnetic layer reach into the antiferromagnetic layer leading to a more complex interface structure regarding the exchange interaction between ferromagnetic and antiferromagnetic spins.

Note, that already at that time an asymmetry of the hysteresis curve itself was found, as can be seen in Fig. 2.1. Today, such asymmetries are in the center of focus, and their investigation will be of central importance for the present work since disclosing their microscopic origin will certainly add to a more comprehensive understanding of the exchange bias effect.

2.2 Theoretical approaches

Even though the exchange bias effect was discovered over 50 years ago, its microscopic origin has long been under debate, and several competing models and theoretical approaches have accompanied this discussion trying to explain this effect or one or the other property connected to it. With the introduction of the domain state model, all the key aspects ranging from training effects, dependence on magnetically diluting the antiferromagnetic, and its layer thickness dependence, over to the experimentally observed asymmetries could be explained within a single model [Miltényi et al., 2000; Nowak et al., 2002b; Beckmann et al., 2003, 2006].

Despite the fact that a concise view of the microscopic origin has long been missing, technically this effect has been made use of in innumerable devices, ranging from so called spin-valves [Dieny et al., 1991; Heim et al., 1994] to read heads working on the basis of the giant magnetoresistance effect. Another idea is to beat the superparamagnetic limit [Skumryev et al., 2003] which is one of the main problems when it comes to increasing the storage density of magnetic media.

Ever since the exchange bias effect has been discovered, theoretical models have been proposed to explain aspects connected to it. The first approach to quantitatively describe the exchange bias effect was already presented by Meiklejohn and Bean themselves. In there intuitive picture they assumed an uncompensated interface between the ferromagnetic cobalt and the antiferromagnetic cobalt oxide.

In their model they postulated a term for the total free energy per unit area, which included terms for the external field, the saturation magnetization of the ferromagnet, its thickness, the antiferromagnet's thickness, its anisotropy constant, an interface coupling constant, and various angles between easy axes and/or field axis. From that term, they deduced an expression for the exchange bias field B_{EB} which was inversely proportional to the ferromagnet's thickness.

However, there are a number of apparent drawbacks within their view of the exchange bias effect. Not only the explanation of various other experimental findings fails, but also the value for the exchange bias field derived from their formula overestimates the effect by several orders of magnitude. Besides that, their phenomenological approach does not give rise to an interface magnetization, and fails to explain the stability of such during reversal.

Beyond this first attempt, a considerable number of models have been proposed. Most of them can be subdivided into two categories: the first one includes models where domain walls in the antiferromagnet are perpendicular to the ferromagnetic-antiferromagnetic interface, the second one includes those where these walls are aligned parallel to this interface. The models falling into the second category, however, cannot explain essential features of exchange bias systems. For instance, the experimentally observed irreversible magnetization [Pollak et al., 1988] of the antiferromagnet cannot be explained when assuming domain walls parallel to the interface of the heterostructure.

In the following, three of the models falling in either the one or the other category will be discussed. Then, in the next chapter, an overview of asymmetric magnetization reversal will be given followed by a detailed introduction to the domain state model.

2.2.1 Random field model

In the work of Malozemoff [1987] the main assumption is the rough interface between the ferromagnet and the antiferromagnet which is introduced to explain the formation of domain walls perpendicular to the interface. A sketch of such a rough interface is displayed in Fig. 2.3.

Assuming an antiferromagnetic, i. e. negative, coupling between the ferromagnet and the antiferromagnet, leads to broken bonds in the case of a parallel alignment of adjacent spins across the interface. Assuming further that the ferromagnet remains single domain, the antiferromagnet breaks up into domains – with domain walls perpendicular to the interface – when cooled below the Néel temperature of the antiferromagnet. In this view, a large number of domains would lower the interfacial but enhance the domain wall energy. The optimal size of the domains is then calculated to be

$$L \approx \pi \sqrt{\frac{J_{\mathrm{AFM}}}{D_{\mathrm{AFM}}}}, \tag{2.1}$$

where J_{AFM} denotes the exchange constant and D_{AFM} the anisotropy constant of the antiferromagnet.

In the following, Malozemoff presumes – in the context of a random field – that for N antiferromagnetic spins on a rough interface on average $r\sqrt{N}$ spins are uncompensated, where r is a number in the order of unity. For an arbitrary

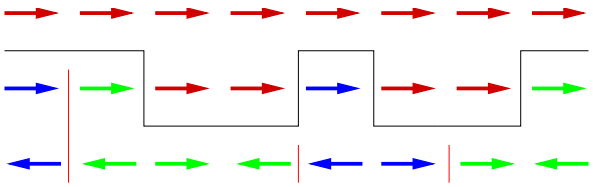

Figure 2.3: Sketch of perpendicular domain walls which in Malozemoff's view are supposed to originate from the interface roughness.

lattice constant a, in an area with lateral size L one obtains a total number of $N = (L/a)^2$ spins. This leads to the following expression for the exchange bias field

$$B_{\mathrm{EB}} = -\frac{2r\sqrt{J_{\mathrm{AFM}} D_{\mathrm{AFM}}}}{\pi^2 m_{\mathrm{F}} t_{\mathrm{F}}}, \tag{2.2}$$

with m_{F} denoting the saturation magnetization of the ferromagnet. This model shows a fairly good agreement with several experimental results found in exchange bias systems, for instance, it predicts a decent value for the exchange bias field and can explain the training effect. But for one, the statistical argument is rather dissatisfactory, and for the other, it could not be shown so far that the unidirectional exchange anisotropy solely depends on the existence of a rough interface. Rather, the formation of domain walls in the antiferromagnet only due to interface roughness is energetically not favorable and has never been proven.

While Malozemoff's model makes use of a so called fully compensated antiferromagnetic structure with a rough interface, there also exist models assuming uncompensated interfacial spin structures.

2.2.2 Perpendicular interfacial coupling

On the basis of micromagnetic numerical simulations, Koon [1998] showed the existence and stability of unidirectional anisotropy in thin films with fully compensated antiferromagnetic interfaces, i. e., there are an equal number of interfacial antiferromagnetic spins on each sublattice. Here, domain walls parallel to the interface occur and account for the observed displacement of the hysteresis curve. In his calculations a perpendicular orientation of the antiferromagnetic spins with respect to the adjacent ferromagnetic interfacial spins was shown to be stable. This perpendicular coupling is referred to as spin-flop coupling.

In his model he assumes a single-crystal body centered tetragonal antiferromagnetic structure as shown in Fig. 2.4 (top), and included a uniaxial anisotropy for the antiferromagnet along the [001]-axis and no intrinsic anisotropy for the ferromagnet. Besides, the motion of the spins is restricted to a plane parallel to the interface.

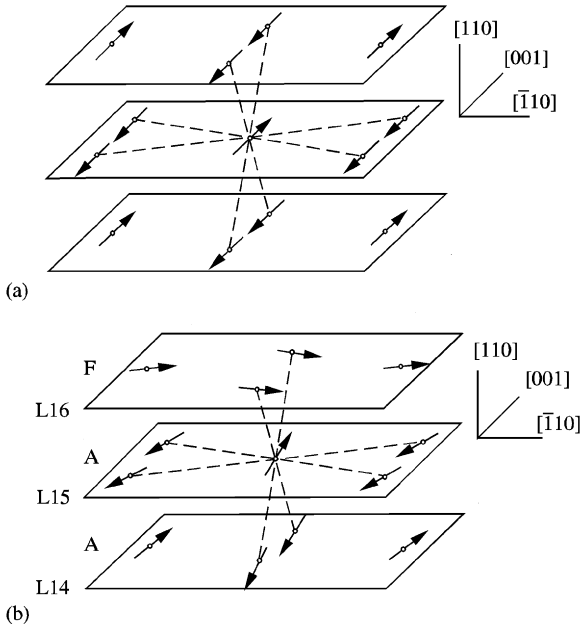

Figure 2.4: Spin flop coupling in multilayers with a fully compensated ferromagnetic-antiferromagnetic interface. The top figure shows the magnetic structure of the $\langle 110 \rangle$ oriented antiferromagnetic body with the exchange bonds displayed as dashed lines. The bottom figure shows the lowest energy spin configuration near the interface plane. For a detailed discussion see the text ([Koon, 1998]).

For perfectly antiparallel aligned antiferromagnetic spins no net moment acting on the ferromagnet would be observed. However, in his calculations an energetically more favorable spin configuration was found as shown in Fig. 2.4 (bottom), caused by the coupling to the ferromagnet.

Surprisingly, this energy minimum occured for a perpendicular coupling of the ferromagnetic and antiferromagnetic spins across the interface. Koon's model seems to be rather suggestive and can explain other experimental findings such

as positive exchange bias. However, Schulthess and Butler [1998] showed that the observed unidirectional anisotropy vanishes if one uses an additional degree of freedom for the antiferromagnetic spin, i. e., they used a three dimensional instead of an XY Heisenberg model. Thus, Koon does not provide a general explanation for the exchange bias effect.

2.2.3 Antiferromagnetic grains

A different approach for explaining exchange bias is presented by Stiles and McMichael [1999] who assume a granular structure for the antiferromagnet with a stable magnetic order. Thus, one has to deal with a polycrystalline antiferromagnetic structure, which is characterized by an arbitrary orientation of the uniaxial anisotropies for the grains. In their view, the reason for the shift of the hysteresis curve in multilayer systems is attributed to this granular structure which supplies a stable magnetic moment even when exposed to an external field.

Two sections of an antiferromagnetic grain are sketched in Fig. 2.5. Stiles and McMichael assume that each of such a grain is found to be in one of two states. Far from the ferromagnetic-antiferromagnetic interface the states are only different regarding the direction of the sublattice magnetization which either points into $\pm\hat{\mathbf{u}}$-direction being parallel to the easy axis. The coupling to a uniformly magnetized ferromagnet winds up a partial domain wall for each of these states. Thus the degeneracy which is observed in the absence of the ferromagnet and an external field is lifted. The unidirectional anisotropy is then assumed to be a result of the energy barrier which for magnetization reversal is proportional to the change in energy plus a domain wall energy.

The idea that parallel domain walls in the antiferromagnet account for the exchange bias effect – as proposed by Stiles and McMichael – was also discussed in a recent work [Scholl et al., 2004] in terms of an antiferromagnetic exchange spring. Using x-ray magnetic linear dichroism the formation of a planar antiferromagnetic domain wall in a Co/NiO system was observed.

Yet, within this model there remains a lack of understanding for other experimentally observed features connected to exchange bias such as the training effect, or why magnetically diluting the antiferromagnet leads to an enhanced exchange bias field. The theoretical model which among others addresses this issue is the domain state model [Miltényi et al., 2000; Keller et al., 2002; Nowak

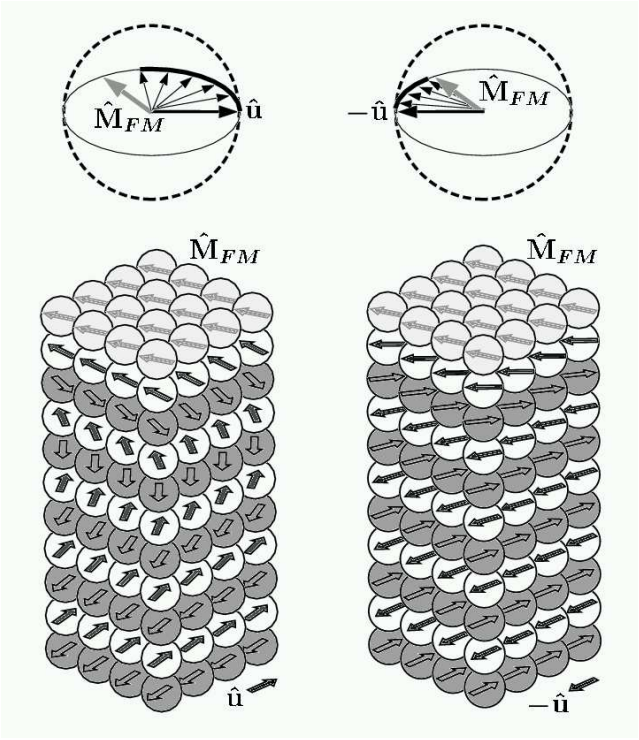

Figure 2.5: Parallel domain walls in an antiferromagnetic grain. The white spheres are antiferromagnetic atoms on the lattice in contact with the ferromagnet (light gray spheres), the dark gray spheres are located on the other sublattice. For a detailed description see the text ([Stiles and McMichael, 1999]).

et al., 2002b], and it will be introduced in the following.

2.2.4 Domain state model

Recently, it has been shown both experimentally [Keller et al., 2002] and theoretically by means of Monte Carlo simulations [Nowak et al., 2002b] that structural disorder[2] plays a crucial role for the exchange bias effect. Within the so-called

[2]In this case this structural disorder is introduced by magnetically diluting the antiferromagnet, i. e., antiferromagnetic moments throughout the volume are replaced by nonmagnetic

domain state model many features connected to this effect can be explained, and it is demonstrated that the introduction of disorder within the volume part of the antiferromagnet significantly enhances exchange bias. This is due to the formation of domains in the volume part of the antiferromagnet carrying a net magnetization which is stable during reversal.

With an exemplary configuration of the antiferromagnetic spins of such a domain as sketched in Fig. 2.6 it will be shown that the domains originate from the magnetic defects. This argumentation is based on the work of Imry and Ma [1975], where the authors investigated the *Random Field Ising Model*.

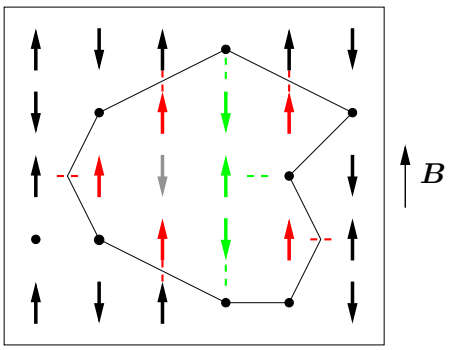

Figure 2.6: Sketch of a domain in a DAFF illustrating the Imry-Ma argument and the metastable domain; Spins with broken bonds are marked red, uncompensated one are green (Figure taken from [Nowak et al., 2002b]).

The antiferromagnetic domain shown in Fig. 2.6 is characterized by a magnetization opposite to the externally prevailing order. Considering the imbalance of the uncompensated spins (green) which are due to magnetic defects and the broken bonds (red), it is obvious that for external magnetic fields B with $B > 5/3\, J_{\mathrm{AFM}}$[3] the displayed spin configuration will be stabilized by such a field B.

Apparently, domain walls will preferentially pass through magnetic defects since this is energetically favorable. Also, the metastability of the domains becomes obvious as their walls are pinned at such defects. If the external field

ones. That the kind of disorder introduced into the system plays only a secondary role is discussed in Chapter 7.

[3] J_{AFM} is the constant for the antiferromagnetic exchange coupling.

B will drop below the value of $5/3J_{\mathrm{AFM}}$, a reversal of the entire domain would be favorable. However, owing to the energy barrier separating the two states before and after the domain is reversed one observes slow dynamics, i. e., a non-exponentially relaxation of relevant quantities on extremely long time-scales [Han et al., 1992; Nowak et al., 1996; Staats et al., 1998], and the system displays properties resembling those of spin glasses. Such domains will be metastable and decay extremely slow. As it will be shown in the results obtained from simulations, this will lead to a stable surplus net magnetization which develops when the DAFF[4] is cooled in an external field from its paramagnetic phase below the temperature $T_i(B)$.

This way a unidirectional anisotropy has been introduced into the antiferromagnet, and it is crucial for the understanding of the exchange bias effect within the domain state model.

With this description of the domain state model in mind, general conclusions can be drawn regarding theoretical approaches incorporating planar domain walls. In such models, assuming domain walls parallel to the interface, the unidirectional anisotropy is caused by parallel aligned spins at the domain boundaries. With an increasing defect concentration in the antiferromagnet, it is energetically favorable that the boundaries are located at such defects. Thus, the number of aligned magnetic moments is lowered, and the energy stored in the domain walls is reduced. As a consequence, a reduced exchange bias field would be expected, contrary to the experimental findings mentioned above.

After this overview of the theoretical models for exchange bias a brief overview of the experiments dealing with asymmetries will be given. They will be of major interest for the present work as their explanation within the domain state model will add to an even more complete view of this theoretical approach.

[4]Diluted Antiferromagnet in a Field.

3 Asymmetric magnetization reversal at a glance

As pointed out earlier, already in the work of Meiklejohn and Bean an asymmetrically shaped hysteresis loop is shown. Yet, at that time the authors focused on the more prominent feature of the shifted hysteresis curve rather than on such a minuscule side effect. However, in recent years this asymmetry in exchange bias systems has been investigated in much detail.

On the one hand, such an asymmetry is a rather peculiar phenomenon since it is not found in other hysteretic physical systems. This fact by itself justifies the risen interest in this effect. On the other hand, the main goal behind this effort is to gain a deeper insight into the microscopic origin of the underlying physics of the exchange bias effect.

Therefore, promising models for the exchange bias effect are those that also provide an explanation for these asymmetries. However, for such asymmetries, it remains a rather challenging task to be adequately described within a theoretical approach. The reason for this is that this phenomenon is observed in numerous experimental set-ups, most of them having the asymmetric hysteresis loop as their only common feature. To illustrate how manifold this subarea of the exchange bias effect is, a number of these experiments and their findings are presented in the following.

3.1 Exchange bias systems with twinned antiferromagnets

Asymmetrically shaped hysteresis loops have been known ever since the work of Meiklejohn and Bean, and similar findings have been observed in a number of experiments, for example in the works of Ambrose and Chien [1998] and Nogués et al. [1999].

The first work addressing this peculiarity in detail was presented by Fitzsimmons et al. [2000]. Using polarized neutron reflectometry, they investigated the magnetization reversal behavior of Fe coupled to MnF_2. Using this technique,

not only the magnetization component parallel to the external field but also the projection perpendicular to that direction was experimentally accessible. From the reflectivity profiles the kind of reversal mechanism could be deduced. They report that magnetization reversal on either side of the hysteresis loop can occur via nucleation and propagation of domain walls or via rotation of the sample magnetization, depending on two things:

- the orientation of the external field during field cooling and hysteresis cycling with respect to the crystallographic directions of the antiferromagnetic twins, and

- whether the measurement is made on the increasing or decreasing branch of the loop.

The inset of Fig. 3.1 clarifies the meaning of the crystallographic orientation of the antiferromagnetic twins. The insets show the antiferromagnetic crystal domain structure of MnF_2 as it was grown on the substrate MgO as quasiepitaxial thin films. One domain is oriented such that $[1\bar{1}1]$ MnF_2 is parallel to [110] MgO, while the other domain is oriented with [001] MnF_2 parallel to [110] MgO.

If the external field during the field cooling process and hysteresis bisects these two domains, the reversal mechanism on the decreasing branch is by coherent rotation while on the opposite one it is by nucleation and domain wall propagation, hence an asymmetric reversal is observed. If this external field is pointing along the direction of one of the antiferromagnetic domains, the reversal mechanism is symmetric, as on both sides of the hysteresis loop coherent rotation is observed.

The authors argue that the bisector of the antiferromagnetic twins constitutes an easy axis for the magnetization direction, which, in conjunction with an assumed 45° coupling between the ferromagnet and each of the antiferromagnetic domains, either leads to the formation of domain walls or to gradual rotation of the magnetization. That these experimental results can be explained utilizing the domain state model for exchange bias with appropriate adaptions applying to the twinned antiferromagnetic structure [Beckmann et al., 2006], will be discussed in Chapter 6.

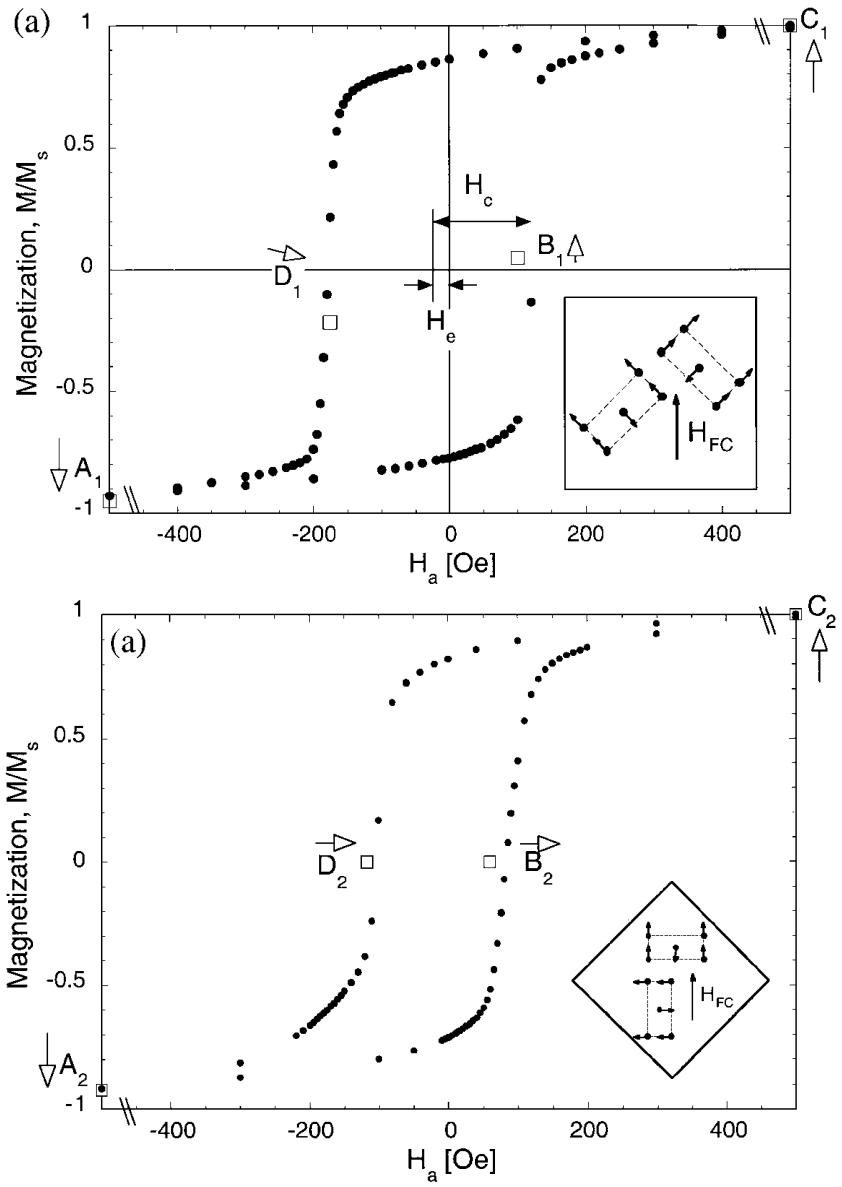

Figure 3.1: Hysteresis for different orientations of the external field during the cooling procedure and the hysteresis measurement. In the top figure the external field is oriented along the bisector of the antiferromagnetic twins (see inset), in the bottom one it points along one of the crystallographic axes of these ([Fitzsimmons et al., 2000]).

3.2 Asymmetries in systems with uniaxial anisotropies

So far, it has not been shown experimentally that an asymmetric reversal mode can also occur in compound systems where the antiferromagnet only shows a uniaxial anisotropy rather than a twinned or polycrystalline structure. It has even been conjectured by Fitzsimmons et al. [2002] that such asymmetries can only occur in systems with a twinned antiferromagnetic structure. Nevertheless, there are works that address the issue of asymmetries where either the ferromagnet displays a uniaxial anisotropy [Camarero et al., 2005], or where such an anisotropy is implicitly assumed for the antiferromagnet [Tillmanns et al., 2005].

The former one, where Co/IrMn compound systems are studied, puts its emphasis on the competing anisotropies between the unidirectional exchange anisotropy and an uniaxial anisotropy within the ferromagnet, where the ferromagnetic anisotropy was set by annealing and a field cooling process. A variation of the angle between the external field and the applied field during hysteresis leads to either symmetric or asymmetric reversal modes, most obviously characterized by different transverse magnetic components of the ferromagnetic magnetization on opposite branches of the hysteresis loop. The presented theoretical model which is used to quantitatively described their findings makes use of a modified Stoner-Wohlfarth model [Stoner and Wohlfarth, 1949]. The energy per unit volume of the system is assumed to be given by

$$E = -M_{\mathrm{S}} H \cos(\theta) - K_{\mathrm{E}} \cos(\theta - \alpha) - K_{\mathrm{U}} \cos^2(\theta - \alpha), \tag{3.1}$$

where M_{S} is the ferromagnetic saturation magnetization, H the applied field, and θ and α are the angles between the applied field and the magnetization and the anisotropy directions, with parameters K_{E} (exchange anisotropy) and K_{U} (unidirectional anisotropy). By minimizing the expression of Eqn. 3.1 hysteresis loops can be obtained. Despite the fact, that there is a striking agreement of numerically calculated and experimentally measured hysteresis loops (see Fig. 3.2), objections have to be raised. As the authors themselves admit, effects of the antiferromagnet are not taken into account – i. e., the micro-structure, anisotropies, etc. are entirely disregarded. Also, an explanation for the microscopic origin of the observed angular dependence is lacking since only a phenomeno-

logical approach with fitting parameters to experimental data is given.

Most important, however, the agreement of experimental and numerical data is only superficial. A net magnetization equal to unity is intrinsic to the Stoner-Wohlfarth model. Therefore, when the magnetization parallel to the external field, $M_\perp$, goes to zero the transverse component, $M_\parallel$, must equal unity, as in this model the magnetization reversal of the assumed macro-spin is always by coherent rotation and the net magnetization is always constant; this discrepancy is not addressed by the authors. Besides, for the very same reason, thermal effects cannot be accounted for, either.

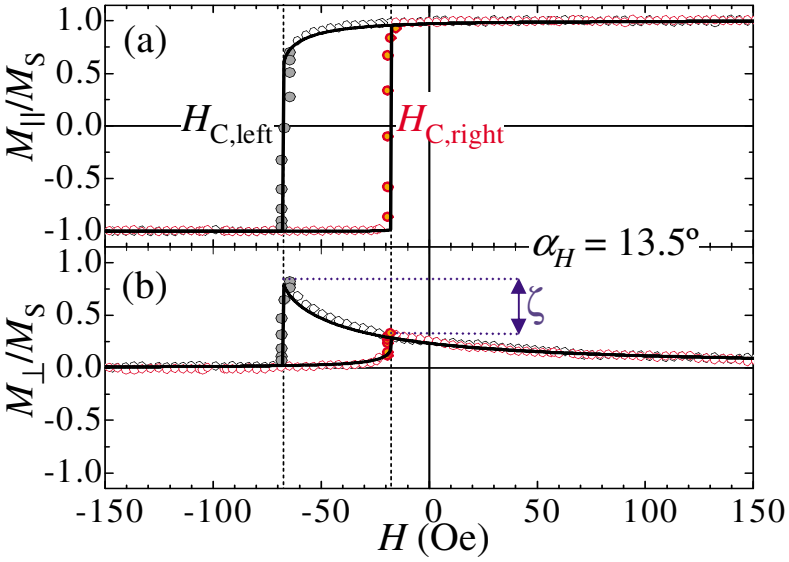

Figure 3.2: Fitted hysteresis loops for the parallel (top) and transverse (bottom) magnetization within a Stoner-Wohlfarth model ([Camarero et al., 2005]).

Nevertheless, despite the fact that this phenomenological approach fails to correctly describe asymmetrical reversal modes when only uniaxial anisotropies are assumed it will be shown in this work that the aforementioned restriction to twinned antiferromagnetic structures does not hold. Rather, numerical simulations within the domain state model will be the basis to show that under certain conditions asymmetric reversal modes should also be observed in compound systems where the antiferromagnet only shows a uniaxial anisotropy rather than a

twinned or polycrystalline structure.

3.3 Asymmetric reversal in patterned structures

For asymmetries to occur in exchange bias systems it has been shown so far, that the micro-structures of the involved materials seem to play a decisive role. Therefore, such systems consisting of continuous thin films have been studied in great detail. Yet, for the development of magneto-electric switching devices, i. e. spin valves, and for magnetic random access memory storage devices, it would be important to investigate the properties of exchange bias systems in patterned films as a function of the structure size. Beyond that, the interest in nanostructured systems has also risen as exchange bias may play an essential role in beating the superparamagnetic limit [Skumryev et al., 2003].

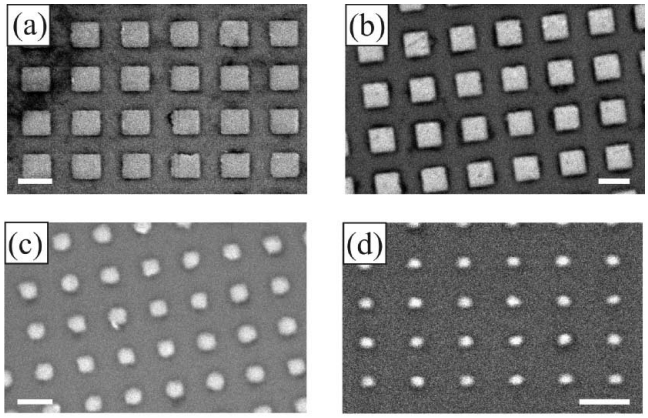

Figure 3.3: Images of Co/CoO square dot arrays obtained by scanning electron microscopy. The interdot distance is kept constant while the lateral size is varied from 900 nm (a), over to 800 nm (b), and 400 nm (c), down to 200 nm (d) ([Girgis et al., 2003]).

Not surprisingly, the asymmetries observed in continuous thin films also affect patterned exchange bias systems [Eisenmenger et al., 2005]. More interestingly, though, asymmetric reversal modes can also be triggered by patterning exchange bias systems [Girgis et al., 2003]. Here, the authors explored Co/CoO dot arrays with variable lateral size of these dots while the intermediate distance between neighboring dots was kept constant. As it is shown in Fig. 3.4, depending on the lateral size of the square dot arrays asymmetrically shaped hysteresis loops were obtained, and the authors explain this effect in terms of a balance between the magnetostatic interdot interaction energy and the exchange anisotropy energy. Another interesting observation is the effect that with decreasing system sizes the exchange bias effect decreases before it eventually approaches zero.

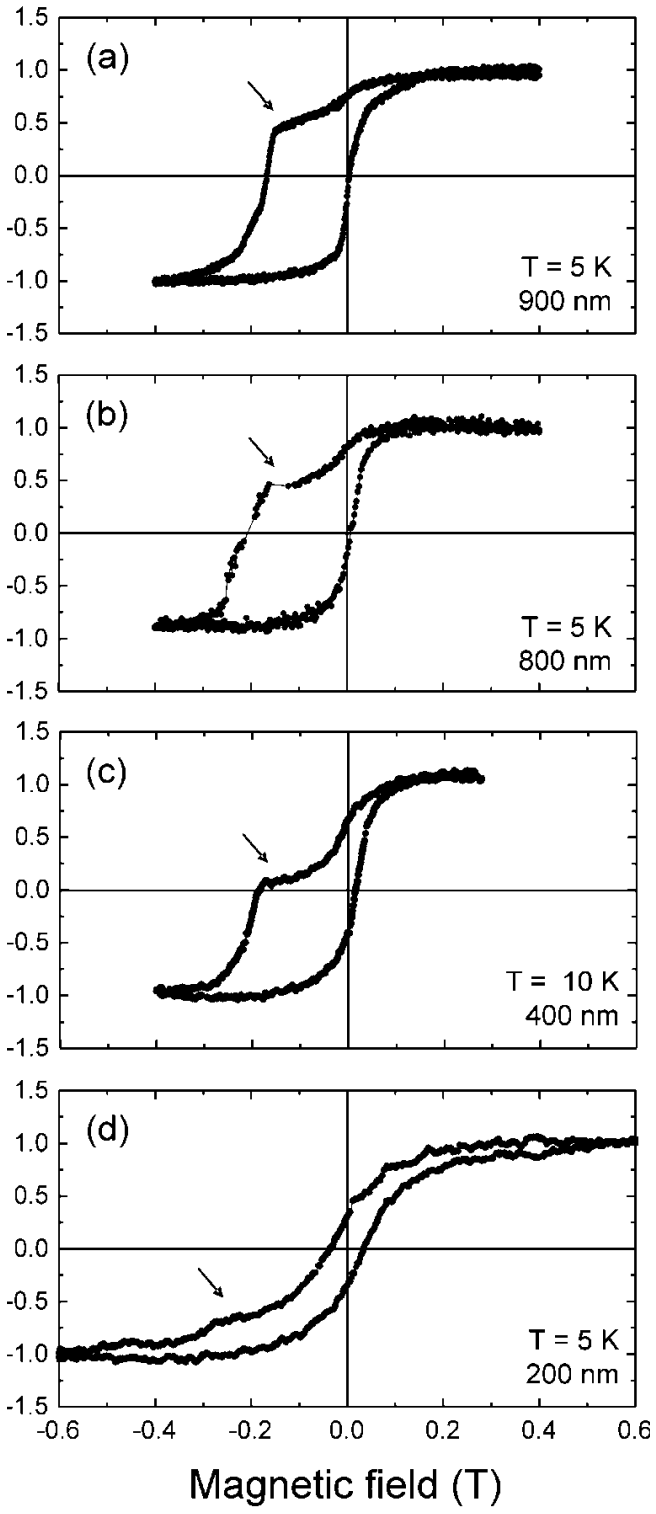

Figure 3.4: Hysteresis loops of Co/CoO square dot arrays with four different dot sizes (see Fig. 3.3). An intermediate magnetization saturation in the upper branch (indicated by the arrows) leading to an asymmetric reversal mode is assumed to be linked to magnetostatic coupling between the dots ([Girgis et al., 2003]).

These examples presented in this chapter vividly demonstrate the complexity connected to asymmetries which are found in exchange bias systems. Therefore, one key aspect of the presented work will be to show that within the framework of the domain state model such asymmetries can be explained. Both for systems displaying uniaxial anisotropies but also for those showing a more complex structure within the antiferromagnet, Monte Carlo simulations are used to explain corresponding experimental findings.

In order to do so, in the following chapter the domain state model and the corresponding numerical methods which are employed will be introduced and discussed in detail.

4 Model and methods

The compound systems studied in this work consist of ferromagnetic and antiferromagnet layers. These two flavors of magnetism are distinguished by different transition temperatures – the Curie temperature T_C for ferromagnetic and the Néel temperature T_N for antiferromagnetic systems – below which a spontaneous ordering occurs, while above their critical temperatures they remain in the paramagnetic phase. On the basis of a cubic lattice, such magnetic systems are modeled where on each lattice site a classical magnetic moment is located, i. e., realistic crystal structures are not considered.

This approach can be motivated in a number of ways. On the one hand, such a spin model emerges from a quantum mechanical, localized spin model as it was introduced by P. Dirac in 1923. For the description of localized electrons in orthogonal orbitals, he introduced the following energy term as a consequence of the Pauli exclusion principle

$$-\sum_{i<j} J_{i,j}\left[\frac{1}{2}+2\boldsymbol{S}_i\cdot\boldsymbol{S}_j\right],$$

when formulating the Hamilton function. Here, $\boldsymbol{S}_i$ and $\boldsymbol{S}_j$ are spin variables on the lattice sites i and j, respectively. This suggested to take this spin-dependent energy term as the basis for a spin-spin exchange interaction in a vector model.

On the other hand, the choice of a simple cubic lattice results in a drastic simplification for the numerical effort. This also means that the main emphasis is put on qualitative aspects, rather than trying to obtain results which quantitatively fit with experimental data.

In the following, the details of this model will be given along with the most important assumptions made for the ferromagnet and the antiferromagnet. Besides, the special properties of the antiferromagnet, which will be of major importance for any further discussion of the domain state model, will be addressed.

4.1 The classical Heisenberg model for magnetic layers

The model which is used to describe the magnetic layers is based on the classical Heisenberg Hamilton function

$$\mathcal{H}_J = -J \sum_{\langle i,j \rangle} \boldsymbol{S}_i \cdot \boldsymbol{S}_j, \tag{4.1}$$

where the spin variables $\boldsymbol{S}_i = \boldsymbol{\mu}_i/\mu$[1] describe the magnetic moment on the lattice site i. Note, that these spin variables are normalized. The constant J originates from the exchange integral which is dependent on the distance $|\boldsymbol{r}_{i,j}|$ between spins on lattice site i and j. Since this exchange interaction is extremely short-ranged, it is sufficient to consider only the exchange between adjacent spins. Hence, for a positive value $J > 0$ a parallel alignment of the spins is energetically favorable, whereas a negative value $J < 0$ leads to an antiparallel alignment.

So far, Eqn. 4.1 describes a completely isotropic system, i. e., the relevant variable for minimizing the energy is the angle ϕ between adjacent spins, rather than an angle between a spin and a certain direction in space. To describe an anisotropic magnetization within a system, as it is often observed experimentally, another term needs to be introduced to account for this.

One reason for such anisotropies is the dipole-dipole interaction of the magnetic moments. Even though it is orders of magnitude smaller than the exchange interaction, its contribution may be significant since it is long-ranged. As a consequence, the interactions between all spins of the systems have to be considered. The corresponding term for the Hamilton function is given by

$$\mathcal{H}_w \propto \sum_{i<j} \frac{3\left(\boldsymbol{S}_i \cdot \boldsymbol{e}_{i,j}\right)\left(\boldsymbol{e}_{i,j} \cdot \boldsymbol{S}_j\right) - \boldsymbol{S}_i \cdot \boldsymbol{S}_j}{r_{i,j}^3}, \tag{4.2}$$

where $\boldsymbol{e}_{i,j}$ is the unit vector pointing along the direction of $\boldsymbol{r}_{i,j}$, which represents the vectors connecting lattice sites i and j.

Since the interaction between all spins have to be considered, for a straightforward calculation of the corresponding double sum involving N magnetic moments, N^2 calculations are needed. This is a numerical effort too large for many

[1] μ is of the order of the Bohr magneton.

systems to be included as such. However, one can make use of fast Fourier transform techniques [Press et al., 1990] to reduce the number of calculations of the long-range interaction [Yuan and Bertram, 1992; Berkov et al., 1993] to the order of $N \log N$.

Despite the speed-up gained from using fast Fourier transform techniques as compared to calculating the double sum of Eqn. 4.2, the long-ranged dipolar interactions are often times not included. Especially, for geometries resembling infinitely extended rotational ellipsoids, assuming its major axis to be aligned with the z-axis, the following term can be motivated [Hubert and Schäfer, 1998]

$$\mathcal{H}_D = -D \sum_i S_{i,z}^2, \tag{4.3}$$

which approximates the dipolar interaction for the magnetic layers considered here. The constant D is referred to as anisotropy constant. In the case of $D > 0$ an orientation of the spins along the z-axis is energetically favorable, whereas the case of $D < 0$ would lead to an in-plane orientation normal to the z-axis. In the former case one refers to such a direction as easy axis, for the latter this constitutes a hard axis. Since the geometry of the system plays an important role when considering this kind of anisotropy, the preceding term is often referred to as shape anisotropy.

Another source of anisotropy in magnetic systems is the so-called crystallographic anisotropy. Its origin lies in the spin-orbit coupling which incorporates the coupling of the spins to the crystallographic structure. In the most simple case such an anisotropy would be uniaxial. Therefore, it can also be described using the term of Eqn. 4.3.

Since one of the major aspects of this work is the investigation of magnetization reversal processes, the coupling to an external field $\boldsymbol{B} = (B_x, B_y, B_z)$ has to be considered, too. The corresponding contribution to the Hamilton function, namely the Zeeman energy, is given by

$$\mathcal{H}_B = -\boldsymbol{B} \cdot \sum_i \boldsymbol{S}_i. \tag{4.4}$$

The resulting Hamilton function describing a ferromagnet can be composed of the terms $\mathcal{H}_J$, $\mathcal{H}_D$ and $\mathcal{H}_B$. The inclusion of the long-ranged dipolar interaction by means of fast Fourier transform techniques will be explicitly mentioned. The choice of parameters and constants will be given in the corresponding sections.

4.2 Infinite anisotropies and dilution

So far, the terms contributing to the Hamilton function describing the magnetic system all include spin variables with continuous degrees of freedom. However, in numerous works where exchange bias systems are explored, the antiferromagnetic material displays a strong uniaxial anisotropy [Keller et al., 2002; Nogués and Schuller, 1999]. Therefore, in many cases it is justified to simulate the antiferromagnet within the Ising model, which emerges from the classical Heisenberg model described in the previous section when infinite anisotropies are assumed. If this anisotropy axis is assumed to be along the z-axis, then only two spin orientations are possible, i. e., $\boldsymbol{S}_i = \sigma_i \hat{\boldsymbol{z}}$, with $\sigma_i = \pm 1$. In the following, the variables σ_i are referred to as Ising spin variables with a reduced magnetic moment μ_i.

Within the scope of this work another rather important assumption is made regarding the antiferromagnet which is motivated by experimental observations. It has been shown that disorder in the antiferromagnet plays a decisive role in exchange bias systems [Miltényi et al., 2000]. The larger this disorder is, the more distinct the unidirectional anisotropy in such multilayer systems. For instance, if the antiferromagnet consists of epitaxially grown NiO as compared to polycrystalline NiO, the exchange bias field is reduced to half of its value [Michel et al., 1997].

One possibility to model structural disorder within the antiferromagnet is by magnetically diluting the system, i. e., some lattice sites are left without a magnetic moment. As a result, a magnetic interaction between adjacent lattice sites may not be present. This leads to the so-called site-diluted antiferromagnet. It is important to note that this site-dilution of the antiferromagnet is only one way to introduce structural disorder, and that it is not important in which way disorder manifests itself in the antiferromagnet. In Chap. 7 it will be shown that a different kind of structural disorder will lead to the same qualitative results.

To begin with, the site-diluted antiferromagnet will be considered, though. The dilution of an Ising antiferromagnet, following the description of the relevant contributions given in Eqns. 4.1 and 4.4, is accomplished by the following approach

$$\mathcal{H}_{\mathrm{AFM}} = -J \sum_{\langle i,j \rangle} \epsilon_i \epsilon_j \sigma_i \sigma_j - B \sum_i \epsilon_i \sigma_i \tag{4.5}$$

where quenched disorder is introduced by setting $\epsilon_{i,j} = (0, 1)$. In the case of $\epsilon_i = 1$ lattice site i is occupied with a magnetic moment, whereas in the case of $\epsilon_i = 0$ it is left empty and is referred to as a magnetic defect.

Note that since the spins are oriented antiparallel in the ordered phase, the contribution coming from the dipolar interaction will be negligible and therefore not be included.

The system which is described by Eqn. 4.5 has been subject of intense studies in the past. Therefore, for a detailed discussion of the properties of diluted antiferromagnets in a field the reader is referred to the works of Kleemann [1993] and Belanger [1998].

So far, the theoretical basis which is important for the understanding of the domain state model has been addressed. The numerical aspects and the simulation method will be discussed in the following. Furthermore, the system parameters which are common to all simulations will be specified.

4.3 Numerical simulation

The multilayer systems which are subject of this work will be investigated by means of the so called Monte-Carlo simulation [Binder and Heermann, 1997]. This method allows for the treatment of complex systems without knowing any specific time scales of the underlying processes. Because of the fact that only the more probable states of all possible ones are calculated, it is necessary to minimize any occurring fluctuations. This is even more true since in the present case multilayers are investigated where the antiferromagnet is randomly diluted. Taking an average over many defect realizations is inevitable.

The conditions which have to be met for the Monte-Carlo simulation of the system introduced in the preceding chapter shall be discussed in this section.

4.3.1 Monte-Carlo simulation

Consider a spin system which is in contact with a heat bath at finite temperature T causing random spin flips. In general, this leads to a time dependent probability distribution $P_q(t)$ of spin states $\boldsymbol{q}(t)$, and its evolution in time is

described by the master equation [Reif, 1965]. It can be written in the form

$$P_{\boldsymbol{q}}(t+\Delta t) - P_{\boldsymbol{q}}(t) = \sum_{\boldsymbol{q}'} \left(P_{\boldsymbol{q}'}(t) W_{\boldsymbol{q}'\to\boldsymbol{q}} - P_{\boldsymbol{q}}(t) W_{\boldsymbol{q}\to\boldsymbol{q}'} \right). \tag{4.6}$$

The probability that the system will be in a state $\boldsymbol{q}$ at time t is described by $P_{\boldsymbol{q}}(t)$. This state can change over to a different one with the transitional probability W. Often times, it is common to write the left hand side of Eqn. 4.6 in a differential notation. However, this will not be done here since in the present form, a direct access to the Monte-Carlo simulation is provided when considering states at different times t and $t + \Delta t$.

Physically, it is required that for the evolution in time the system eventually reaches thermal equlibrium,

$$\lim_{t\to\infty} P_{\boldsymbol{q}}(t) = P_{\boldsymbol{q}}^{\mathrm{eq}}. \tag{4.7}$$

For the described canonical ensemble the distribution in thermal equilibrium is given by the Boltzmann distribution

$$P_{\boldsymbol{q}}(t) = P_{\boldsymbol{q}}^{\mathrm{eq}} = \frac{1}{Z} \exp\left(-\frac{E(\boldsymbol{q})}{k_{\mathrm{B}} T} \right), \tag{4.8}$$

which is independent of time; i. e., if at time t the system is in thermal equilibrium, $P_{\boldsymbol{q}}(t) = P_{\boldsymbol{q}}^{\mathrm{eq}}$, then this is also the case at time $t + 1$ for $P_{\boldsymbol{q}}(t + 1)$. Consequently, considering Eqn. 4.6 this leads to

$$\sum_{\boldsymbol{q}'} \left(P_{\boldsymbol{q}'}^{\mathrm{eq}} W_{\boldsymbol{q}'\to\boldsymbol{q}} - P_{\boldsymbol{q}}^{\mathrm{eq}} W_{\boldsymbol{q}\to\boldsymbol{q}'} \right) = 0. \tag{4.9}$$

In order to solve this equation, usually the stronger condition of *detailed balance* [Reif, 1965; Binder and Heermann, 1997], describing the ratio of the transitional probabilities, is assumed to be fulfilled, making each term in Eqn. 4.9 vanish,

$$P_{\boldsymbol{q}'}^{\mathrm{eq}} W_{\boldsymbol{q}'\to\boldsymbol{q}} = P_{\boldsymbol{q}}^{\mathrm{eq}} W_{\boldsymbol{q}\to\boldsymbol{q}'}. \tag{4.10}$$

For the underlying equilibrium distribution given in Eqn. 4.8, one then obtains for the above given expression the ratio

$$\frac{W_{\boldsymbol{q}\to\boldsymbol{q}'}}{W_{\boldsymbol{q}'\to\boldsymbol{q}}} = \exp\left(-\frac{E(\boldsymbol{q}') - E(\boldsymbol{q})}{k_{\mathrm{B}} T} \right). \tag{4.11}$$

Among others, this condition is satisfied independently of any choice of ω_0 by the so-called *heat-bath* probability

$$W_{\boldsymbol{q}\to\boldsymbol{q}'} = \frac{\omega_o}{1+\exp\left(\frac{E(\boldsymbol{q}')-E(\boldsymbol{q})}{k_\mathrm{B}T}\right)}. \tag{4.12}$$

In a numerical simulation, a series of states $\boldsymbol{q}(t) \to \boldsymbol{q}(t+1) \to \ldots$ will be generated, a so-called *Markov chain*, for which certain rules apply: starting from a state $\boldsymbol{q}(t)$ one chooses a state $\boldsymbol{q}(t+1)$ randomly and accepts it with a certain transitional probability W.

In this work, for choosing subsequent states $\boldsymbol{q}$ in the numerical simulations, the so-called *single-spin flip* [Nowak, 2001] is used, which generally is a threefold procedure: one spin is chosen from the lattice, then a new direction for this spin is determined, and, finally, the energy difference ΔE between the initial and final configuration is calculated. The new spin orientation is then accepted with the given probability of Eqn. 4.12.

Another requirement which will be imposed on the numerical simulation is ergodicity, i. e., any configuration can be reached after generating a series of new states $\boldsymbol{q}$ from an arbitrary initial configuration. Then, one can show that when these two conditions – *detailed balance* and ergodicity – are fulfilled, the equilibrium distribution will be reached [Binney et al., 1992].

For the implementation of the *single spin flip* dynamics, the first two steps of that procedure deserve careful attention. The first part, choosing a spin from the lattice, can be performed in several ways, for example by systematically scanning through the lattice or by randomly choosing spins from it. The only prerequisite is to statistically select each spin the same number of times.

For the second part, choosing a new spin orientation, there exist a number of different possibilities. For an Ising system, this choice is rather simple since here only two possible spin orientations are available, i. e., the spin variable can change from σ_i to $-\sigma_i$. For a Heisenberg model, this trial step is referred to as *reflection trial step* (see Fig. 4.1). It is important to note that in this case it has to be combined with other kinds of trial steps. Just using reflection trial steps by itself does not guarantee ergodicity when considering a Heisenberg model with its continuous degrees of freedom – the phase space is a unit sphere.

One which is often used for this matter consists of a small deviation from the initial orientation of the spin (Fig. 4.2). In this case, a new direction of the spin

Figure 4.1: Spin configurations before and after the so called *reflection trial step*, the direction of the spin is reversed.

is chosen with uniform probability within a cone with a given opening angle around the initial spin direction. For low anisotropies, this technique is likely to yield coherent rotation as reversal mechanism. It is important to note that the spin can only move in small steps, and in order to reverse its direction it must overcome any energy barriers which are, for instance, due to anisotropies.

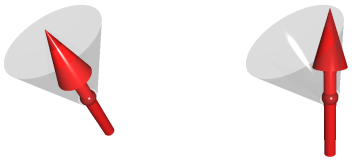

Figure 4.2: Spin configurations before and after the so called *small trial step*. The new spin direction (right) is chosen with uniform probability within a cone around the initial spin direction.

In the case of large anisotropies, the previously described method might not be very efficient. To circumvent this, a different approach is to randomly choose a new spin direction (Fig. 4.3). Then, no energy barrier has to be overcome, and the phase space can be efficiently sampled. This kind of trial step also samples the entire phase space.

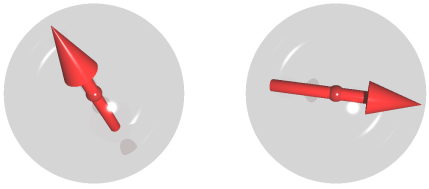

Figure 4.3: Spin configurations before and after the so called *universal trial step*. Here, a new spin direction (right) is chosen arbitrarily, independently of the initial spin direction.

For the efficiency of the simulation, it is important to bear in mind what kind of system is investigated. E. g., for an Ising model, only the reflection

trial step is a sensible – or rather: permissible – choice. For Heisenberg models, it is allowed to use a combination of the aforementioned trial steps. The only prerequisite is to guarantee ergodicity. What is actually used for the simulation within this work will be described in the specific sections.

4.3.2 Simulating magnetic multilayers

After this introduction to the Monte-Carlo simulation technique, the specific model for the ferromagnetic-antiferromagnetic multilayers under consideration and its corresponding Hamilton function will be discussed. Owing to the complexity of the large systems which will be simulated, this discussion will be given on the basis of a smaller system. The graphical illustration of the system will be of special interest since the spin configurations allow for a deeper insight into the reversal mechanisms beyond the pure data of the simulated magnetization components during hysteresis.

Color-coding

One important aspect for the investigation of magnetic multilayers in this work is the illustration of the magnetic moments on each lattice site. The fact that different reversal modes may even be obtained from indistinguishable hysteresis curves demands for a closer look at the actual spin structure during reversal. For instance, a fanning mode where the ferromagnet breaks up into two domains of almost equal size rotating away from each other can hardly be distinguished from a mode where the reversal is by nucleation and domain wall propagation, because in both cases the transverse magnetic component – often used to characterize reversal modes – will more or less equal zero. From the technical point of view, in the simulation the spin direction at any given lattice site is accessible. To display its orientation, it is useful to color-code the direction because this leads to a clearer view of the collective orientation for larger systems. Therefore, in any spin structure that will be discussed, the spin orientation is color-coded as sketched in Fig. 4.4. Note, that this color-coding is within the monolayer; gray-scaled spins will indicate a direction pointing along the x–axis, i. e., out-of-plane.

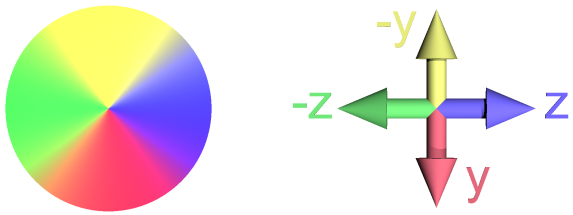

Figure 4.4: Color-coding of spin directions. The spin directions (right side) within the y–z plane are colored according to a color wheel (left side).

Geometry of a $(3+1) \times 5 \times 5$-system

In the following, an exemplary discussion of the model for ferromagnetic-antiferromagnetic multilayers will be given by means of a $(3+1) \times 5 \times 5$-system as shown in Fig. 4.5. This system consists of three antiferromagnetic layers exchange coupled to one ferromagnetic layer; the lateral dimensions along the y– and z–direction are 5×5. Here, both for the ferromagnet and the antiferromagnet a Heisenberg model is used. However, the anisotropy of the displayed antiferromagnet will be large enough to reach the limiting case of an Ising system. The corresponding easy axis will be aligned with the z–axis. Furthermore, in this work both open and periodic boundary conditions are employed. For the latter one, the system is periodic within the y–z plane, while the system remains open along the x–direction. An external magnetic field $\boldsymbol{B}$ is assumed to lie in the y–z plane, and any angles will be measured with respect to the z–axis and within the y–z plane.

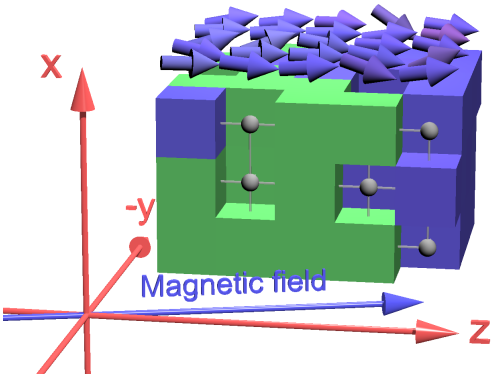

Figure 4.5: Sketch of a multilayer system with dimensions $5 \times 5 \times (3+1)$. The top layer displays the ferromagnet, below which three diluted antiferromagnetic layers with the corresponding domain structure are shown. The gray spheres indicate sites with no magnetic moment.

For the magnetically diluted antiferromagnet in Fig. 4.5, the staggered magnetization is shown, i. e., the direction of every other spin is reversed. For

clarification, in Fig. 4.6 the underlying spin structure of the middle antiferromagnetic layer of the system which is displayed in Fig. 4.5 is shown with its corresponding staggered spin structure. Since the orientation of the spins is indicated both by the direction of the arrows and the color-coding, the arrows will be replaced by boxes. This will support better visualization of domains, especially for larger systems sizes. The Hamilton function which describes this exemplary model will be given in the next section.

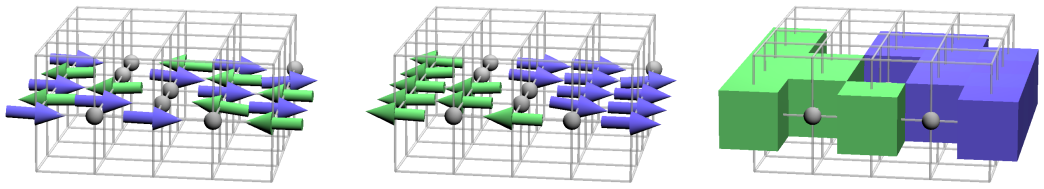

(a) Antiferromagnetic spin structure.

(b) Staggered magnetization, the spins of one sublattice are reversed.

(c) Removing redundancy by replacing arrows with boxes.

Figure 4.6: Middle layer of the diluted antiferromagnet of Fig. 4.5. Note that the domain wall passes through magnetic defects.

Hamilton function

The Hamilton function for the exchange coupled multilayer system shown in Fig. 4.5 consists of three parts which describe the ferromagnetic and the antiferromagnetic contribution and the coupling across the ferromagnetic-antiferromagnetic interface.

The contribution originating from the ferromagnet incorporates the exchange interaction, two anisotropy terms, and the coupling to the external field. The first anisotropy term defines an easy axis parallel to the z–axis, the second one describes a hard axis out of plane which accounts for the shape anisotropy, which is due to the dipolar interaction; thus, spins will tend to keep within the y–z

plane. With these assumptions the following Hamilton function is obtained

$$\mathcal{H}_{\mathrm{FM}} = -J_{\mathrm{FM}} \sum_{\langle i,j\rangle \in \mathrm{FM}} \boldsymbol{S}_i \cdot \boldsymbol{S}_j - \sum_{i \in \mathrm{FM}} \left(d^z_{\mathrm{FM}} S^2_{iz} + d^x_{\mathrm{FM}} S^2_{ix} + \boldsymbol{B} \cdot \boldsymbol{S}_i \right). \tag{4.13}$$

Here, $\sum_{\langle \ldots \rangle}$ indicates the sum over all nearest neighbors of lattice site i. The anisotropy constant d^z_{FM} (d^x_{FM}) is positive (negative) in the case of the easy (hard) axis.

The contribution of a diluted antiferromagnet was presented in Eqn. 4.5 of Sec. 4.2. However, here a system with a Heisenberg model for the antiferromagnet is discussed, which leads to the following term

$$\mathcal{H}_{\mathrm{AFM}} = -J_{\mathrm{AFM}} \sum_{\langle i,j\rangle \in \mathrm{AFM}} \boldsymbol{\sigma}_i \cdot \boldsymbol{\sigma}_j - \sum_{i \in \mathrm{AFM}} \left(d^z_{\mathrm{AFM}} \sigma^2_{iz} + \boldsymbol{B} \cdot \boldsymbol{\sigma}_i \right). \tag{4.14}$$

Note, that in contrast to the Hamilton function for an Ising system given in Eqn. 4.5, the spin variables σ are now written in a vectorial form.

The remaining part is the contribution of the exchange coupling across the interface. It is assumed that the ferromagnet and the antiferromagnet are both modeled on a simple cubic lattice. Therefore, only the coupling of adjacent spins across the interface has to be taken into account, which leads to the following expression

$$\mathcal{H}_{\mathrm{INT}} = -J_{\mathrm{INT}} \sum_{\langle i \in \mathrm{AFM}, j \in \mathrm{FM}\rangle} \epsilon_i \boldsymbol{\sigma}_i \cdot \boldsymbol{S}_j. \tag{4.15}$$

The notation $\sum_{\langle \ldots \rangle}$ describes a sum over adjacent spins if the spin on lattice site i is in the antiferromagnetic and the one on site j in the ferromagnetic layer.

All three contributions, $\mathcal{H}_{\mathrm{FM}}$, $\mathcal{H}_{\mathrm{AFM}}$, and $\mathcal{H}_{\mathrm{INT}}$, add to the complete Hamilton function. Thus, the basis for a simulation will be a sum of all three terms,

$$\mathcal{H} = \mathcal{H}_{\mathrm{FM}} + \mathcal{H}_{\mathrm{AFM}} + \mathcal{H}_{\mathrm{INT}}. \tag{4.16}$$

For any further investigations, the preceding Hamilton function may be slightly altered. For instance, if an Ising model is assumed for the antiferromagnet, or if systems with more than one easy axis for the antiferromagnet will be discussed. Details of such adaptions will be given where applicable.

After the modeling of magnetic multilayers has been outlined and introduced along with the corresponding Hamilton function, in the next chapters results

obtained from Monte-Carlo simulations based on the presented model will be given and discussed in detail. For a beginning, a system is investigated where the antiferromagnet is characterized by just one easy axis. In this case, it will be shown that a variation of the direction of the external field during hysteresis will lead to different reversal mechanisms for the ferromagnet.

5 Asymmetries in multilayers with uniaxial anisotropies

In this chapter an important outstanding problem of exchange bias systems will be addressed: the explanation of asymmetry of reversal modes during hysteresis. As it has been discussed already in Sec. 3, asymmetric reversal modes can occur in many experimental systems. However, a systematic theoretical investigation of this effect has been lacking so far.

Recently, this issue has been addressed in a diploma thesis, results of which have been published by Beckmann et al. [2003]. This chapter takes up the subject again by giving a review of the explanation of the origin of asymmetric reversal modes. Beyond that extended results concerning asymmetries in multilayers with uniaxial anisotropies are presented along with results on the training effect and the influence of parameter variation with respect to the occurrence of the asymmetric reversal modes.

In the following it will be shown that the occurrence of an asymmetry depends on the angle between the external magnetic field and the easy axis of the antiferromagnet. Systematically varying this angle reveals a rich variety of different reversal modes. The findings are not only important for a deeper understanding of the exchange bias effect but also essential for a correct interpretation of the complex reversal behavior observed experimentally.

To begin with, the choice of system parameters will be elucidated, followed by a detailed description of the simulation process which illustrates how the angular dependence is investigated. Then, the results together with an explanation of which will be given.

5.1 System parameters

Since prominent exchange bias systems, for instance CoO or FeF2, have large anisotropies, this can be taken as a motivation for modeling the antiferromagnet as an Ising system. As a consequence, the computational time needed for simulation is drastically reduced. However, it is important to note, that the

basic features of the domain state model for exchange bias are also found in systems where the antiferromagnet is modeled as a Heisenberg system [Nowak et al., 2002a; Misra et al., 2004]. Since the antiferromagnet is modeled as an Ising system, its contribution to the Hamilton function as discussed in Sec. 4.3.2 has to be slightly modified, the complete function has the following form

$$\begin{aligned}\mathcal{H} = & - J_{\mathrm{FM}} \sum_{\langle i,j\rangle \in \mathrm{FM}} \boldsymbol{S}_i \cdot \boldsymbol{S}_j - \sum_{i \in \mathrm{FM}} \left(d^z_{\mathrm{FM}} S^2_{iz} + d^x_{\mathrm{FM}} S^2_{ix} + \boldsymbol{B} \cdot \boldsymbol{S}_i \right) \\ & - J_{\mathrm{AFM}} \sum_{\langle i,j\rangle \in \mathrm{AFM}} \epsilon_i \epsilon_j \sigma_i \sigma_j - B_z \sum_{i \in \mathrm{AFM}} \epsilon_i \sigma_i \\ & - J_{\mathrm{INT}} \sum_{\langle i \in \mathrm{AFM}, j \in \mathrm{FM}\rangle} \epsilon_i \sigma_i S_{jz}.\end{aligned} \tag{5.1}$$

The choice of the parameters considerably influences the behavior of the system, and the multitude of the involved constants poses a challenging task. On the one hand, the constants have to be chosen such that their relations among each other remains in physically sensible limits. On the other hand, the selected parameters have to yield large – if not maximum – effects in order to clearly stand out from any statistical fluctuations.

Therefore, the values for the exchange constants, $J_{\mathrm{FM}}, J_{\mathrm{AFM}}$ and J_{INT}, the number of ferromagnetic and antiferromagnetic layers, the lateral dimensions, and the values for the dilution within the volume, p_{vol}, and at the antiferromagnetic interface layer, p_{int}, will be set according to the simulation results of the work of Nowak et al. [2002b]. There, the systematic investigation of the domain state model has shown that a maximum effect, i. e., largest exchange bias field B_{EB}, is obtained under the following conditions: the dilution within the volume is set to $p_{\mathrm{vol}} = 0.6$, at the interface it is $p_{\mathrm{int}} = 0.5$, the number of antiferromagnetic layers is $t_{\mathrm{AFM}} = 3$; for the ferromagnet one monolayer is considered, $t_{\mathrm{FM}} = 1$.

Furthermore, the anisotropy constants need to be set. The value for the shape anisotropy, which was explained to be originating from the long-ranged dipolar interaction, will be set to $d^x_{\mathrm{FM}} = -0.2 J_{\mathrm{FM}}$. The easy axis within the ferromagnet being parallel to the z–axis is introduced by setting $d^z_{\mathrm{FM}} = 0.02 J_{\mathrm{FM}}$. The relation between the ferromagnetic and antiferromagnetic exchange constant will be set complying with experimental findings, $J_{\mathrm{AFM}} = -J_{\mathrm{FM}}/2$. For the exchange coupling across the interface, neither the order of magnitude nor the sign of the

corresponding exchange constant J_{INT} is known. Thus, it is set to $J_{\mathrm{INT}} = J_{\mathrm{FM}}/2$ according to the work of Nowak et al. [2002b].

The lateral dimensions will be set to $L_y = L_z = 128$, and periodical boundary conditions within the y–z plane are implemented. A systematic variation of the lateral dimension is not carried out, since finite size effects [Batlle and Labarta, 2002] are not relevant for our investigation. Nowak et al. [2002b] have pointed out, that the given lateral size is sufficient so that a typical domain structure within the antiferromagnet can develop.

5.2 Procedure for simulating hysteresis

For the investigation of the angular dependence of the reversal mechanism, hysteresis loops are simulated for angles between 0° and 72° with an increment of 4°. Initially, the system is cooled in an external field $B_{\mathrm{FC}} = J_{\mathrm{FM}}$ pointing along the z–axis, i. e., $\theta = 0°$, from $k_{\mathrm{B}}T_{\mathrm{i}} = J_{\mathrm{FM}}$ to $k_{\mathrm{B}}T_{\mathrm{f}} = 0.1J_{\mathrm{FM}}$ in steps of $k_{\mathrm{B}}\Delta T = -0.002J_{\mathrm{FM}}$. This is from above to below the ordering temperature of the antiferromagnet.

At each temperature step 500 Monte-Carlo steps – a single spin flip for antiferromagnetic spins and a small trial step for the ferromagnetic spin as described in Sec. 4.3.1– are performed, and during this procedure the typical domain state within the antiferromagnet develops along with its excess magnetization along the cooling field direction.

The system configuration at the temperature T_{f} is stored, as it will be the starting point for the consecutive simulations of the hysteresis at different angles θ of the external magnetic field $\boldsymbol{B}$. This way the initial conditions for different angles θ are identical, i. e., the same defect realizations and cooling field orientations for each series of angles are used; rotating the external field is done after the initial field cooling process. This way it is assured that the results will solely depend on the angle θ.

After this field cooling procedure each hysteresis loop starts with the external magnetic field set to a value of $B = 0.4J_{\mathrm{FM}}$ at an angle θ. This field is reduced in steps of $\Delta B = 0.004J_{\mathrm{FM}}$ down to $B = -0.4J_{\mathrm{FM}}$. Then, the external field is increased in the same manner to its initial value[1]. When this hysteresis loop

[1] These two ranges for the external field will be referred to as decreasing and increasing branch of the hysteresis loop.

is completed, the initially saved configuration is restored, then the angle θ is increased by 4° and the next hysteresis loop is simulated.

At each point during hysteresis, the first 40 Monte-Carlo steps are discarded to let the system relax. Then 340 Monte-Carlo steps are carried out and thermal averages are calculated, for instance, the y– and z–component of the magnetization of the ferromagnetic layer, and the antiferromagnetic magnetization along with the staggered magnetization. To minimize effects of statistical fluctuations, the results are averaged over six different defect realizations of the antiferromagnet, i. e., the randomly diluted antiferromagnet is initialized with different seeds for the pseudo random number generator.

5.3 Exchange bias field and coercivity

To illuminate the effects of the coupling to an antiferromagnet and the variation of the direction of the external field, the simulated hysteresis curves will be investigated. Especially, it will be distinguished between the projection $m_{\parallel}$ along the magnetic field $\boldsymbol{B}$ and the perpendicular component $m_{\perp}$. Here, the magnetization per spin in the ferromagnetic layer is the relevant quantity and it is given by $\boldsymbol{m} = \frac{1}{N}\sum_{i\in\mathrm{FM}} \boldsymbol{S}_i$, with N being the number of spins in the ferromagnetic layer. In Fig. 5.1 typical hysteresis loops both for the longitudinal and perpendicular component of the ferromagnet for three different angles θ are shown. The loops for different angles θ are taken from the same simulation series, i. e., the defect realization and the initial configuration after the initial field cooling process were identical.

For a further discussion of the depicted curves it is noteworthy to explain the way in which the hysteresis loops are cycled through. The parallel projection of the magnetization $m_{\parallel}$ along the external field as shown in Fig. 5.1 (top) is labeled with numbers 1 through 4.

At the beginning, the system is saturated and the spins are aligned with the external field. Then, this field is reduced and at point 2 the parallel component $m_{\parallel}$ vanishes before the magnetization of the system is reversed (point 3). The spins are now pointing opposite to their initial direction. In the same manner the external field is increased again, and at point 4 the projection $m_{\parallel}$ reaches zero again. Finally, the system has completed a hysteresis cycle when reaching point 1. The points 2 and 4, where $m_{\parallel}$ crosses the field axis are referred to as

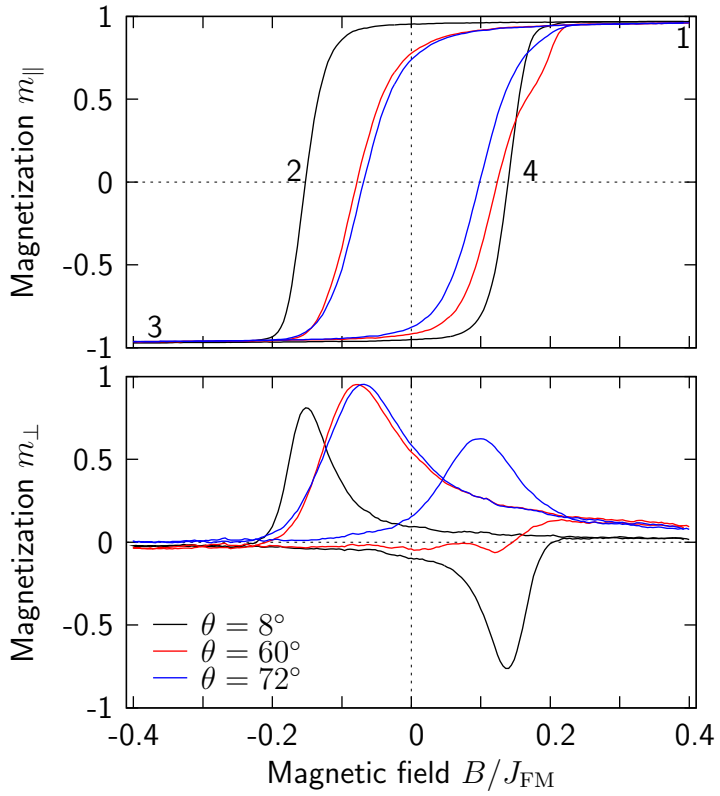

Figure 5.1: Hysteresis loops for $\theta = 8°, 60°$, and $72°$. Shown are the projections along (top) and perpendicular to (bottom) the external magnetic field $\boldsymbol{B}$. The points 1 through 4 in the top figure indicate the way in which the hysteresis is run through (see text for description, [Beckmann et al., 2003]).

coercive fields B^- (2) and B^+ (4).

From the hysteresis curves in Fig. 5.1 a number of effects linked to the angular dependence can be observed, most obviously displayed in the transverse magnetization. On a second glance, one notices a different behavior for the coercive fields, and, finally, the exchange bias field itself seems to vary when rotating the external field away from the easy axes.

To quantify the last two observations, Fig. 5.2 shows the angular dependence both for the exchange bias field B_{EB} and the coercive fields B^- and B^+. For small angles θ the exchange bias field B_{EB} is within the range of previously simulated exchange bias fields [Nowak et al., 2002b], which was to be expected since the parameters used are identical. However, for larger angles the absolute value of B_{EB} decreases, and for angles $\theta \geq 20°$ its value even becomes positive.

Experimentally a positive exchange bias field has been observed in many systems. For instance, for FeF_2 systems Nogués et al. [1996] found a positive value

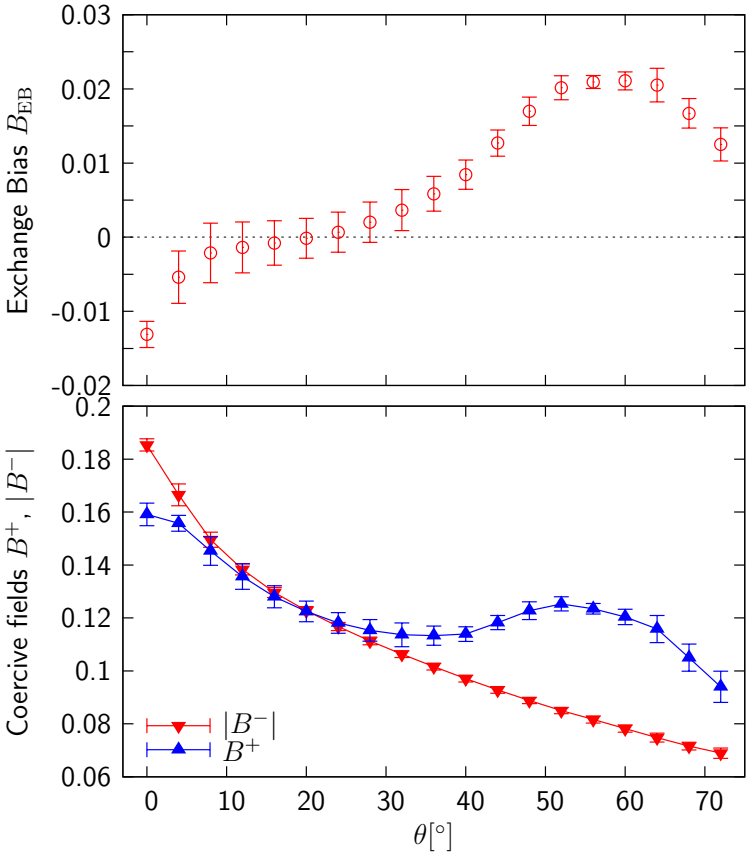

Figure 5.2: Angular dependence of exchange bias (top) and coercive (bottom) fields. The observed positive exchange bias seems to be closely connected to the differing angular dependence of the coercive fields ([Beckmann et al., 2003]).

of this quantity in dependence of the magnitude of the cooling field. They explained this effect with a different coupling of the antiferromagnetic layer.

In another experiment, where the angular dependence of the exchange bias field itself was subject of the investigation [Shi and Lederman, 2002], a positive value was observed as well. However, this was the case for angles $\theta > 90°$, which corresponds to measurements where the cooling field is applied opposite to the external field. Thus, in the context of this discussion, this effect should be regarded as "artificial". A complete understanding for the positive value found in the simulation is still lacking.

A look at the coercive fields (bottom of Fig. 5.2) may give a hint into the right direction. Apparently, the angular dependence is different for the two coercive fields B^- and B^+. On the one hand, a monotonic decrease of B^+ indicates a

Stoner-Wohlfarth-like behavior. On the other hand, there is a range of angles where with increasing θ the coercive field B^+ also increases contrary to intuition. The origin of this different angular dependence will be disclosed in the following, when the different reversal modes will be discussed.

5.4 Reversal modes and in–plane magnetization paths

In the previous section, the hysteresis loops for the parallel and perpendicular projection of the magnetization for the angles $\theta = 8°, 60°$ and $72°$ shown in Fig. 5.1 already allow for a discussion of the reversal modes for the different angles. However, it turns out that plotting the in–plane magnetization of the ferromagnet displays this angular dependence even more clearly. In Fig. 5.3 the magnetization component m_y is plotted versus m_z, with m_z (m_y) denoting the magnetization parallel (perpendicular) to the easy axis of the ferromagnet and antiferromagnet. For each plot, labels 1 and 3 indicate points with maximum external field $|\boldsymbol{B}|$, labels 2 and 4 points where $m_{\|}$ vanishes; these points correspond to those given in Fig. 5.1.

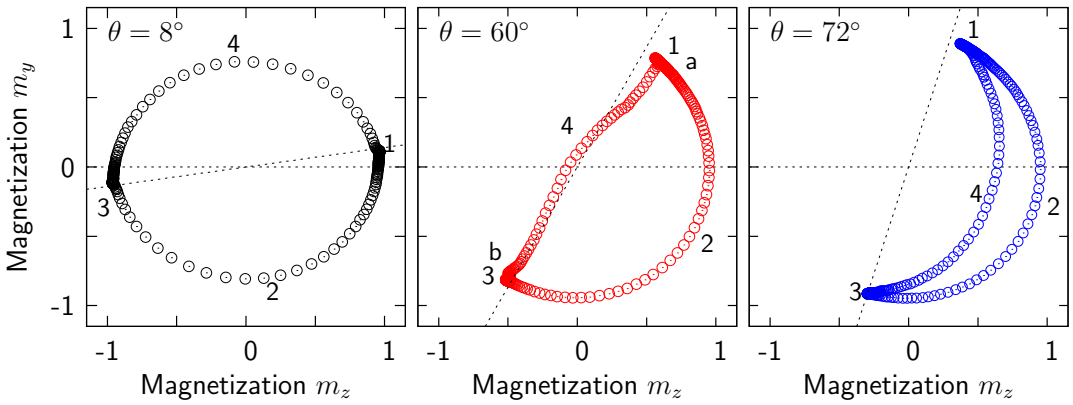

Figure 5.3: In–plane magnetization m_z versus m_z of the ferromagnetic layer for angles $\theta = 8°, 60°$, and $72°$. Points 1 through 4 correspond to those given in Fig. 5.1. The vertical dashed line indicates the orientation of the easy axis of the antiferromagnet, the other one the orientation of the the field axis ([Beckmann et al., 2003]).

For $\theta = 8°, 60°$ and $72°$ a coherent rotation for the decreasing branch is observed. At point 1 the system is exposed to a maximum external field $\boldsymbol{B}$, the system is saturated and the spins are aligned with the external field. When this field is gradually decreased, the magnetic moments will relax towards the closest easy axis, i. e., in this case rotate clockwise. Passing through point 2, the systems displays a coherent rotation as its magnetization significantly deviates from zero, before the magnetization is eventually reversed (point 3). Here, a maximum negative external field $B = -0.4J_{\mathrm{FM}}$ is applied. This reversal mechanism for the decreasing branch is identical for any angle θ, the magnetization reversal always occurs by a coherent rotation.

For the increasing branch this is not true any more. For $\theta = 8°$ the reversal mechanism is the same as for the decreasing branch. A significant magnetic moment perpendicular to the external field during reversal is observed, the systems rotates coherently. For $\theta = 60°$ the perpendicular contribution is negligible, the magnetization path follows the direction of the external field, and a highly nonuniform reversal mode is obtained which is characterized by a vanishing total magnetization.

For $\theta = 72°$ the contribution perpendicular to the external field during reversal on the increasing branch is finite again. Two aspects are noteworthy, though. The net contribution $m_\perp$ is smaller than for the increasing branch. And, even more surprisingly, the system rotates away from its closest easy axis. Thus, magnetization reversal is by coherent rotation via the same side for both branches of the hysteresis loop.

The evolution of the reversal mechanism in dependence of the angle between the easy axis of the antiferromagnet and the direction of the applied field is shown clearly in Fig. 5.4. For angles $\theta \leq 24°$ the simulation yields hysteresis curves where a symmetric reversal mechanism is observed, i. e., both for the decreasing and increasing branch of the hysteresis loop coherent rotation is the dominating reversal mode – the special case for $\theta = 0°$ will be discussed in Sec. 5.5. Then, another reversal mechanism sets in which leads to a nonuniform reversal mode for the increasing branch as compared to a coherent rotation. For $\theta = 60°$ this asymmetry is minimal. Subsequently, coherent rotation will become the prevailing reversal mechanism again. However, contrary to the results for small angles, reversal is now via the same side of the hysteresis loop.

This angular dependence is directly linked to the behavior of the coercive fields as shown in Fig. 5.2. For the coercive field B^- coherent rotation is the

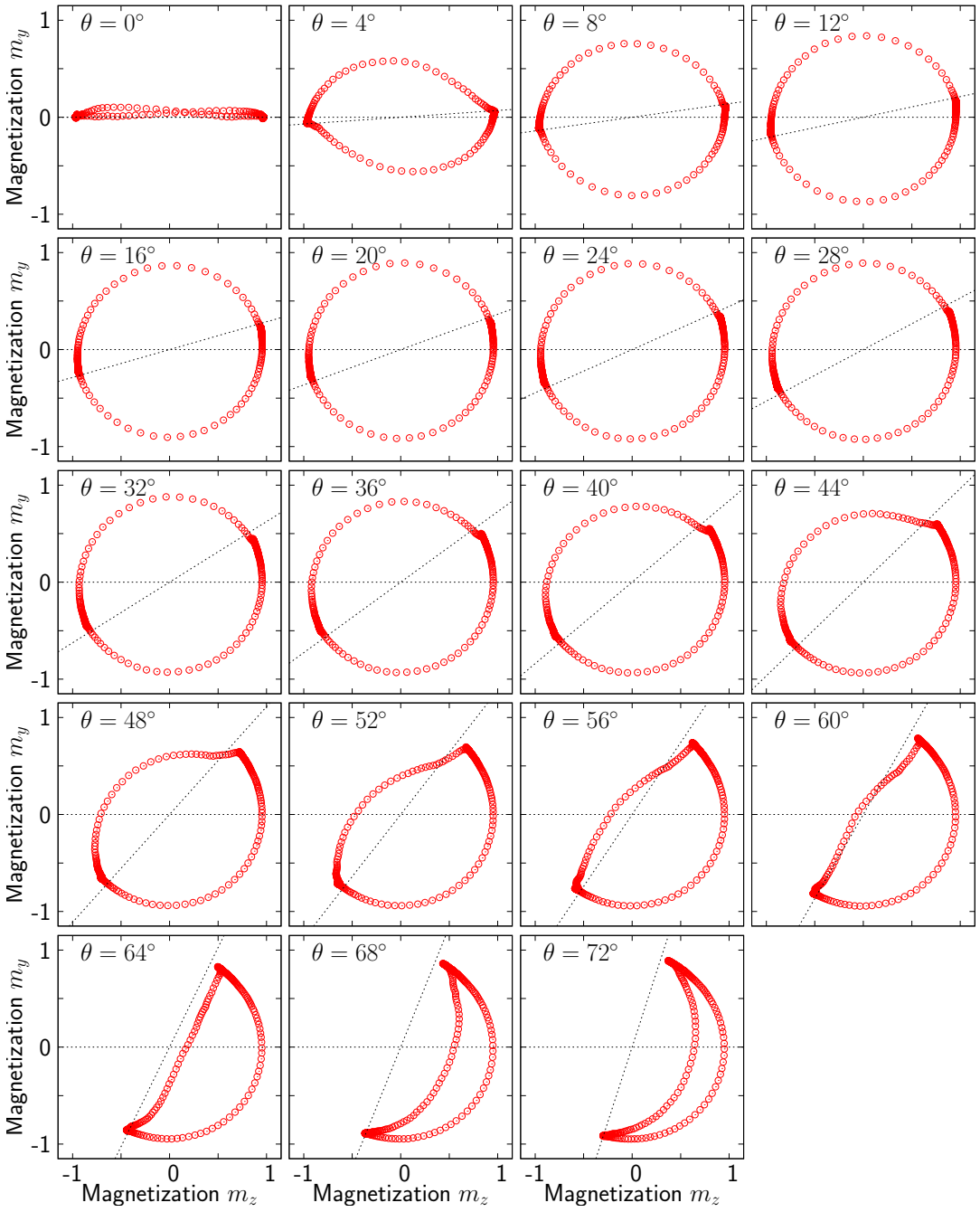

Figure 5.4: In–plane magnetization for $\theta = 0 - 68°$. With the gradual increase of the measuring angle θ the reversal mode for the increasing branch of the hysteresis loop changes from coherent rotation over a nonuniform reversal mechanism to coherent rotation again, this time via the same direction as for the decreasing branch.

dominating reversal mechanism for the complete range of angles θ, and its absolute value decreases monotonically when increasing this angle. For the coercive field on the decreasing branch of the hysteresis loop, B^+, its value is decreasing in the same manner as for B^-, since here coherent rotation is the dominating reversal mode. However, as soon as a different reversal mechanism sets in, this value is increasing until for larger angles coherent rotation is the prevailing reversal mode again, and the value of the coercive field starts decreasing.

5.5 Origin of asymmetric reversal modes

To find an explanation for the asymmetric reversal modes it is necessary to describe the different contributions to an effective field H_{eff} which acts on the ferromagnet during reversal. Three fields are contributing to such an effective field, namely, the exchange field $\boldsymbol{H}_X$ originating from the contact to the antiferromagnet, the external field $\boldsymbol{H}_Z = \boldsymbol{B}$, and the anisotropy field $\boldsymbol{H}_A$. An exchange field which is due to the ferromagnetic layer can be neglected provided this layer is magnetized homogeneously.

The exchange field is directly linked to the interface magnetization of the antiferromagnet since only nearest neighbor interaction are considered. This field only has a component along the z–direction because the antiferromagnet is modeled as an Ising system. That the antiferromagnet reaches a domain state with an excess magnetization after the field cooling process can be seen from Fig. 5.5, where the hysteresis curves for the interface layer are shifted vertically. Note, that for increasing angles the domain for the hysteresis curves decreases. This is due to the fact that the Ising spins are only subject to the projection along the z–axis of both the external field and the exchange field originating from the exchange coupling to the ferromagnet. Both of these components are proportional to $\cos(\theta)$. The antiferromagnet will be exposed to smaller fields with increasing angles θ.

The term $\boldsymbol{H}_A$ is a consequence of the shape anisotropy which led to the introduction of an easy axis parallel to the z–axis as described in Sec. 4.1. Due to this term, spins will preferably rotate towards its closest easy axis.

From the Hamilton function of Eqn. 5.1 the following terms for the fields $\boldsymbol{H}_X$

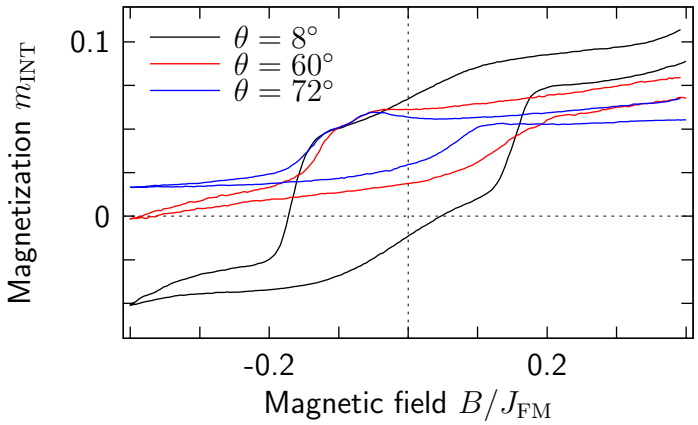

Figure 5.5: Hysteresis of the antiferromagnetic interface layer for $\theta = 8°, 60°$ and $72°$ ([Beckmann et al., 2003]).

and $\boldsymbol{H}_A$ are deduced

$$\boldsymbol{H}_X = J_{\mathrm{INT}} m_{\mathrm{INT}} \hat{\boldsymbol{z}}, \tag{5.2}$$

$$\boldsymbol{H}_A = 2 d^z_{\mathrm{FM}} m_{\mathrm{FM}} \hat{\boldsymbol{z}}. \tag{5.3}$$

The field $\boldsymbol{H}_A$ can be either positive or negative depending on the magnetization m_{FM}. Also, it is apparent that only the projection along the z–axis is relevant, i. e., $\boldsymbol{H}_A$ decreases with increasing angle θ being proportional to $\cos(\theta)$.

Fig. 5.6 shows a sketch of the effective fields acting on the the ferromagnet close to the coercive fields B^- and B^+ before reversal sets in. Here the asymmetry of the observed reversal modes is maximal and the origin thereof can be discussed best. The anisotropy field $\boldsymbol{H}_A$ is in both cases of the same order of magnitude with opposite signs, however. From Fig. 5.5 positive values for the exchange field $\boldsymbol{H}_X$ for the decreasing and increasing branch of the hysteresis loop are obtained.

This leads to the following picture. For the first reversal the effective field H^-_{eff} has a large angle with the external field[2]. I. e., there exists a substantial component perpendicular to the external field leading to a well defined direction of rotation for the ferromagnetic spins. For the second reversal the mentioned angle is considerably smaller with a negligible perpendicular component. Thus, no direction of rotation is predefined leading to the nonuniform reversal modes

[2]To be more precise, it is the angle with respect to the orientation of the magnetization. But this will be aligned with the external field.

with a vanishing magnetization component $m_\perp$.

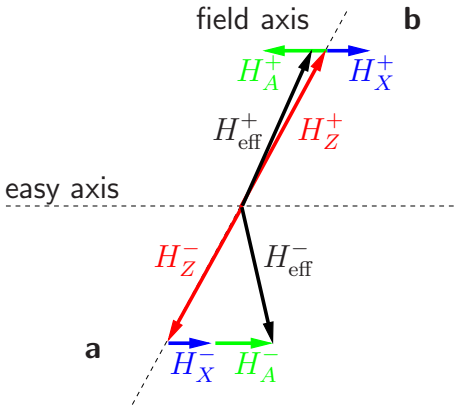

Figure 5.6: Sketch of the effective field H_{eff} for $\theta = 60°$. The fields labeled with $-$ $(+)$ correspond to point a (b) in Fig. 5.3 ([Beckmann et al., 2003]).

Generally, it is the relation between the fields $\boldsymbol{H}_A$ and $\boldsymbol{H}_X$ which determines which kind of reversal will be observed, and the following crude classification can be formulated for the observation of different reversal modes on the increasing branch

$$H_X + H_A : \begin{cases} \ll 0 & \text{coherent rotation via the closest easy axis;} \\ \approx 0 & \text{nonuniform reversal mode;} \\ \gg 0 & \text{coherent rotation via the distant easy axis.} \end{cases}$$

These findings comply with the reversal modes observed for very small angles, especially $\theta = 0°$, where the effective field is more or less aligned with the external field and, therefore, no considerable perpendicular component may be observed. For angles $\theta \lesssim 4°$ in Fig. 5.4 the coherent rotation is less well defined, and for $\theta = 0°$ a nonuniform reversal mode with vanishing perpendicular magnetization components during reversal is obtained since here the effective field and the external field are aligned parallel. This is further supported by the results shown in Fig. 5.7.

Here, the perpendicular magnetization component $m_\perp$ for three different defect realizations of the antiferromagnet is shown. As was to be expected, no significant contribution occurs implying that the reversal mechanism is not dominated by coherent rotation but rather a nonuniform reversal mode is at hand.

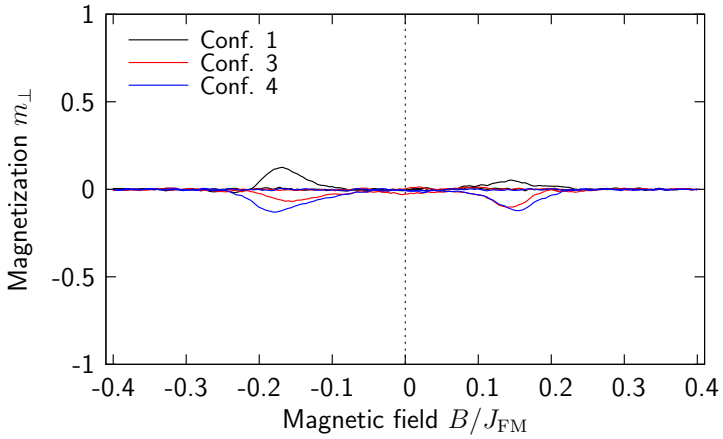

Figure 5.7: Transverse magnetization for $\theta = 0°$ for three different defect realizations of the antiferromagnet.

5.6 Influence of system parameters

In the previous section it has been shown that for an angle of $\theta = 60°$ the obtained asymmetry for the hysteresis is maximal. It needs to be stressed that this specific angle depends on many parameters such as the exchange constants J_{FM}, J_{INT} and J_{AFM}. Also, since the exchange bias field is dependent on the thickness of the antiferromagnetic layer [Nowak et al., 2002b], a variation of it may lead to a different angular dependence, e. g., the maximum asymmetry for hysteresis may occur at different angles θ.

In order to support this, simulations have been performed where the number of the Monte-Carlo steps have been more than doubled, i. e., instead of 380 steps each spins was subject to 800 trials per field value $\boldsymbol{B}$. Also, the range of the external field was decreased from $|\boldsymbol{B}_{\mathrm{max}}| = 0.4 J_{\mathrm{FM}}$ to $0.25 J_{\mathrm{FM}}$. Finally, the thickness of the antiferromagnetic layer was increased by one. Thus, the system consists of four antiferromagnetic layers exchange coupled to a ferromagnetic monolayer. Simulations with these parameters will be labeled with parameter set 2, whereas results from previous simulations with the original settings will be referred to as parameter set 1.

5.6.1 Exchange bias field and coercivity

In Fig. 5.8 the parallel projection of the magnetization $m_{\parallel}$ along the external field is shown for the case where the external field is oriented at an angle of

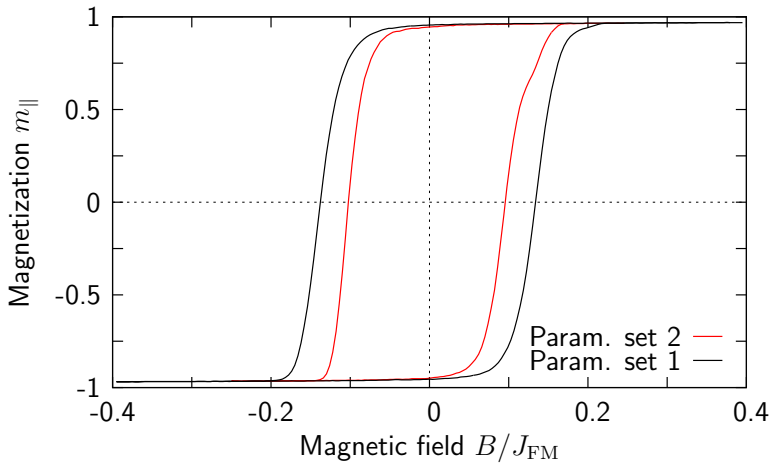

Figure 5.8: Influence of system parameters on hysteresis curve. Both hysteresis curve are simulated with $\theta = 12°$; see text for further details on system parameters.

$\theta = 12°$. The wider opening of the hysteresis curve, i. e., an increased coercivity, of parameter set 1 may be primarily ascribed to the fewer number of Monte-Carlo steps.

In the following six different defect realizations of the diluted antiferromagnet will be considered in order to mitigate influences of statistical fluctuation. The simulation procedure will be the same as described in Sec. 5.2 only changing the system parameters as pointed out above, and the angle θ will be varied between $4°$ and $60°$ with an increment $\Delta\theta = 8°$.

As it turns out, it is worthwhile to take a look at the angular dependence of the exchange bias field and the coercive fields for this series of angles as they are presented in Fig. 5.9. There, both the exchange bias field (top) and the coercive fields (bottom) are compared to the results for parameter set 1 which have already been presented in Sec. 5.3.

Qualitatively, the same angular dependence is obtained, i. e., for increasing measuring angles θ the value of the exchange bias field eventually becomes positive. The absolute value of the exchange bias field is within the same range as for parameter set 1; only for very large angles θ there is a significant deviation when for parameter set 2 the absolute value of this quantity is considerably smaller. It is noteworthy, that for both parameter sets the crossover from negative to positive exchange bias fields seems to take place in the same region of angles θ.

The absolute value of the coercive fields both for the decreasing and increasing branch of the hysteresis loop (bottom of Fig. 5.9) are considerably smaller as

compared to those obtained for parameter set 1. Interestingly enough, though, is the fact that here, too, the same qualitative behavior is found for either coercive field, B^- and B^+.

For the decreasing branch of the hysteresis loop the coercive field B^- decreases monotonically with increasing measuring angles θ. The same behavior has been found for parameter set 1. From the plot of the coercive fields for the increasing branch, B^+, one can tell that for both parameter sets such a behavior is not found. For parameter set 1 this was discussed in Sec. 5.3 where an intermediate increase of this quantity was ascribed to a different reversal mode other than coherent rotation. For parameter set 2 the same seems to be true. There, for angles in the range of $\theta = 30° - 40°$, a monotonic decrease is not obvious any more, but rather an increase seems to take place.

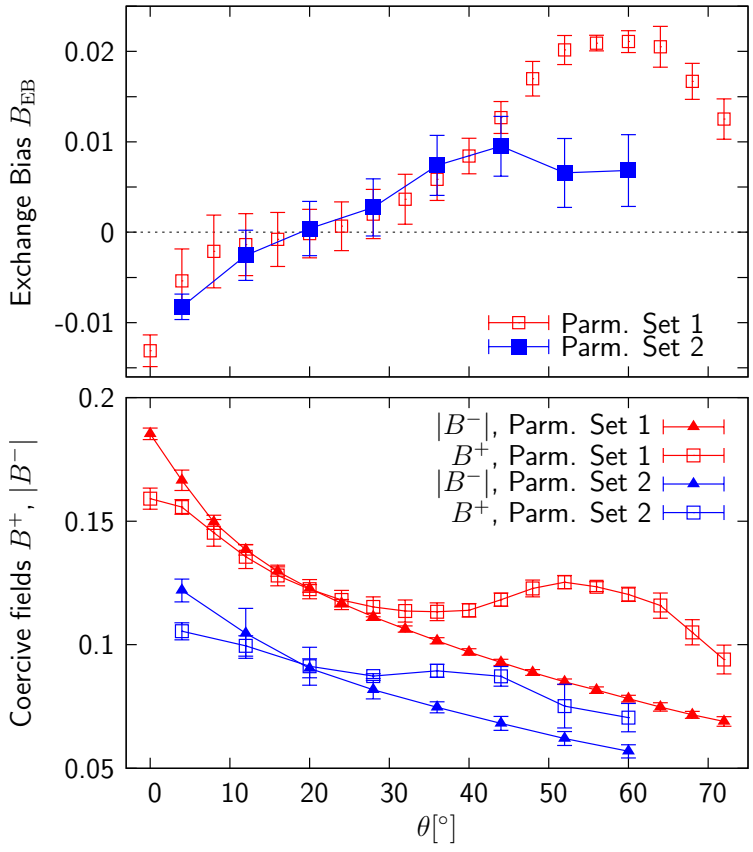

Figure 5.9: Angular dependence of the exchange bias field (top) and the coercive fields (bottom) comparing the two different parameter sets. Note the resemblance of the corresponding angular dependence of the coercive fields for the increasing and decreasing branch of the hysteresis loop. The lines are guides to the eye.

With the knowledge of different reversal modes and the corresponding exchange bias field B_{EB} and coercive fields B^- and B^+ depending on the angle

of measurement one may conjecture that here, too, different reversal modes are responsible for the observed behavior. To verify this the in-plane magnetization paths will be discussed in the following.

5.6.2 In-plane magnetization paths

As it has been shown in Sec. 5.4, plotting the in-plane magnetization paths during hysteresis, i. e., m_y versus m_z, is revealing when characterizing the kind of reversal mode. For a range of measuring angles θ these plots are shown in Fig. 5.10.

For angles up to $\theta = 28°$ reversal modes can be characterized by coherent rotation. Upon reversal on either branch of the hysteresis loop, the magnetization rotates away from the direction of the external field towards its closest easy axis before eventually reversing and then saturating with the magnetization again being aligned with the external field. Note, that for $\theta = 4°$ the reversal on either branch of the hysteresis loop displays a transverse magnetization which is smaller than it is for larger angles θ.

The reason is the same as for the findings of Sec. 5.5, where a less well defined coherent rotation for smaller angles was attributed to the fact that the effective field and the external field are more or less aligned parallel. As a consequence the perpendicular component of the effective field was negligible, and it is this quantity which generally determines whether reversal is by coherent rotation or a non-uniform mode.

Then, for $\theta = 36°$ the magnetization reversal is maximal asymmetric with a coherent rotation for the decreasing branch and a non-uniform reversal mode for the increasing branch where the magnetization path follows the direction of the external field. In this case the transverse component of the magnetization during reversal is negligible.

Upon further increasing the measuring angle θ the same behavior as described previously in Sec. 5.4 is found. Coherent rotation is the prevailing reversal mode, with either branch of the loop rotating via the same side, i. e., for the increasing branch upon reversal the magnetization rotates away from its easy axis.

Generally, for these findings the same explanation holds true as was given in Sec. 5.5. It is the orientation of the effective field with respect to the easy axes of the system which plays a crucial role concerning the reversal mechanism. The choice of system parameters only plays a secondary role and does not lead

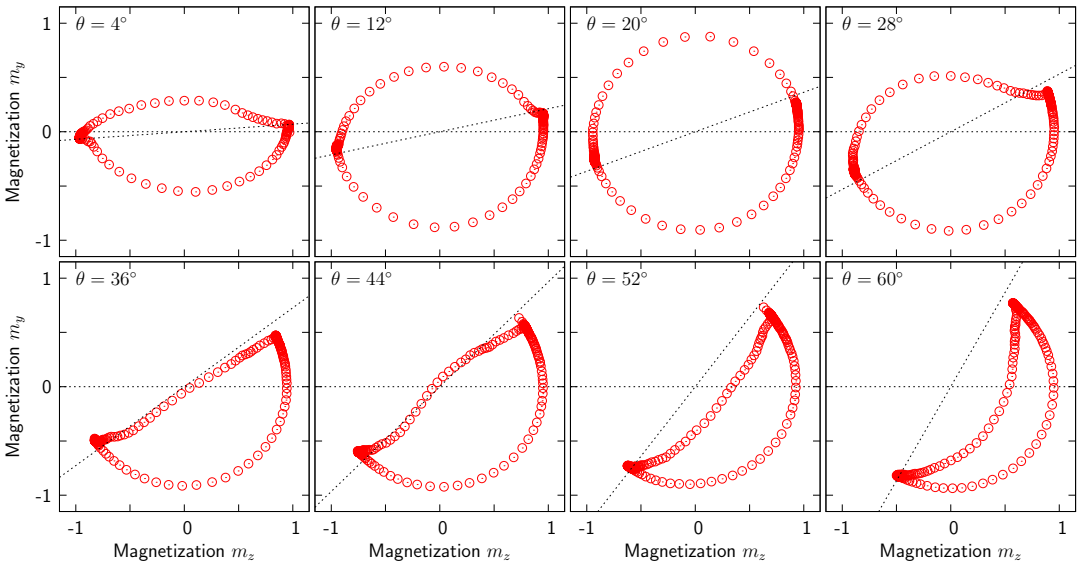

Figure 5.10: In-plane magnetization paths for hysteresis curves obtained for parameter set 2 for measuring angles θ between 4° and 60°. The same behavior as shown in Fig. 5.4 is observed, i. e., with increasing angle θ magnetization reversal for the increasing branch is first via coherent rotation followed by a non-uniform reversal and finally by coherent rotation again; reversal for the decreasing branch is always by coherent rotation.

to a qualitative different behavior. In the present case the angle at which the maximal asymmetric reversal was observed shifted to smaller angles. It is noteworthy, that angles at which reversal is maximal asymmetric and where the coercive field for the increasing branch of the hysteresis loop displays a maximum coincide regardless of the parameter set.

One remaining question is now concerning a possible training effect, i. e., whether the number of consecutive hysteresis cycles has an impact on the reversal mode. To elucidate this, for angles $\theta = 4°$ and 36°, where asymmetry is maximal, simulations are performed on the basis of the parameter set 2.

5.7 Training effect

An important property of exchange bias systems is the training effect which describes the decrease of the exchange bias field B_{EB} when repetitively cycling through hysteresis loops. For the domain state model it has been shown both experimentally [Keller et al., 2002] and theoretically [Nowak et al., 2002b] that after a sharp decrease from the first to the second hysteresis loop the exchange bias field almost remains constant for consecutive hysteresis cycles. In a recent work the power-law decay of the exchange bias field with respect to the number of hysteresis cycles was explained in a phenomenological approach by Binek [2004]. Another interesting feature connected to the training effect was reported in the work of Hochstrat et al. [2002], where this effect mainly originates from the reduction of the coercive field B^- on the decreasing branch of the hysteresis loop while B^+ remains almost constant.

However, so far the training effect has not been considered within the context of asymmetric reversal modes. To investigate this within the domain state model in connection with the angular dependence two different measuring angles were chosen to be subject of simulations. The first one being $\theta = 4^\circ$ which serves as a reference since here for the training effect qualitatively the same behavior should be found as in the cited works of the domain state model as many of the important system parameters are identical. Also, in this case the small misalignment of the direction of the measuring field and the easy axis is close to the geometry of the system considered by Nowak et al. [2002b]. The second angle, $\theta = 36^\circ$, is of more interest since in this case the reversal mode is maximal asymmetric.

5.7.1 Increase of exchange bias

Simulations have been performed as usual, i. e., the same simulation procedure as described earlier is used, the only difference being now that after the initial field cooling process not just one but five hysteresis loops are simulated. Again, results are obtained from six different defect realizations of the diluted antiferromagnet.

In Fig. 5.11 the exchange bias field B_{EB} for the two different measuring angles θ is plotted versus the number N of consecutive hysteresis cycles. For $\theta = 4^\circ$ the usual behavior is found. The initial hysteresis loop yields an exchange bias field

of $B_{\mathrm{EB}} \approx -0.009 J_{\mathrm{FM}}$, for the following loops the absolute value of this quantity is decreasing quickly and settles at approximately $-0.0055 J_{\mathrm{FM}}$.

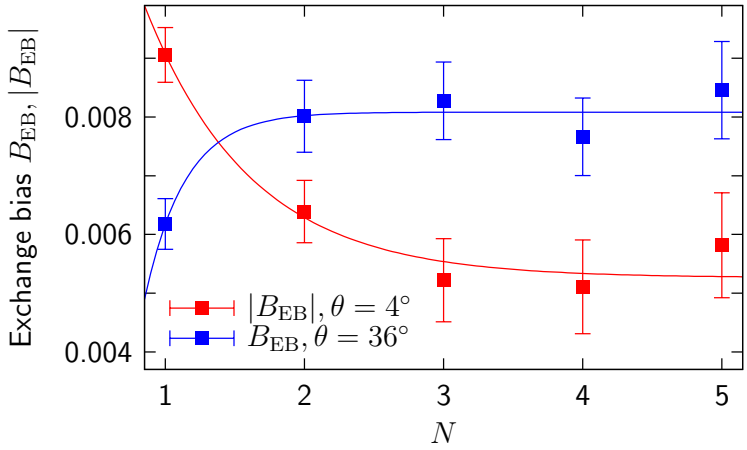

Figure 5.11: Training effect of the exchange bias field for the two different measuring angles $\theta = 4°$ and $36°$. For the latter one the exchange bias field is not only positive but also increases with the number of consecutive hysteresis cycles. The lines are guides to the eye.

For the second measuring angle, $\theta = 36°$, the first loop displays a positive exchange bias field, its value being $B_{\mathrm{EB}} \approx 0.006 J_{\mathrm{FM}}$. Surprisingly enough, for consecutive hysteresis cycles this value even increases and settles at a constant value of $B_{\mathrm{EB}} \approx 0.008 J_{\mathrm{FM}}$. This is a puzzling property which has not been observed in exchange bias systems so far.

To explore in more detail this counter-intuitive feature of a reversed training effect for larger measuring angles the interface magnetization of the antiferromagnet is plotted in Fig. 5.12. It is this layer which carries access magnetization leading to the exchange bias effect.

For $\theta = 4°$ each loop is shifted upwards due to the fact that the antiferromagnet has reached a domain state after the initial field cooling process and carries a net surplus magnetization. Also, the first hysteresis loop (run 1) is not closed on the right-hand side indicating that part of this magnetization is lost during the hysteresis loop. This can be explained by a rearrangement of the antiferromagnet's domain structure during hysteresis. Note, that for this parameter set with its increased number of Monte-Carlo steps this opening is considerably smaller than observed for parameter set 1 as it is shown in Fig. 5.5.

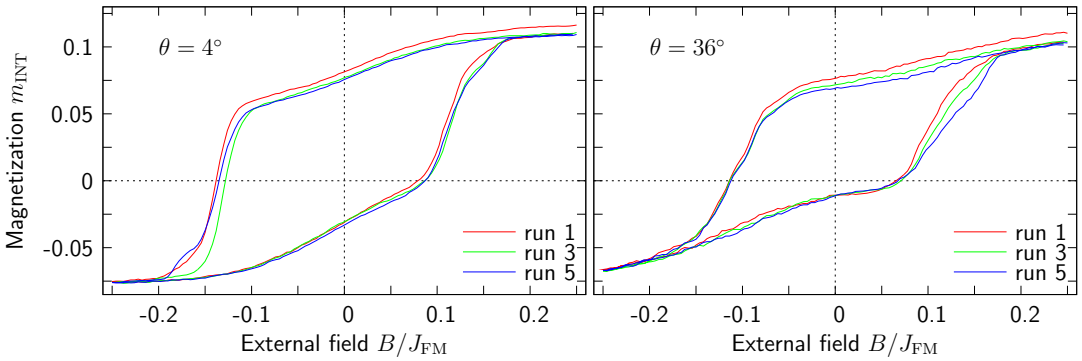

Figure 5.12: Training effect of the interface magnetization for the two different measuring angles $\theta = 4°$ and 36°. In both cases the loops are shifted upwards, and hysteresis loops of the first run are open on the right-hand side.

Surprisingly, for $\theta = 36°$ the plot of the interface magnetization qualitatively looks the same as for the smaller angle. The loops are shifted upwards, as well, and the first hysteresis loop is open on the right-hand side, and there is no apparent difference with respect to the interface magnetization of the first case for $\theta = 4°$ which might give rise to the training effect leading to an increasing exchange bias. Hence, it might be worthwhile to examine the training effect of the coercive fields for these two measuring angles.

In Fig. 5.13 the coercive fields B^- (top) and B^+ (bottom) for $\theta = 4°$ (left axis) and 36° (right axis) are plotted versus the number of consecutive hysteresis cycles. Note that the scales on each axis are identical. For the coercive fields on the decreasing branch, B^-, for $\theta = 4°$ a decrease is obtrusive, i. e., the absolute value of this quantity decreases. Initially, its value is $B^- \approx -0.123 J_{\mathrm{FM}}$, and after five consecutive hysteresis cycles it is approximately given by $-0.118 J_{\mathrm{FM}}$. For the increasing branch, values of $B^+ \approx 0.105 J_{\mathrm{FM}}$ for the first and $B^+ \approx 0.107 J_{\mathrm{FM}}$ for the fifth hysteresis loop are obtained.

For the second angle, $\theta = 36°$, the most obvious difference is the more or less constant value of the coercive field B^- on the decreasing branch of the hysteresis loop, while for the increasing branch a similar behavior as for $\theta = 4°$ is shown. The value B^- is given by $-0.072 J_{\mathrm{FM}}$ and remains constant with repetitively cycling through hysteresis loops. For the increasing branch, B^+

increases slightly approximately from $0.085 J_{\mathrm{FM}}$ to $0.089 J_{\mathrm{FM}}$.

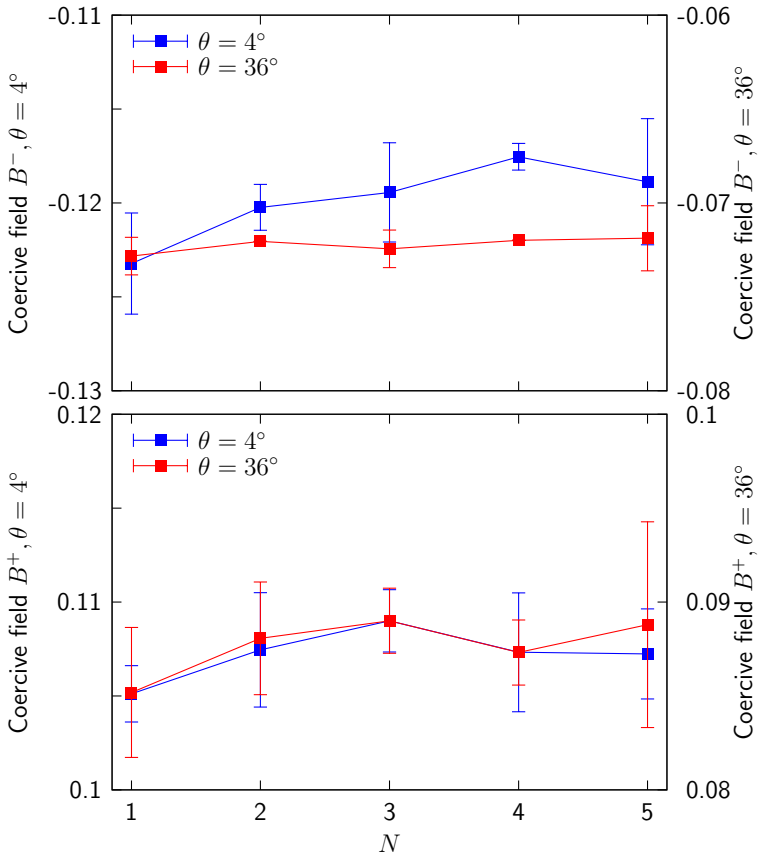

Figure 5.13: Training effect of the coercive fields B^- and B^+ for the two different measuring angles $\theta = 4°$ (left axis) and 36° (right axis). Note the different range on the y-axes. The scales are identical, though.

Therefore, while for the measuring angle $\theta = 4°$ the training effect of the exchange bias field is mainly due to the decrease of the absolute value of the coercive field on the descending branch, B^-, which outweighs negligible changes of the coercive field B^+ on the ascending branch, it is the increase of the coercive field B^+ with B^- remaining constant that causes the increase of the exchange bias field to occur for the measuring angle $\theta = 36°$. Thus, one may conjecture that it is an effect connected to the decreasing branch of the hysteresis loop. So far it has been the increasing branch of the hysteresis loop which has caught much of the attention since it is here where different reversal modes occur in dependence of the angle of measurement, whereas on the decreasing branch of the hysteresis loop coherent rotation is the only reversal mode which is observed.

5.7.2 Magnetization reversal for trained hysteresis

The question arises, whether or not the reversal modes itself are affected when cycling through the hysteresis loops consecutively. Different reversal mechanism for consecutive hysteresis cycles may explain the observation of of the observed increase of the exchange bias field. That reversal mechanisms may indeed be subject to a training effect has been shown experimentally by Brems et al. [2005], where an asymmetric reversal mode was obtained for the untrained hysteresis loop and a symmetric mode for consecutive hysteresis loops.

To answer the above stated question the in-plane magnetization paths will be investigated. In Fig. 5.14, m_z versus m_y is plotted for $\theta = 4°$ (left) and $\theta = 36°$ (right). These hysteresis curves from one specific defect realization of the antiferromagnet – a total of six defect realizations have been considered – are exemplary for the remaining ones.

For the small angle a symmetric hysteresis with coherent rotation is observed for each consecutive hysteresis cycle. Only slight variations concerning the transverse magnetization are visible, e. g., this component seems to slightly decrease for runs 1 through 3. But the loop of run 4 is almost identical to the one of run 1. For the last run, also for the decreasing branch a slightly smaller transverse component can be seen. Overall, there is no distinct training effect concerning the kind of magnetization reversal, the observed variations of the transverse components on either branch of the hysteresis loops can be ascribed to thermal fluctuations.

The same picture emerges for the loops shown for $\theta = 36°$. For each loop magnetization reversal is asymmetric with a coherent rotation on the decreasing branch and a non-uniform reversal on the increasing regardless of the number of consecutive hysteresis cycles. Especially, a distinctive difference between first and second loop, as it has been observed experimentally, is not apparent. Here, no significant change takes place.

This may be partly due to the fact that for the antiferromagnet an Ising system is considered. Therefore, only the projection of the external field along the easy axis is relevant which is being proportional to $\sin(\theta)$. The same holds true for the exchange field provided by the ferromagnet. For larger angles θ it is only during reversal when this field may considerably influence the antiferromagnet. The largest effects are then to be expected for coherent rotation when the ferromagnet uniformly sweeps via the easy axis of the antiferromagnet. For less

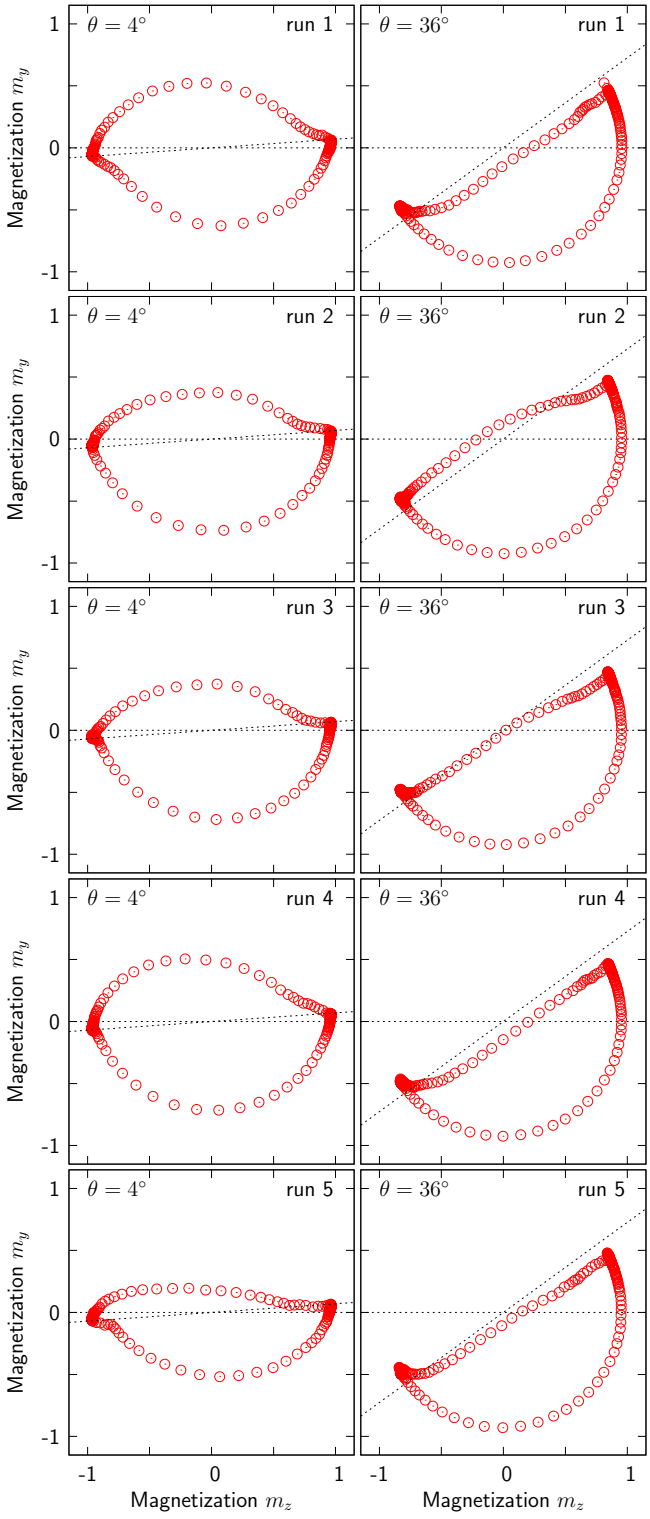

Figure 5.14: In-plane magnetization reversal for consecutive hysteresis cycles for $\theta = 4°$ (left) and $\theta = 36°$ (right). The former one displays a symmetric reversal for each of the consecutive runs, while for the latter one reversal is asymmetric with coherent rotation on the decreasing and a non-uniform reversal on the increasing branch.

uniform reversal modes, e. g., nucleation with domain wall propagation, this effect will not be as pronounced as in the previous case since then, for instance, reversal may be via opposite directions locally[3].

Moreover, the assumption that it is the coercive field on the decreasing branch which gives rise to the increase of the exchange bias field for consecutive hysteresis cycles is unsustainable. Here, a well pronounced coherent rotation is found for each single loop regardless of the number of consecutive hysteresis cycles. Therefore, other effects are likely to be responsible for this puzzling property and an explanation is not readily available from the present simulation data.

In the following, this chapter concludes with a detailed characterization of the reversal modes by means of the spin configurations of the ferromagnetic layer observed during reversal.

5.8 Spin configurations

It has been pointed out in Sec. 4.3.2 that a closer look at the spin configurations of the magnetic system may give more insight into the actual reversal mechanism than the pure simulation data allow for. Moreover, the domain state of the antiferromagnet is best displayed in such a graphical presentation. Therefore, the antiferromagnetic domain state will be discussed, then the asymmetric reversal mode for $\theta = 60°$ will be illuminated.

5.8.1 Antiferromagnetic domain state

In Fig. 5.15 the staggered spin configuration of the antiferromagnet during the field cooling process for two different temperatures is depicted. Note, that for a dilution $p_{\mathrm{vol}} = 0.6$ of the antiferromagnet the Néel temperature is approximately given by $T_N = 1.8 J_{\mathrm{INT}}/k_{\mathrm{B}}$ [Usadel and Nowak, 1992]. Therefore, in Fig. 5.15a at a temperature of $k_{\mathrm{B}}T = 0.994 J_{\mathrm{FM}}$ the antiferromagnet is still in its paramagnetic phase and the majority of the spins will be aligned with the external field (color coding blue and green changes frequently since the staggered spin configuration is shown). In Fig. 5.15b the temperature is below the ordering temperature of the diluted antiferromagnet and the domain structure which has developed during field cooling is clearly identifiable.

[3]For a detailed discussion see Sec. 5.8

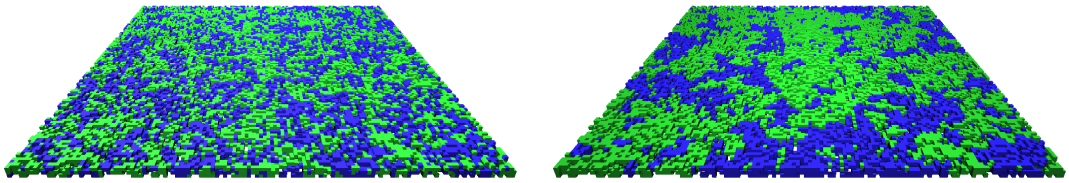

(a) Staggered spin structure for $k_{\mathrm{B}}T = 0.994J_{\mathrm{FM}}$ right after initialization of the simulation procedure.

(b) Staggered spin structure for $k_{\mathrm{B}}T = 0.1J_{\mathrm{FM}}$. At this temperature the hysteresis loops are simulated.

Figure 5.15: Staggered spin structure of the antiferromagnetic during field cooling.

5.8.2 Ferromagnetic spin configuration during reversal

To qualify the often used term of a nonuniform reversal mode slightly more precise, it is helpful to take a look at the spin configurations of the ferromagnet during the reversal process. From a series of snapshots it will be possible to distinguish between modes resembling, for instance, coherent rotation or nucleation with domain wall propagation. Exemplary, this discussion will be by means of the reversal mode for $\theta = 60°$. Here, both a coherent rotation and a nonuniform reversal mechanism were observed. A series of spin configurations of the ferromagnet for the descending and ascending branch of the hysteresis loop around the coercive fields B^- and B^+ are shown in Fig. 5.16.

For the decreasing branch in Fig. 5.16a the coherent rotation is obvious. Each snapshot is colored uniformly, thus the spins are mostly aligned parallel. Initially, the spins are aligned with the external field at an angle of $\theta = 60°$ with respect to the easy axis of the antiferromagnet (top snapshot, blue-yellow colored). Then, the spins relax towards the closest easy axis (second snapshot, blue colored); eventually, the magnetization is reversed and the spins are aligned with the external field again (third and fourth snapshot, blue-red and red colored).

For the increasing branch shown in Fig. 5.16b close to the coercive field B^+ the spins are aligned with the external field (first snapshot, red-green colored); then, regions evolve (second snapshot) where the spins either rotate towards

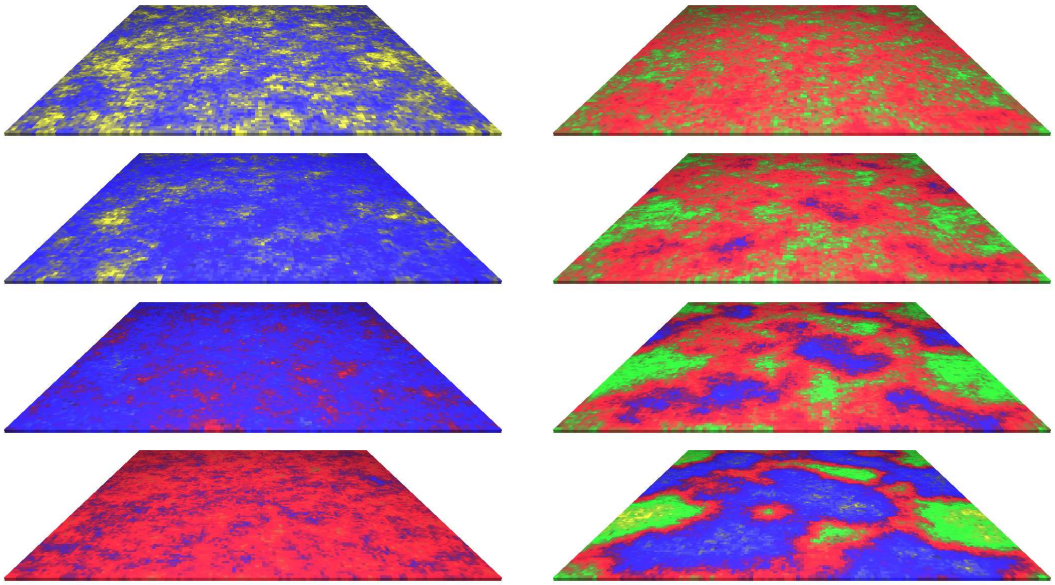

(a) Snapshots during reversal around B^- for the decreasing branch of the hysteresis loop. Each spin configuration is colored uniformly indicating a coherent rotation.

(b) Snapshots during reversal around B^+. Differently colored regions indicate areas where the spins reverse via opposite directions.

Figure 5.16: Spin configurations of the ferromagnet close to the coercive fields where reversal sets in. For $\theta = 60°$ reversal asymmetry is maximal.

the closest easy axis (green colored) or away from it (blue colored). These regions grow (third and fourth snapshot) before the system will eventually be reversed. It is noteworthy that this reversal mechanism cannot be considered as a nucleation process with subsequent domain wall propagation, which would be characterized by domain walls sweeping across the ferromagnet, and it is thus best described by nonuniform.

So far, an explanation of the origin of the asymmetric reversal modes observed in ferromagnetic-antiferromagnetic multilayer systems with uniaxial anisotropies has been given in the context of the domain state model. The next step is to understand the reversal mechanism as they are observed in systems where the

antiferromagnet displays a more complex structure. Therefore, in the following chapter systems will be investigated where a so-called twin structure for the antiferromagnet is considered while the main properties of the ferromagnet are left unchanged in order to explicitly explore the influence of the antiferromagnetic structure.

6 Asymmetries in multilayers with twinned antiferromagnetic structures

In the previous chapter the asymmetries and the origin thereof in exchange bias systems have been investigated, where the most characteristic feature of the antiferromagnet was its strong uniaxial anisotropy. Hence, the antiferromagnet was modeled as an Ising system. However, in numerous experimental works it is emphasized that the antiferromagnet does not feature a strong uniaxial anisotropy but rather displays cubic anisotropy [Hoffmann, 2004], or it shows a so-called twinned structure [Fitzsimmons et al., 2000, 2002; Tillmanns et al., 2005; Nogués et al., 1999; Pechan et al., 2002]. In this case, there is not one single easy axis for the antiferromagnet but rather a distribution of easy axes. In many cases, these are aligned perpendicular to each other within the film plane. For instance, in the case of antiferromagnet FeF_2 this is a result of the growth process, where a lattice with a rectangular structure, e. g., the (110)-plane of the FeF_2 is grown onto a substrate with a quadratic lattice, such as the (100)-plane of MgO. A further illustration of the experimental details and especially the crystal structure of FeF_2 is given in the work of Nogués et al. [1999].

In the works mentioned above it is pointed out that the orientation of the external field with respect to the easy axes of the antiferromagnet during the field cooling process may have a significant impact on the kind of reversal mode which occurs during hysteresis. Probably the most prominent example for observed asymmetries in systems with a twinned antiferromagnetic structure is given in the work of Fitzsimmons et al. [2000], which was discussed in detail in Sec. 3.1. They showed that one obtains a symmetric reversal behavior for the ferromagnet, i. e.,the same reversal mechanism – in this case coherent rotation – is observed on either side of the hysteresis loop, when cooling and measuring the sample in a field pointing along the direction of one of the easy axes of the antiferromagnet (see bottom of Fig. 3.1). In contrast to that, if this is done along the direction of the bisector of both of the easy axes, an asymmetric reversal mode is observed. Here, a coherent rotation for the decreasing branch and nucleation for the increasing branch of the hysteresis loop are obtained. Furthermore, in a more recent work [Tillmanns et al., 2005] it was shown that

a variation of the sample orientation during the measurement leads to different reversal mechanisms, both symmetric and asymmetric, even when the cooling procedures were identical.

In order to explore this behavior within the framework of the domain state model, the conditions for the antiferromagnet displaying only a uniaxial anisotropy need to be relaxed. This is obvious, since an angular dependence of the direction of the cooling field is not to be expected when the antiferromagnet is modeled as an Ising system with only one easy axis. In this case, a variation of the direction of the external field during cooling would be equivalent to a variation of its strength, because for the antiferromagnetic Ising spins only the projection along the z-direction would be relevant. Therefore, in order to mimic a distribution of easy axes within the antiferromagnet, the most simple approach is to introduce two easy axes for the antiferromagnet which are perpendicular to each other and within the film plane. The details for the necessary modifications of the geometry and the Hamilton function of the system will be outlined in the following section.

6.1 Modification of the antiferromagnetic system

In order to model the system where the antiferromagnet displays a so-called twinned structure, some conditions need to be met, particularly concerning the lateral dimensions of the areas with one easy axis. By means of electron-beam- or x-ray-diffraction [H. Dosch, 1987] the orientation of the easy axes of a sample can be determined. However, experimentally there are only very few prerequisites regarding the spacial dimensions of the antiferromagnetic twin structure. I. e., the question dealing with the size of the regions where only one of the easy axes is found often times remains open.

Yet, Liu et al. [2001] and Fitzsimmons et al. [2001] report in their works, that the ratio of the size of the ferromagnetic domains and the size of regions with a single easy axes within the antiferromagnet are roughly 100:1, where the lower boundary of the size of the antiferromagnetic twin-structure can be obtained by means of the Scherrer-relation [Warren, 1990] when evaluation Bragg reflections, and it is given by 10 ± 1 nm. This would suggest that the ferromagnet is exposed to an effective field provided by the antiferromagnet.

Generally, such a system would be comparable to a system with a single easy

axis as it was discussed in the previous chapter. Therefore, the case of small antiferromagnetic twin structures will be investigated, such that the ferromagnet can be influenced locally by the underlying antiferromagnetic structure. This will be possible when the lateral dimensions of antiferromagnetic areas with a uniaxial anisotropy are larger than the ferromagnetic domain wall width which is given by $\delta = \sqrt{J/(d2)}$ [Hubert and Schäfer, 1998; Malozemoff and Slonczewski, 1979], with the given parameters this leads to $\delta = 5$[1].

Hence, the lateral size for the area with a single uniaxial anisotropy will be set to $l_y \times l_z = 32 \times 32$. With adjacent regions of antiferromagnetic twins and their easy axis being perpendicular to each other a checkerboard-like structure as shown in Fig. 6.1 is the result. It displays 4×4 patches of the antiferromagnetic areas with uniaxial anisotropy leading to an overall system dimension of 128×128. Also, the direction of the easy axes of the ferromagnet is indicated by the black line bisecting the two easy axes of the antiferromagnet. The reason for this assumption is to not favor any particular direction due to the exchange coupling to the antiferromagnet, and thus implying an asymmetry within the system.

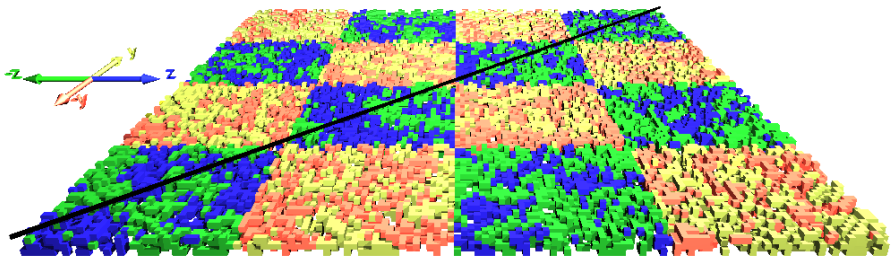

Figure 6.1: Staggered spin configuration of the twinned antiferromagnet. The red/yellow and green/blue colors render the twin structure with two easy axes perpendicular to each other. One is aligned along the y axis (red/yellow), the other along the z axis (green/blue). The black line bisecting these two axes illustrates the direction of the easy axis of the ferromagnet.

[1] $J = J_{\mathrm{FM}} = 1$ and $d = D_{\mathrm{FM}} = 0.02 J_{\mathrm{FM}}$.

6.1.1 Hamilton function of the twinned system

With the previously mentioned modifications in mind it is easy to specify the corresponding Hamilton function. Starting point is the Hamilton function given in Eqn. 5.1, which basically describes a ferromagnet modeled as Heisenberg system exchange coupled to an antiferromagnet described as an Ising system. Only the terms for the ferromagnetic anisotropy – a new direction of the easy axes is to be considered – and the areas with different uniaxial anisotropies for the antiferromagnet need to be adapted. The Hamilton function of the system is thus given by

$$\begin{aligned}\mathcal{H} = & - J_{\mathrm{FM}} \sum_{\langle i,j\rangle \in \mathrm{FM}} \boldsymbol{S}_i \cdot \boldsymbol{S}_j - \sum_{i \in \mathrm{FM}} \left(d_{\mathrm{FM}} (\boldsymbol{n} \cdot \boldsymbol{S}_i)^2 + d^x_{\mathrm{FM}} S^2_{ix} + \boldsymbol{B} \cdot \boldsymbol{S}_i \right) \\ & - J_{\mathrm{AFM}} \sum_{\langle i,j\rangle \in \mathrm{AFM_{x,y}}} \epsilon_i \epsilon_j \boldsymbol{\sigma}_i \boldsymbol{\sigma}_j - \sum_{i \in \mathrm{AFM_{x,y}}} \epsilon_i \boldsymbol{\sigma}_i \boldsymbol{B} \\ & - J_{\mathrm{INT}} \sum_{\langle i \in \mathrm{AFM_{x,y}}, j \in \mathrm{FM}\rangle} \epsilon_i \boldsymbol{\sigma}_i \boldsymbol{S}_j .\end{aligned} \tag{6.1}$$

Again, $\boldsymbol{S}_i$ and $\boldsymbol{\sigma}_i$ are Heisenberg and Ising spin variables at lattice site i, respectively, the first one being a classical Spin vector while the latter is described as $\boldsymbol{\sigma}_i = \sigma_i \cdot \hat{\boldsymbol{y}}$ for $i \in \mathrm{AFM}_y$ or $\boldsymbol{\sigma}_i = \sigma_i \cdot \hat{\boldsymbol{z}}$ for $i \in \mathrm{AFM}_z$, where $\mathrm{AFM}_{y,z}$ denotes areas of the antiferromagnet with its easy axis being parallel to the y- or z-axis, respectively. $\boldsymbol{n}$ is the unit vector along the direction of the easy axis of the FM which is aligned along the bisector of the easy axes of the AFM as discussed before. This anisotropy is taken into account by introducing the term $d_{\mathrm{FM}}(\boldsymbol{n} \cdot \boldsymbol{S}_i)^2$.

It is important to note, that only the geometry of the system has been adapted. The values for any exchange and anisotropy constants will be the same as for the previous simulations described in Sec. 5.1. Thus, the exchange constants are set to $J_{\mathrm{AFM}} = -J_{\mathrm{FM}}/2$ and $J_{\mathrm{INT}} = -J_{\mathrm{AFM}}$ and the anisotropy constants are set to $d_{\mathrm{FM}} = 0.02 J_{\mathrm{FM}}$ and $d^x_{\mathrm{FM}} = -0.2 J_{\mathrm{FM}}$ for the ferromagnet. Also, the dimensions of the system remain the same, i. e., one ferromagnetic monolayer exchange coupled to a diluted antiferromagnetic film consisting of three monolayers is considered. The values for the dilution are set $p_{int} = 0.5$ for the interface layer and $p_{vol} = 0.6$ for the remaining two layers.

6.1.2 Procedure for simulating hysteresis

Generally, the procedure for simulating the hysteresis loop are the same as described in Sec. 5.2, only that an additional variation of the orientation of the external field has to be considered. The simulation procedure is illustrated by means of Fig. 6.2. ϕ denotes the angle between the external field $\boldsymbol{B}_{\mathrm{FC}}$ during field cooling, whereas θ is the one to which this initial angle is changed for the simulation of the hysteresis loop itself. Two different angles ϕ will be considered and for each cooling field direction hysteresis loops for angles $\theta = 0° - 50°$ in steps of $\Delta\theta = 10°$ are calculated.

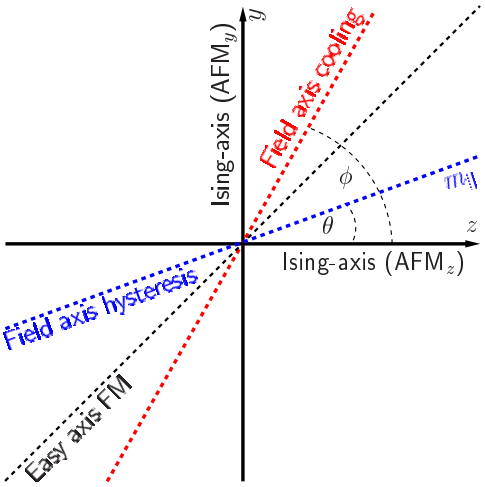

Figure 6.2: Top view of the orientation of the field axes during the initial cooling and for the hysteresis loops. The angles θ and ϕ are measured with respect to one of the easy axes of the antiferromagnet (z-axis).

In detail, the following procedure for simulating the hysteresis loop for the two different angles ϕ and the series of angles θ is performed: Initially, the ferromagnet is set to be aligned along the direction $\boldsymbol{n}$, which is along its easy axis, for cooling in an external field $\boldsymbol{B}_{\mathrm{FC}} = 0.4J_{\mathrm{FM}}$. Then, the angle ϕ is set to either 0° or 45°, respectively, which is either along one easy axis of the antiferromagnet or along the bisector of both. In the next step the system is cooled from its initial temperature $k_{\mathrm{B}}T = J_{\mathrm{FM}}$ to $k_{\mathrm{B}}T = 0.1J_{\mathrm{FM}}$ in steps of $\Delta k_{\mathrm{B}}T = -0.002J_{\mathrm{FM}}$, which is from above to below the Néel temperature of the antiferromagnet.

At each temperature step 600 Monte-Carlo steps are performed. Again, the same Monte-Carlo simulation techniques are employed, i. e., a single-spin flip for antiferromagnetic spins and a small trial step for the Heisenberg spins of the ferromagnet. Then, hysteresis curves for different angles θ are calculated. In

order to do so, the external field is reduced from $B = 0.32 J_{\mathrm{FM}}$ to $B = -0.32 J_{\mathrm{FM}}$ in steps of $\Delta B = 0.004 J_{\mathrm{FM}}$ before being increased in the same manner to its initial value. Here, for each field step 500 Monte-Carlo steps are performed. For the ferromagnet, periodic boundary conditions within the film plane are imposed. For the antiferromagnet this is not necessary since adjacent areas $\mathrm{AFM}_{y,z}$ have their easy axes perpendicular to each other, thus no interaction between their spins can occur.

It has to be pointed out, that there are slight modifications concerning the simulation procedure besides the investigation of the cooling field direction. The range in which the hysteresis loops are simulated is smaller than it was previously when investigating multilayers with uniaxial anisotropies, which leads to a reduced numerical effort. It has been shown to be sufficiently large such that at each maximum external field $\boldsymbol{B}$ the saturation magnetization is reached. Also, the range of angles θ is smaller since rather significant effects could already be observed in this range. Finally, the number of Monte-Carlo steps has been increased owing to the additionally introduced antiferromagnetic anisotropy axis. It is possible that this additional anisotropy demands for an increased number of Monte-Carlo steps in order to reach quasi-equilibrium at each field value. The results that will be presented in the following have been obtained from a single defect realization. In order to check that different defect realizations of the antiferromagnet lead to the same qualitative behavior the results were averaged over four different defect realizations.

6.2 Cooling field dependence of reversal modes

Before the main results are discussed that were obtained from the simulations the angular dependence of the exchange bias field itself will be briefly addressed. As it has been the case in the previous chapter, the value of the exchange bias field and its angular dependence on the cooling and measuring field, respectively, only plays a secondary role. The result of the simulations showed that contrary to experimental findings [Shi and Lederman, 2002; Camarero et al., 2005; Dekadjevi et al., 2006] a pronounced angular dependence of the exchange bias field is not found, as it is shown in Fig. 6.3.

There, for the two cooling field directions with $\phi = 0°$ and $\phi = 45°$ the exchange bias field B_{EB} is plotted versus the angle of measurement, θ, ranging

from 0° to 60° with an increment of 10°. For neither one of the cooling field directions a pronounced angular dependence is obvious.

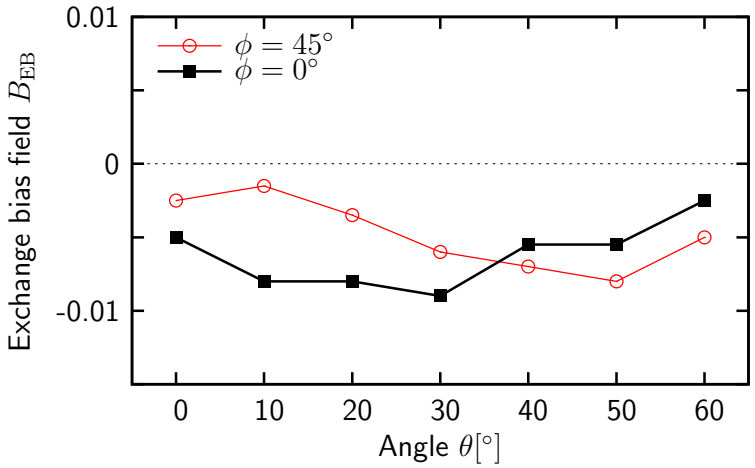

Figure 6.3: Angular dependence of the exchange bias field B_{EB} for the two cooling field directions with angles $\phi = 0°$ and $\phi = 45°$.

Also, the value of the exchange bias field is considerably smaller than in previous simulations within the domain state model. A reason for this may be the fact that the surplus magnetization which leads to exchange bias is provided by the independent patches of antiferromagnetic twins. Within each twin with its quasi-open boundary conditions the ratio of reversible and irreversible magnetization – influencing the coercivity and exchange bias field – is shifted towards the former one. Besides, in simulations within the domain state model the exchange bias field has always been rather small as compared to the coercivity. As a consequence, any angular dependence regarding this quantity will not be extraordinarily pronounced, if visible at all.

Therefore, the emphasize will be put on the discussion of the reversal modes which depend on the direction of the cooling field. It will be shown that the direction of rotation for magnetization reversal is given by the frozen magnetization provided by the antiferromagnet. Also, reversal is mostly less coherent as compared to the single crystal case. Despite the fact that some hysteresis loops appear symmetric, the reversal modes themselves are not necessarily the same on either side of the hysteresis loop.

6.2.1 Coherent rotation versus nonuniform reversal mode

In this section the dependence of the reversal modes on the cooling field direction will be discussed. To do so, in Fig. 6.4 for the two cooling field directions the

in-plane magnetization of the ferromagnet with its ascending (blue open circles) and descending branch (closed red squares) is plotted as m_y versus m_z for a series of angles θ, with m_z (m_y) denoting the magnetization parallel to the Ising axis of antiferromagnetic twins AFM_z (AFM_y). This in-plane magnetization is illustrated in the same manner as described in 5.4, i. e., each plot starts at the right corner corresponding to the magnetization for the maximum external field value $B_{\max}$. Here the spins of the ferromagnet are aligned with the external field, its direction being indicated by the solid black line. In the left corner the magnetization points into the opposite direction when exposed to the maximum negative field $-B_{\max}$. Note, that the magnetization of the ferromagnet for a maximum external field is always aligned with this field since its absolute value is considerably larger than the anisotropy of the ferromagnet.

From the series of in-plane magnetization paths for both cooling field directions different reversal modes are found. On the one hand, reversal can be considered as coherent rotation when the magnetization path is shaped semicircle-like. On the other hand, if this path lies mostly on the external field axis such a reversal mode will be called nonuniform which is characterized by a negligible transverse magnetization component.

When talking about coherent rotation as the predominant reversal mechanism one has to bear in mind that in the simulations thermal effects are taken into account. As a consequence the magnetization magnitude – especially in zero field close to reversal – depends on the temperature. Furthermore, it also depends on the direction with respect to the easy axes and the external field, i. e., when the magnetization is oriented perpendicular to the external field or any easy axis its magnitude inevitably has to be lower than the corresponding saturation magnetization. In that sense, the magnetization is never fully saturated and a reversal could be called coherent when the magnetization magnitude significantly deviates from zero during reversal.

Also, characterizing a reversal mode as nonuniform deserves careful attention. Such a reversal mode – where the magnetization magnitude breaks down to zero during reversal – might have different origins. For instance, domain wall propagation, nucleation, or even a local coherent rotation, which will be discussed in the next section, may all lead to a vanishing transverse magnetization during reversal.

From the set of magnetization curves in Fig. 6.4 two different reversal mechanisms can be identified. Most clearly the differences can be seen in the series

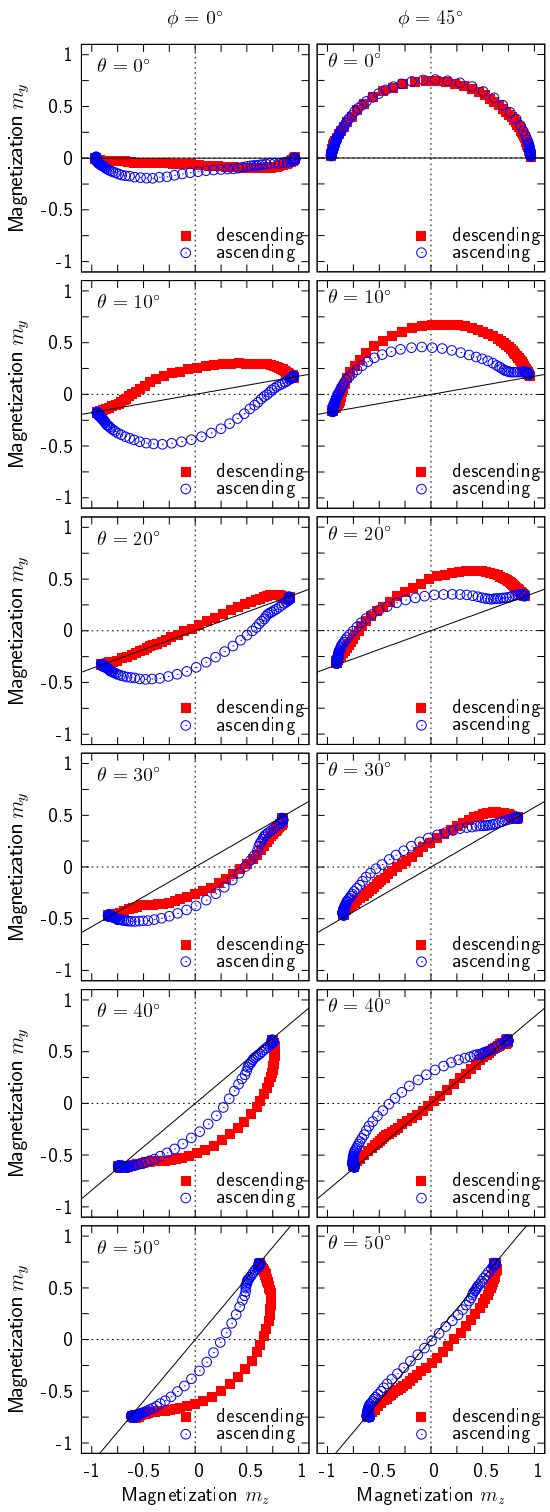

Figure 6.4: In-plane magnetization of hysteresis loops with the descending (red closed squares) and ascending branch (blue open circles) for angles $\theta = 0° - 50°$ for two cooling field directions with angle $\phi = 0°$ (left) and $\phi = 45°$ (right). The field axis for the hysteresis is aligned at an angle of θ for each loop as indicated by the solid black line.

of the magnetization curves for $\theta = 0°$ shown in the first line of Fig. 6.4. In this case, while for $\phi = 0°$ only a negligible transverse magnetization component is present, there is a clear coherent rotation for magnetization reversal for $\phi = 45°$. It is apparent that the reason for this behavior lies in the different frozen magnetizations of the antiferromagnet induced during the field cooling process.

In the first case (left row), the cooling field is aligned parallel to one easy axis (z axis) of the antiferromagnet. Thus, only the spins with this easy axis will carry a surplus net magnetization pointing into the z direction. Consequently, for the hysteresis loop with $\theta = 0°$ there is only a surplus net magnetization provided by the antiferromagnet which is parallel to the external field. Hence, the magnetization reversal for both branches of the hysteresis loop is nonuniform. The situation changes, once the field for the hysteresis loop is not perfectly aligned with the z axis any more. Then, there are projections of the antiferromagnetic net magnetization both along and perpendicular to the external field. This leads to a reversal mechanism which shows a non-negligible transverse component. For increasing angles θ, the antiferromagnetic magnetization projection perpendicular to the external field also increases. For $\theta = 20°$ the reversal can be considered asymmetric as for the decreasing branch a nonuniform reversal is obtained whereas for the increasing branch a coherent rotation is the predominant reversal mechanism. For angles $\theta \geq 30°$ the rotation of the magnetization is via the same side for both branches of the hysteresis loop.

It is noteworthy, that these findings are qualitatively in agreement with recent experimental results [Tillmanns et al., 2005], even though the range of angles where these effects occur is different. This can be seen from Fig. 6.5, where the transverse magnetization components of hysteresis loops are shown for a range of measuring angles ϕ_H after the sample, Fe/FeF_2 with a twinned structure for the antiferromagnet, has been cooled in an external field, which is aligned with one easy axis of the antiferromagnet. A direct comparison with the numerical results is difficult since the experimental results do not reveal a quantitative magnitude for the magnetization component $M_\perp$. However, the same qualitative behavior can be identified, i. e., within a narrow range of measuring angels the reversal mechanism changes from symmetric (e. g. $\phi_H \approx 0°$), which corresponds to to the case of $\phi = 0°, \theta = 0°$ in the simulation, over to an asymmetric reversal mode with one branch displaying a coherent rotation while the other one has a negligible transverse component ($\phi_H \approx 2°$). This case is found for the same

cooling field direction with $\theta = 20°$ in the simulation. Finally, the reversal is symmetric again, with both branches rotating coherently via the same side ($\phi_H \geq 4°$), which is the same behavior found in the simulation ($\theta \geq 30°$).

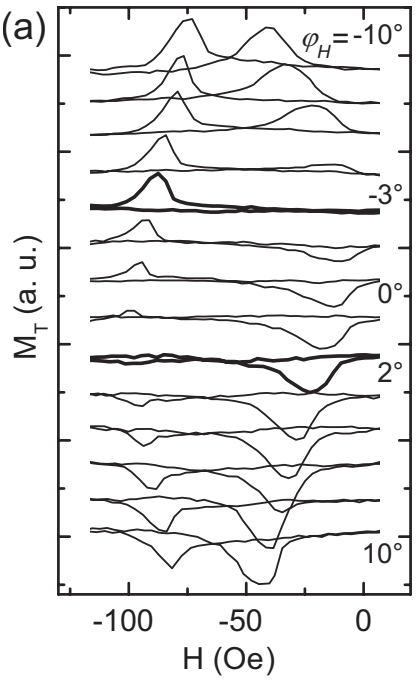

Figure 6.5: Transverse magnetization component of Fe/FeF_2 hysteresis loops for a series of measuring angles after field cooling along one easy axis of the antiferromagnet ([Tillmanns et al., 2005]).

Besides the agreement with recent experimental results, it has to be pointed out that these effects are qualitatively the same as they were found for the system where the antiferromagnet only showed a uniaxial anisotropy, as it was shown in Sec. 5.4. In Fig. 5.4 the same evolution of the reversal mechanism is observed in the case for the antiferromagnet with a twinned structure. For $\theta = 0°$ a symmetric reversal is obtained with negligible transverse components for both branches of the hysteresis loop. When the angle θ is increased , the reversal will eventually become symmetric, before for very large angels, $\theta \geq 68°$, the reversal is also symmetric but with both branches rotating via the same side of the hysteresis loop.

The situation for the reversal mechanism changes significantly, when the direction of the cooling field is aligned with the bisector of the twinned structure of the antiferromagnet. As a consequence of this cooling process both regions $AFM_{y,z}$ carry a net surplus magnetization. Therefore, even for $\theta = 0°$ there already exists a non-null projection of the antiferromagnetic net magnetization

perpendicular to the external applied field. This leads to a reversal mode which is predominantly characterized by a coherent rotation on either side of the hysteresis loop. Again, it is worth noting that both times the rotation is via the same direction in contrast to a pure Stoner-Wohlfarth behavior. If θ is increased now, this leads to a decreasing projection perpendicular to the external field. Thus, the reversal mechanism becomes less and less coherent before eventually there is no transverse component any more.

6.2.2 Asymmetric magnetization reversal and spin configurations

It has been pointed out that a closer look at the spin configurations allows for a deeper insight into the reversal mechanisms. This is even more true in the case of the reversal mechanism in the present case, where the antiferromagnet displays a twinned structure. Intuitively, one would not expect that the reversal mechanisms for the increasing and decreasing branch of the hysteresis loop for $\phi = 45°, \theta = 30°$ are different, since its in-plane magnetization path shown of Fig. 6.4 looks rather symmetric. But surprisingly, a closer look at the spin configurations of the ferromagnet for external field values close to the coercive fields reveals certain asymmetries.

A series of snapshots of the ferromagnetic spin configurations both for the increasing and decreasing branch of the hysteresis loop is shown in Fig. 6.6. Either series shows the spin configurations in an interval of $\Delta B = 0.08 J_{\mathrm{FM}}$ around the corresponding coercive fields. In Fig. 6.6a the series displays the spin configurations for the decreasing branch of the hysteresis loop. Here, the twinned structure of the underlying antiferromagnet is mapped onto the ferromagnet, an effect which has also been observed experimentally [Nolting et al., 2000; Ohldag et al., 2001]. The obtained reversal mode locally shows a coherent rotation depending on how the easy axis of the antiferromagnet underneath is oriented. However, the global magnetization of the ferromagnetic film has a negligible transverse magnetization due to the fact that this coherent rotation is via opposite directions. Therefore, the corresponding transverse contributions cancel out each other.

For the increasing branch shown in in Fig. 6.6b there are again larger regions displaying a coherent rotation. This time, though, the spin structure is not related to the underlying twinned structure of the antiferromagnet. Nevertheless,

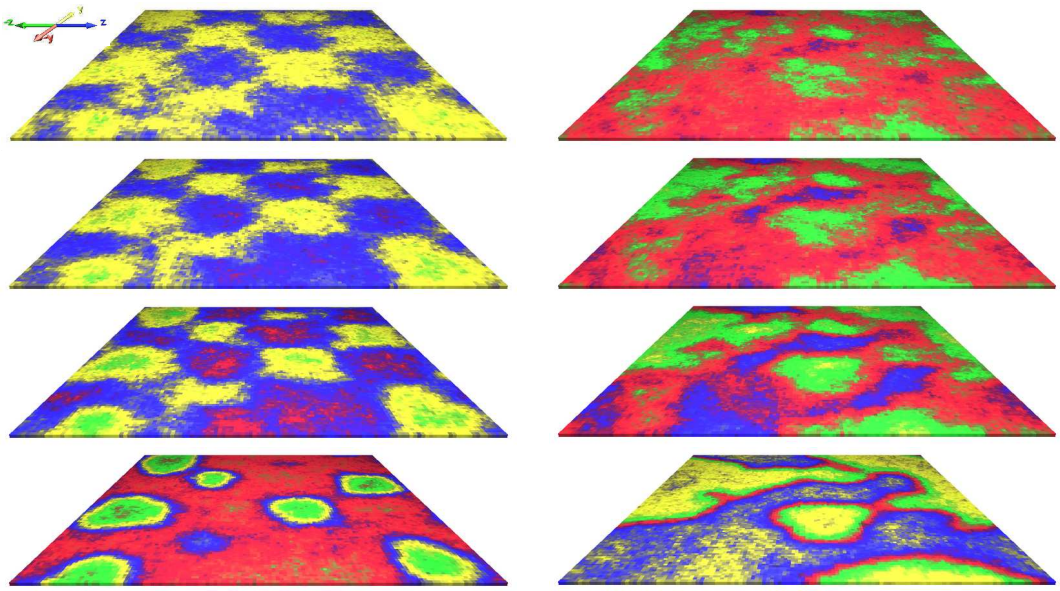

(a) Snapshots during reversal around B^-. The antiferromagnetic twin structure is mapped onto the ferromagnet during reversal.

(b) Snapshots during reversal around B^+. Large areas are displayed where the spins reverse via opposite directions.

Figure 6.6: Spin configurations of the ferromagnet around the the coercive fields for $\phi = 45°$ and $\theta = 30°$. The spawned interval for both decreasing and increasing branch is $\Delta B = 0.08 J_{\mathrm{FM}}$. In both cases a nonuniform reversal mode is observed, i. e., larger regions show coherent rotation but for different regions via opposite directions.

due to the fact that its transverse component during reversal is also negligible and that the reversal mode cannot be characterized by domain wall propagation or nucleation, this mode is also referred to as nonuniform.

The question remains whether these findings can also explain the experimental results of Fitzsimmons et al. [2000]. It turns out that this is possible to a certain extent. In order to do so the corresponding cooling field and measuring field directions shown in Fig. 3.1 have to be identified in Fig. 6.4. The case that the external field during the cooling procedure and the measurement are aligned

with one easy axis of the antiferromagnet is shown in the left column of Fig. 6.4 ($\phi = 0°$) and small angles $\theta = 0°, 10°$.

The special case of $\theta = 0°$, where all relevant anisotropy and field axis are perfectly aligned, shall not be considered in this context. It has already been pointed out for systems with uniaxial anisotropies that in this case only nonuniform reversal modes can be observed. However, as soon as any of the relevant axes deviates from a perfect alignment, i. e., the external field is parallel to the easy axis both of the ferromagnet and the antiferromagnet, a rather different behavior for the reversal mechanism is observed, as it has been shown in Secs. 5.5 and 6.2.2. A perfect alignment of all of the relevant field and anisotropy axes might be hard to accomplish experimentally. Therefore, the argumentation will focus on angles slightly larger than in this special case.

Considering the case of $\theta = 10°$ and $\phi = 0°$ as shown in Fig. 6.4, the corresponding reversal mechanism can be regarded as symmetric – even though if coherent rotation is not very pronounced in this case. Bearing in mind that the results obtained experimentally by neutron scattering techniques do not yield quantitative but rather qualitative values for the reversal mechanisms, one has – if not a perfect agreement with the corresponding results – still at least no contradiction regarding this case.

The second case, which is where the external field during the cooling process and the measurement is pointing along the bisector of the antiferromagnetic twins, is shown in the right column of Fig. 6.4 ($\phi = 45°$) where θ is in the range of $30° - 50°$. As it has been shown already, the attempt to characterize the reversal mechanism only by taking the hysteresis loop into account fails. Rather, one has to take a closer look at the spin configurations during the reversal both for the decreasing and increasing branch of the hysteresis loop as shown in Fig. 6.6. For decreasing field values a negligible transverse magnetization component is observed. However, the spin configurations disclose a coherent rotation on the length scale of the antiferromagnetic twins and they are directly linked to its checkerboard-like structure.

Experimentally, such a reversal mode is likely to be characterized as coherent rotation in the case that the measuring technique is not sensitive to the sign of the transverse magnetization component. For the increasing branch a nonuniform reversal mode, just as it is the case in the experiment, is found. Therefore, there is an agreement between the cited experimental results and the presented simulation results: coherent rotation on the decreasing branch of the hysteresis

loop and a nonuniform reversal mode with a negligible transverse component on the increasing branch.

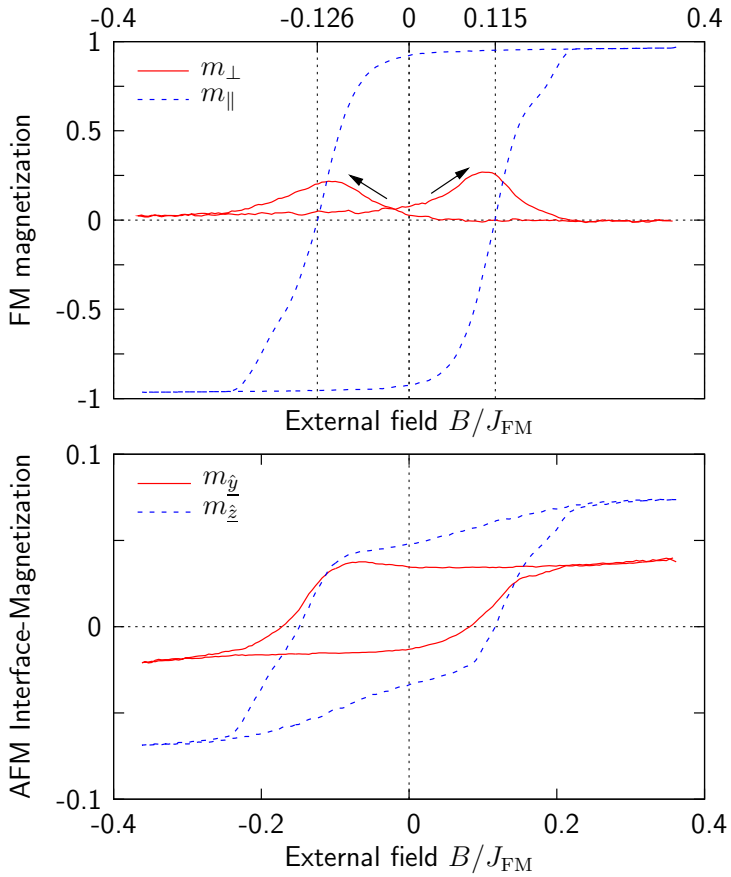

Figure 6.7: Hysteresis loops for the parallel and perpendicular component of the ferromagnetic layer (top), and the magnetization of the regions $\mathrm{AFM}_{y,z}$ of the antiferromagnetic interface layer (bottom) versus the external field ($\phi = 45°, \theta = 30°$).

Finally, the question is why such an asymmetry during the reversal can be observed with the ferromagnet showing a twinned structure during reversal only on one side of the hysteresis loop. One prerequisite is the aforementioned size of the antiferromagnetic twins. Their dimensions were set large enough such that the domain wall width, given by $\delta = 5$, of the ferromagnet is considerably smaller. In Fig. 6.7 (top) the parallel and perpendicular component of the ferromagnetic magnetization is plotted versus the external field – and, as it is often the case, it does not reveal any details relevant for the discussion of the reversal modes. The reason for the asymmetry is given from the antiferromagnetic interface magnetization as it is shown in Fig. 6.7 (bottom). The regions of special interest are the ones where the external field is close to zero. Here, contributions from the external field are negligible, thus it is the exchange field

provided by the antiferromagnetic interface layer which is playing the key role.

For a decreasing external field B at remanence there is a magnetization close to $m = 0.05$ for both the AFM_z and the AFM_y region. This causes the ferromagnetic layer to selectively align along either direction given by the underlying antiferromagnetic interface magnetization.

However, for an increasing external field B at remanence, the situation is rather different. The magnetization m_y in the region AFM_y is close to zero, thus providing an exchange field to the ferromagnet too small to influence its magnetization direction significantly. Besides, the regions AFM_z carry a magnetization m_z which is smaller than it was the case for the decreasing fields.

In conclusion, these results together with the findings of the previous chapter, where exchange bias systems with uniaxial anisotropies have been investigated, allow for a correct interpretation of experimentally observed asymmetric reversal modes. Thus, the domain state model successfully explains yet another property connected to the exchange bias effect. To support the main idea that it is structural disorder within the antiferromagnet which is essential for a domain state within the antiferromagnet to occur a different kind of structural disorder for the antiferromagnet will be considered. Rather than a site-diluted antiferromagnet exchange coupled to a ferromagnet a bond-diluted antiferromagnet will be considered for simulation.

7 Domain state model with bond disorder

It has been shown so far that the domain state model successfully explains exchange bias and many features connected to it. Not only does it show a very good agreement with corresponding experimental results [Nowak et al., 2002b; Keller et al., 2002], where – among others – the dependence on dilution, positive exchange bias, temperature and time dependence, the dependence on the thickness of the antiferromagnetic layer, and the training effect could be explained. But it also explains the origin of asymmetric reversal modes that are found in systems with uniaxial anisotropies [Beckmann et al., 2003] and those where the antiferromagnet displays a twinned structure [Beckmann et al., 2006]. However, despite its success with explaining a large number of effects associated with exchange bias, there are common objections concerning the domain state model.

One of which is, that in experimental setups the antiferromagnetic samples are not diluted intentionally, and it is claimed that exchange bias is also found in systems where the antiferromagnet is not diluted in any way. The other concern is that the value for the dilution of the antiferromagnet where the exchange bias effect is maximal occurs at rather large dilutions. The latter issue has already been addressed in a recent work of Spray and Nowak [2006], where the optimal dilution of the bulk of the antiferromagnet is found to be much less than in previous simulations – here, the optimal value has been $p_{\mathrm{vol}} = 0.5$ – when also taking into account an interface mixing with ferromagnetic spins reaching into the antiferromagnetic interface layer. The former one, however, is still under debate and there is a risen interest to resolve this issue.

It seems to be important to stress, that it is not the magnetic dilution of the antiferromagnet itself, but rather the structural disorder that is introduced this way, which plays the crucial role when investigating exchange bias systems. In order to show that any kind of structural disorder should lead to the same qualitative results the domain state model will be adapted, and a random bond instead of a random site model will be utilized. Some of the most characteristic features connected to exchange bias will be shown to also occur in such a model, such as the resulting domain state of the antiferromagnet, the dependence of the

exchange bias field on the dilution and the temperature dependence. To begin with, the necessary adaptation of the model will be explained together with the corresponding Hamilton function.

7.1 Adaption of the random site model

The starting point for the investigation of a random bond model for ferromagnetic-antiferromagnetic multilayers will be the domain state model for exchange bias which incorporates a site diluted antiferromagnet. Recalling the picture of the site diluted domain state model shown in Fig. 4.5 the difference with respect to a bond diluted model as it is shown in Fig. 7.1 is apparent. Again, the basis is a simple cubic lattice both for the ferromagnet and the antiferromagnet. The ferromagnet is modeled as Heisenberg system as well as the antiferromagnet and it displays a small anisotropy along the z axis with the anisotropy constant set to $d^z_{\mathrm{FM}} = 0.02 J_{\mathrm{FM}}$. Describing the antiferromagnet within the Heisenberg model relaxes the constraints given by the Ising model. Furthermore, the dipolar interaction is accounted for in the same way as before, which is by introducing a hard axis along the x axis, preferentially keeping the spins within the y-z plane, the corresponding anisotropy term is given by $d^x_{\mathrm{FM}} = -0.2 J_{\mathrm{FM}}$.

For the antiferromagnet the situation is different, now. Rather than introducing structural disorder by randomly leaving lattice sites within the antiferromagnetic layers empty, the exchange constants between adjacent spins are randomly set to zero within the bulk. For the coupling across the ferromagnetic-antiferromagnetic interface an intermixing of ferromagnetic and antiferromagnetic bonds is assumed representing a minimal roughness which can be expected to exist in any real system. Note that this intermixing of bonds is a different approach than intermixing ferromagnetic and antiferromagnetic spins. The current approach leads towards a spin glass within the interface layer. It has been shown very recently that compound systems consisting of a ferromagnet exchange coupled to a spin glass exhibits all the key features of usual exchange bias systems [Ali et al., 2007].

However, a systematic investigation of this intermixing has been beyond the scope of this work. But a crude investigation for the bond diluted model showed that large effects are for instance found when there is a rather small fraction of ferromagnetic bonds.

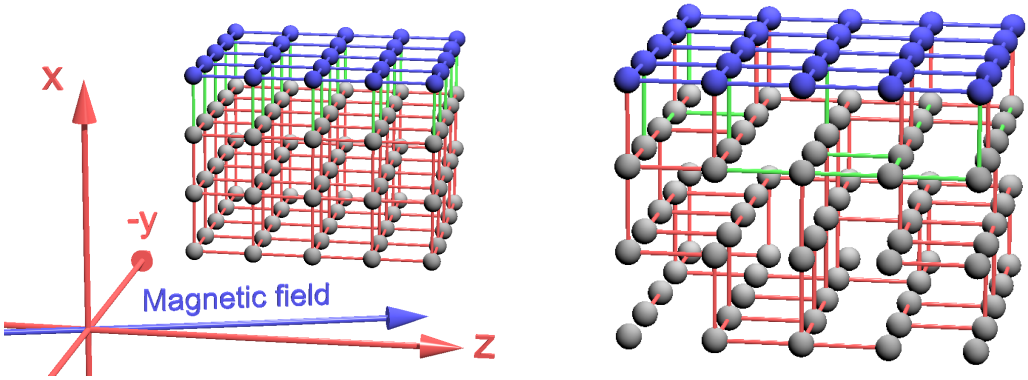

(a) Undiluted antiferromagnet with $p_{\mathrm{vol}} = 0.0$.

(b) Diluted antiferromagnet with dilution $p_{\mathrm{vol}} = 0.5$.

Figure 7.1: Sketch of a random bond model on a simple cubic lattice. The coloring is as follows: blue for a ferromagnetic (J_{FM}), red for a antiferromagnetic (J_{AFM}) coupling. For the coupling across the interface, a fraction of the bonds is ferromagnetic (green; here $J_{\mathrm{INT}} = J_{\mathrm{FM}}/2$) and a fraction of the remaining bonds antiferromagnetic (J_{AFM}).

For the simulations a fraction $R_{\mathrm{FM}} = 0.3$ of the exchange constants J_{ij} between spins of adjacent sites of the ferromagnetic and antiferromagnetic layer and between those within this antiferromagnetic interface layer is set to a value of $J_{\mathrm{INT}} = J_{\mathrm{FM}}/2$. The remaining portion of the interface exchange constants and throughout the volume of the antiferromagnet is set to zero with probability p_{vol}; antiferromagnetic bonds not set to zero or J_{INT} have a value of $J_{\mathrm{AFM}} = -J_{\mathrm{FM}}/2$. Note that in the case of dilutions $p_{\mathrm{vol}} \lesssim 0.57$ the portion of antiferromagnetic bonds will exceed the ferromagnetic ones. This means that then the exchange interaction across the interface will be mostly antiferromagnetic.

The corresponding Hamilton function is easily adapted from Eqn. 5.1 and for the present case of the bond diluted system is given by

$$\begin{aligned}\mathcal{H} = & - \sum_{\langle i,j\rangle\in\mathrm{FM}} J_{ij}\boldsymbol{S}_i\cdot\boldsymbol{S}_j - \sum_{i\in\mathrm{FM}}\left(d^z_{\mathrm{FM}}S^2_{iz} + d^x_{\mathrm{FM}}S^2_{ix} + \boldsymbol{B}\cdot\boldsymbol{S}_i\right) \\ & - \sum_{\langle i,j\rangle\in\mathrm{AFM}} J_{ij}\boldsymbol{\sigma}_i\boldsymbol{\sigma}_j - \sum_{i\in\mathrm{AFM}}\boldsymbol{B}\boldsymbol{\sigma}_i - \sum_{i\in\mathrm{AFM}} d^z_{\mathrm{AFM}}\sigma^2_{iz} \\ & - \sum_{\langle i\in\mathrm{AFM},j\in\mathrm{FM}\rangle} J_{ij}\boldsymbol{\sigma}_i\boldsymbol{S}_j.\end{aligned} \tag{7.1}$$

As usual, the first line describes the energy contribution of the ferromagnet, the second line the one of the antiferromagnet, and the last one includes the term accounting for the coupling across the ferromagnetic-antiferromagnetic interface. The exchange constants J_{ij} are set as described above. For the antiferromagnetic layers the value of anisotropy is set to $d^z_{\mathrm{AFM}} = 1.0$ and is assumed to be aligned along the same direction as for the ferromagnet, which is along the z axis.

The geometry of the system will not be subject of any systematic investigation, i. e., a thickness dependence of the exchange bias field on number of antiferromagnetic layers will not be carried out. Therefore, the dimensions are set to (3+1)×128×128 which describes one ferromagnetic monolayer exchange coupled to three antiferromagnetic layers both with lateral dimensions of 128×128.

7.2 Monte-Carlo simulations for the random bond model

For the Monte-Carlo simulations a combination of the different trial steps discussed in Sec. 4.3.1 will be used. For the ferromagnet the usual small trial step will be utilized as its properties, e. g., the easy and hard axes, are identical to those of previous simulations. For the antiferromagnet, which is now modeled as Heisenberg system, at least one additional trial step should be used owing to the relatively large anisotropy along the z axis. In detail, a combination of the small, the universal, and the reflection trial step will be used, where for each chosen spin of the antiferromagnetic lattice one of the above mentioned trial steps will be randomly chosen with probabilities $p_{\mathrm{STS}} = 0.6$, $p_{\mathrm{UTS}} = 0.2$, and $p_{\mathrm{RTS}} = 0.2$, for the small, the universal, and the reflection trial step, respectively.

In order to show that the bond diluted model for ferromagnetic-antiferro-

magnetic multilayers also shows many of the characteristic features found in simulations of the site diluted model the calculations will be carried out according to the following procedure.

To investigate the influence of the bond dilution, for seven different values of the bond dilution $p_{\mathrm{vol}} = 0.0, 0.1, 0.2, 0.3, 0.4, 0.5$ and 0.7 the antiferromagnet will be initialized as described above. Then, the system will be cooled in an external field $B_{\mathrm{FC}} = 0.2 J_{\mathrm{FM}}$ which is aligned at an angle of $\theta = 4^{\circ}$ with respect to the z axis. This is done to avoid that the system gets trapped in a metastable state and to have well defined magnetizations paths as discussed in the previous chapters. At each temperature step 1100 Monte-Carlo steps are performed, discarding the first 100 steps in order to let the system relax. The initial temperature is set to $k_{\mathrm{B}}T = 1.0 J_{\mathrm{FM}}$ which is reduced in steps of $k_{\mathrm{B}}\delta T = 0.01 J_{\mathrm{FM}}$ to three different measuring temperatures $k_{\mathrm{B}}T = 0.5 J_{\mathrm{FM}}, 0.4 J_{\mathrm{FM}}$ and $0.1 J_{\mathrm{FM}}$.

For the hysteresis the external field is initially set to a value of $B_{\mathrm{max}} = 0.16 J_{\mathrm{FM}}$, which is then reduced in steps of $\Delta B = 0.004 J_{\mathrm{FM}}$ down to $-B_{\mathrm{max}}$, before being increased in the same manner to its initial value. The orientation of the external field is the same as for the field cooling process. The same is true for the number of Monte-Carlo steps.

At each temperature and field step thermal averages are calculated for the magnetization components both of the ferromagnet and the antiferromagnet, along with the interface magnetization of the antiferromagnet. The results will be averaged over six different realizations of bond dilution for the antiferromagnet in order to minimize statistical errors.

7.2.1 Domain state of the antiferromagnet

One of the most obvious features found in simulations of the domain state model with a site diluted antiferromagnet was the development of a domain state within the antiferromagnet when cooled below its ordering temperature either in an external field or when being exposed only to the exchange field provided by the ferromagnetic layer. In Fig. 7.2 the domain states found in the bond diluted system for three different values of p_{vol} are compared with the domain states as it develops in a site diluted antiferromagnet for two different values of the dilution. Note, that in the case of the site diluted antiferromagnet an Ising model was incorporated while for the current investigation the antiferromagnet is also modeled as Heisenberg system, yet, with a fairly large uniaxial anisotropy. It

has been shown by Misra et al. [2004] that the domain structure in such systems resemble those found in systems with infinite uniaxial anisotropies assumed for the antiferromagnet.

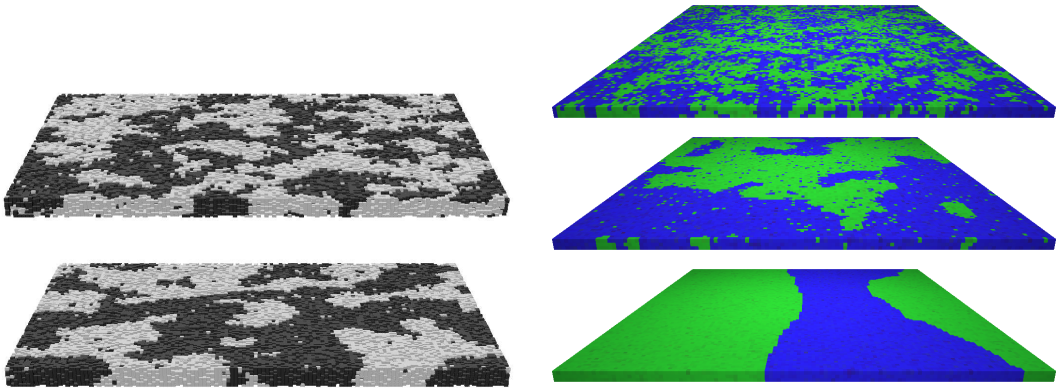

(a) Staggered spin configurations of site diluted antiferromagnets for dilutions $p_{\mathrm{vol}} = 0.5$ (above) and $p_{\mathrm{vol}} = 0.3$ (below). (Ref. [Nowak et al., 2002b]).

(b) Staggered spin configurations of bond diluted antiferromagnets for three different dilutions $p_{\mathrm{vol}} = 0.7$ (above), $p_{\mathrm{vol}} = 0.3$ (middle), and $p_{\mathrm{vol}} = 0.0$ (below).

Figure 7.2: Comparison of domains states for site and bond diluted antiferromagnets after the initial cooling procedure.

In both cases the formation of a domain state is obvious and the fractal structure of the domains observed clearly depends on the dilution, whether it is for the site or bond diluted antiferromagnet. That the formation of domains for decreasing dilution is constricted is easily explained. An increased number of domains would require breaking an increasing number of antiferromagnetic bonds which increases the energy of the system in contrast to systems with larger dilutions where domain walls can pass through defects. The fact that even for zero dilution (bottom of Fig. 7.2b) the systems splits up into two domains can be explained with the intermixing of ferromagnetic and antiferromagnetic bonds within the interface layer.

7.2.2 Influence of temperature and dilution

In the experimental [Keller et al., 2002] and theoretical investigations [Nowak et al., 2002b] of the domain state model the strong dependence of the exchange bias field on the dilution of the antiferromagnet was one of the most important observations. It was argued that dilution favors the formation of domains which leads to an increased magnetization within the antiferromagnet. As a consequence, the resulting exchange bias field is also increased. Here, it will be shown that the same qualitative behavior is found for the model with a bond diluted antiferromagnet.

In Fig. 7.3 the dependence of the exchange bias field B_{EB} on the dilution p_{vol} is shown for three different temperatures $k_{\mathrm{B}}T/J_{\mathrm{FM}} = 0.1, 0.3$ and 0.5. For the latter one, the absolute value of the exchange bias field B_{EB} is zero within error bars for larger dilutions and slightly above zero for lower dilutions. However, it is still fairly small and can be considered negligible.

With decreasing temperature, $k_{\mathrm{B}T} = 0.3J_{\mathrm{FM}}$, the exchange bias effect is apparent and a maximum is displayed for dilutions p_{vol} around 0.3, where the exchange bias field is approximately given by $-0.007J_{\mathrm{FM}}$. For dilutions either going to zero or to 0.3 the exchange bias field approaches a negligible value.

For a temperature of $k_{\mathrm{B}T} = 0.1J_{\mathrm{FM}}$ the effects are even more pronounced, i. e., at a dilution of $p_{\mathrm{vol}} = 0.3$ the absolute value of the exchange bias field is maximal and a value of $|B_{\mathrm{EB}}| \approx 0.1J_{\mathrm{FM}}$ is obtained. For very large dilutions B_{EB} drops to zero, while for the undiluted system exchange bias is negligible but not zero.

One of the most obvious differences concerning the dependence on dilution as compared to the site diluted model is the shifted maximum of the exchange bias field. There, the maximum exchange bias field was found for rather large dilutions of the volume with $p_{\mathrm{vol}} = 0.6$. Here, however, this maximum is now showing at a relatively low dilution, $p_{\mathrm{vol}} = 0.3$, and a value of $|B_{\mathrm{EB}}| \approx 0.1J_{\mathrm{FM}}$ is found. Note, that this is roughly only one quarter of the value found in the original model. However, the emphasis is put on a qualitative comparison, and it is interesting to find the maximum at lower values of dilution p_{vol}.

7.2.3 Magnetization orientation during reversal

Since exchange bias is found to be maximal for rather low dilutions it is interesting to determine the orientation of the ferromagnetic spins with respect to

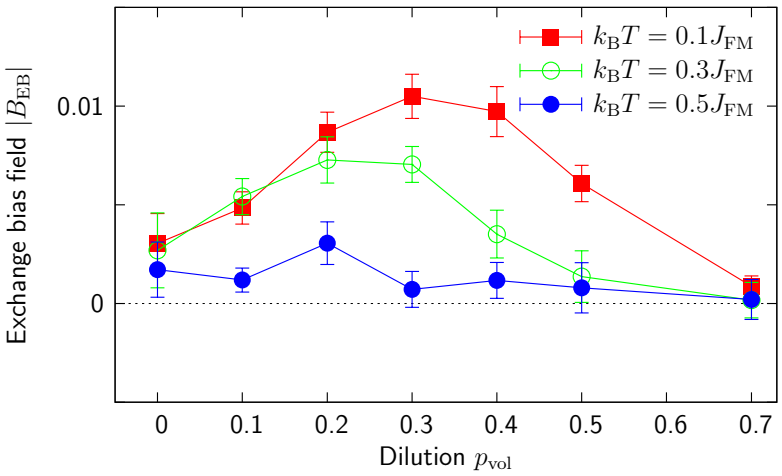

Figure 7.3: Exchange bias field in dependence of the dilution p_{vol} for three different temperatures $k_BT/J_{FM} = 0.1, 0.3$ and 0.5.

the spins of the antiferromagnetic interface layer.

On the one hand, for low dilutions one should expect that in zero field a perpendicular coupling across the ferromagnetic-antiferromagnetic interface should occur since this would minimize the energy, provided that the limiting case of infinite anisotropies is not reached[1]; this is certainly not the case at least for the ferromagnet. One also has to keep in mind that the lower the dilution the larger the domains are. Thus, it is less likely that the energy is minimized when ferromagnetic spins align parallel across adjacent domains of the antiferromagnet.

On the other hand, in the case of a strongly diluted antiferromagnet such a perpendicular coupling does not necessarily have to occur. Now, the number of domains and therefore the number of domain walls increases which consequently leads to an increased energy minimization due to the aforementioned effect of parallel aligned spins across domain wall boundaries.

The plots of Fig. 7.4 support this view of a well predefined magnetization path for lower dilution values p_{vol} where for a vanishing external field the in-plane magnetization vector rotates away from the easy axis both for the decreasing and increasing branch of the hysteresis loop. The lower the dilution is the larger the angle between the easy axis of the ferromagnet and the vector of magnetization in zero field. It is also eye-catching that this angle is always slightly larger for the increasing than for the decreasing branch of the loop.

[1] In this case the system could be described in terms of an Ising model.

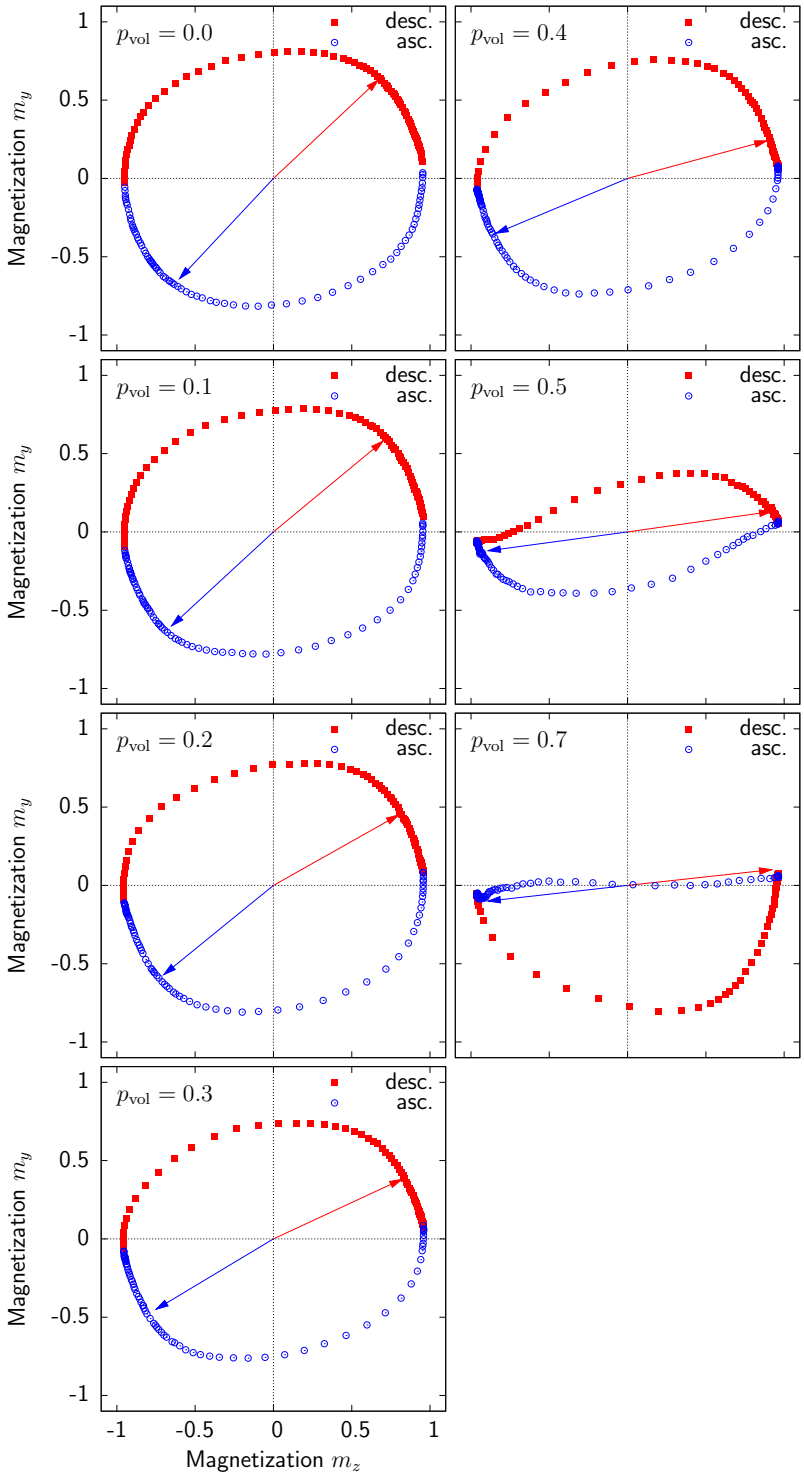

Figure 7.4: Magnetization path during reversal for different values of dilutions p_{vol}. Note that except for $p_{\mathrm{vol}} = 0.7$ for both decreasing and increasing branch the magnetization rotates away from its closest easy axis before reversal takes place. The arrows indicate the remanence magnetization vector for each branch of the hysteresis loop.

This is clearly connected to the exchange bias effect which is caused by the surplus interface magnetization provided by the antiferromagnet. Therefore, the difference between the corresponding angles is largest when the exchange bias effect is maximal, which is the case for $p_{\mathrm{vol}} = 0.3$.

Note, that these findings are contrary to what has been observed for the site-diluted model in the preceding chapters where for small measuring angles, in the present case $\theta = 4°$, coherent rotation has been observed as well, but the magnetization path was less well defined. The most obvious difference, though, is the fact that with decreasing external field values the ferromagnet does not relax towards its closest easy axis but rather rotates away.

As it has been pointed out earlier only for dilutions $p_{\mathrm{vol}} \gtrsim 0.57$ the interface coupling will be mostly ferromagnetic. This is reflected in the plot for $p_{\mathrm{vol}} = 0.7$. Here, upon decreasing the external field the magnetization vector does not rotate away from its closest easy axis but rather keeps aligned with the external field which is aligned at an angle of $\theta = 4°$. Reversal is then by coherent rotation via the closest easy axis for the decreasing branch. For the increasing branch a non-uniform reversal mode is observed where the magnetization path follows the direction of the external field. This is in agreement with the observations made for the site-diluted model where for small measuring angles θ the magnetization path is less well defined (see Sec. 5.5).

To further investigate the effect of a perpendicular coupling the magnetization components of the antiferromagnetic interface layer will be examined. One has to keep in mind that the anisotropy of the antiferromagnet was set to a relatively large value of $d^z_{\mathrm{AFM}} = 1.0$. As a consequence the antiferromagnet is rather stiff and any net magnetization components perpendicular to its easy axis will be accordingly small.

In Fig. 7.5 and 7.6 the magnetization components of the antiferromagnetic interface layer parallel and perpendicular to its easy axis, which is given by the z-axis, is shown. The first thing to notice is the fact that for low dilution values the interface magnetization m^z_{AFM} is negative provided that the ferromagnet is saturated in a positive external field and vice versa. This is due to the fact that the predominant portion of the interface coupling is antiferromagnet. Therefore, for increasing dilutions two effects set in. The ratio of ferromagnetic to antiferromagnetic spins grows in favor of the former one. Also, the overall coupling between the ferromagnetic and antiferromagnetic layer decreases as more interface bonds are set to zero, consequently the exchange coupling is

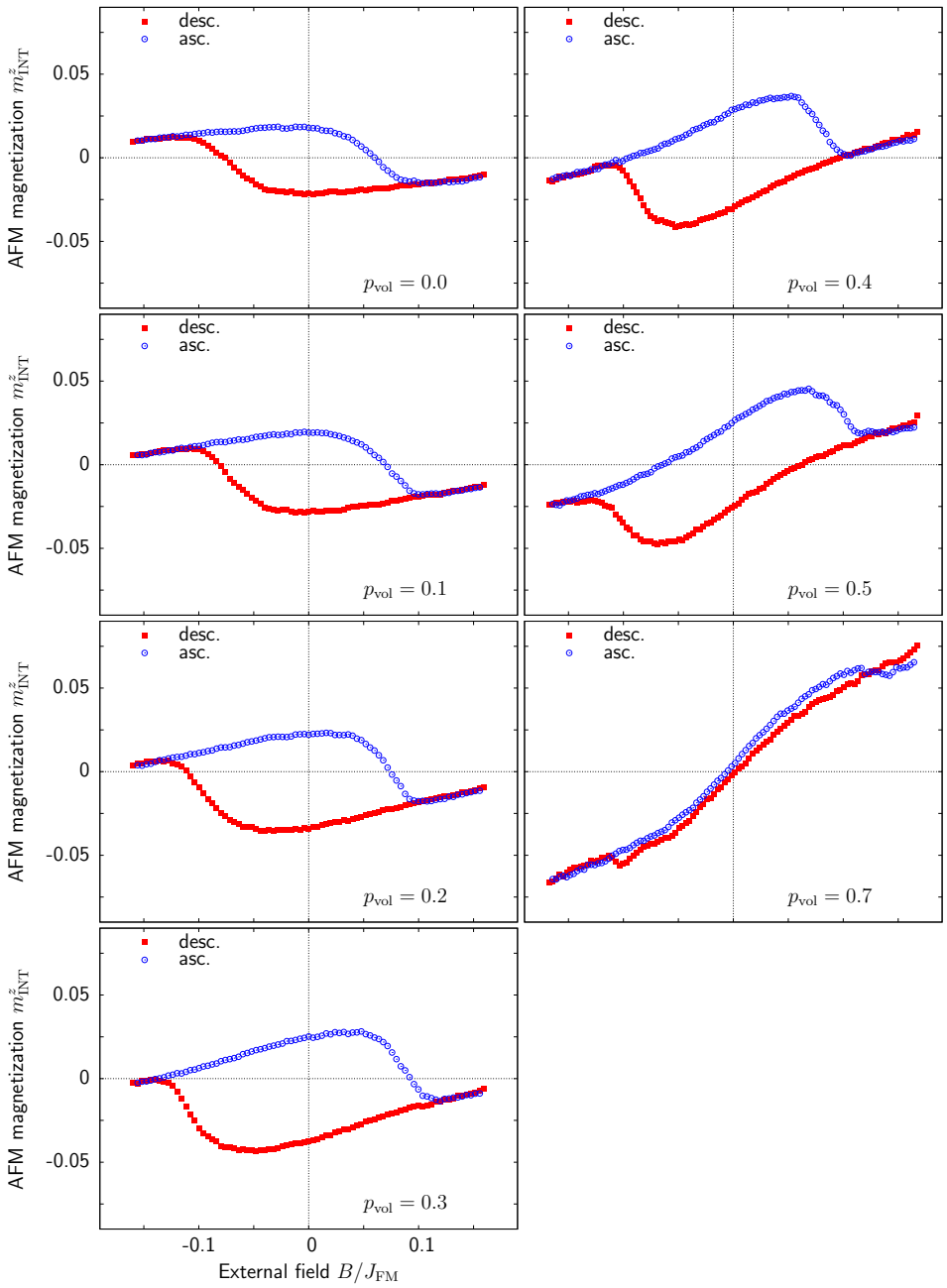

Figure 7.5: Projection of the antiferromagnetic interface magnetization along its easy axis, m^z_{AFM}, for different values of dilution p_{vol}. Except for very large dilutions this magnetization component is opposite to the external field due to the effective negative interface coupling.

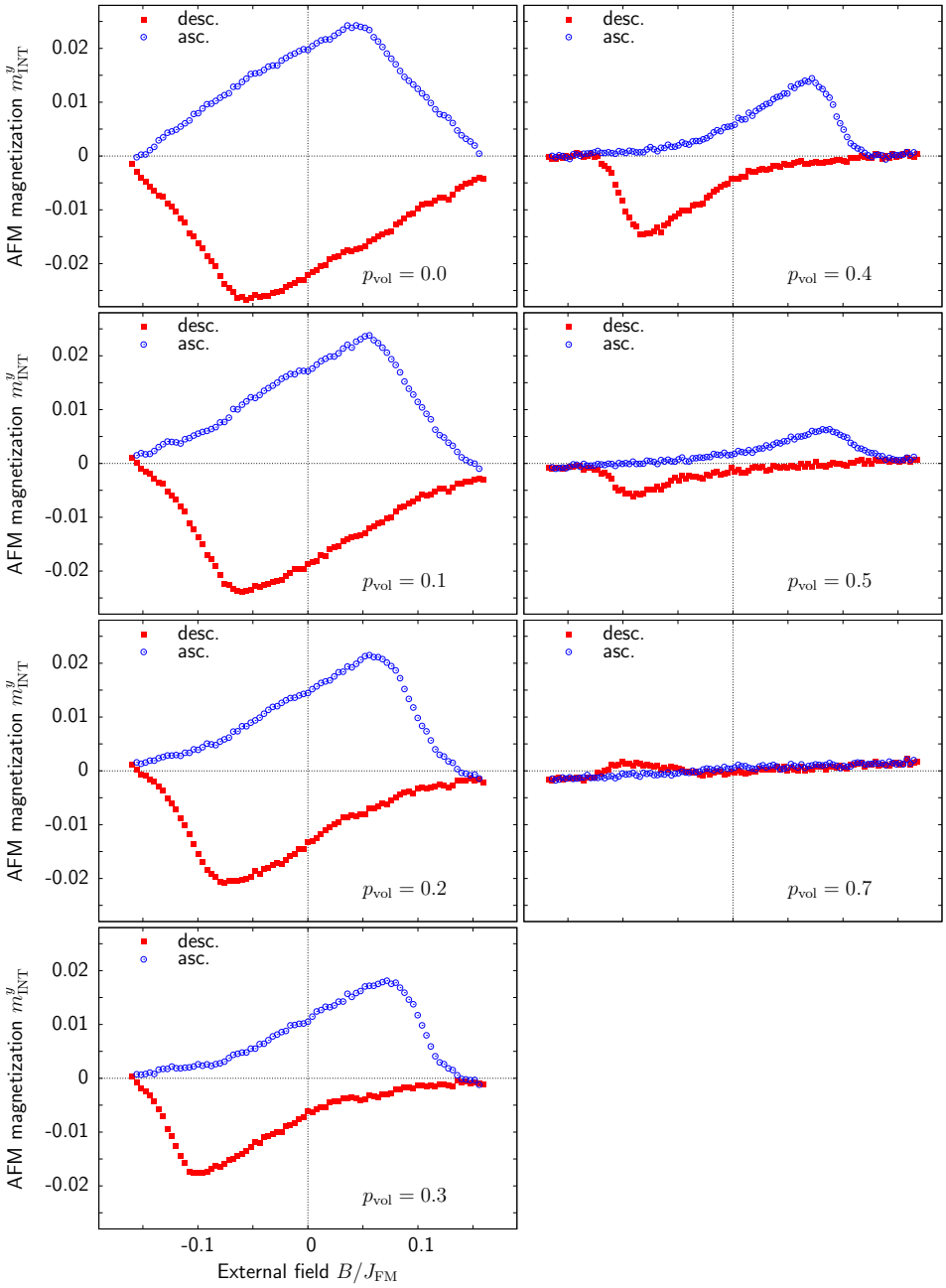

Figure 7.6: Projection of the antiferromagnetic interface magnetization perpendicular to its easy axis, m^y_{AFM}, for different values of dilution. For low dilutions and the external field approaching zero a non-negligible transverse magnetization component indicates a perpendicular coupling with respect to the ferromagnetic layer (see Fig. 7.4)

diminished and the coupling to the external field will become prevailing. This is most obvious in the case of $p_{\mathrm{vol}} = 0.7$ where the magnetization m^z_{AFM} more or less follows the external field.

The second thing which can be observed is the vertical shift for lower dilution values which is due to the fact that the exchange coupling to the ferromagnet is dominated by antiferromagnetic bonds. However, this effect is rather small which is also reflected by the fact that the exchange bias fields are considerably smaller than for the site-diluted case as discussed in Sec. 7.2.2.

For the magnetization component m^y_{AFM}, which is perpendicular to the easy axis of the antiferromagnet, the corresponding plots are shown in Fig. 7.6. Recalling the magnetization paths for the ferromagnetic layer as depicted in Fig. 7.4 one notices that for low dilution values and decreasing absolute value of the external field the net magnetization of this component rotates away from its easy axis. Most notably, it is rotating opposite to the direction of the magnetization of the ferromagnetic layer as shown in Fig. 7.4. This supports the view of a perpendicular coupling for low dilutions. As the value of dilution is increased this effect gradually decreases and vanishes for $p_{\mathrm{vol}} = 0.7$.

In summary it has been shown that structural disorder within the antiferromagnet plays the key role for explaining the microscopic origin of the exchange bias effect, and that within the domain state model different kinds of disorders, namely site or bond dilution, lead to the same qualitative behavior. The findings presented in this chapter are in good agreement with several other theoretical investigations. For instance, qualitatively the same dependence on dilution and temperature [Nowak et al., 2002b] is obtained. Also, in a system described within the Heisenberg model and using a site diluted antiferromagnet a perpendicular coupling across the ferromagnetic-antiferromagnetic interface could be observed for very low dilutions and rather low uniaxial anisotropies of the antiferromagnet [Misra et al., 2004]. However, it was stressed that the occurrence of exchange bias was not attributed to this perpendicular coupling. Also, for larger dilutions and for stronger anisotropies this effect vanished.

A feature which so far has not been observed experimentally nor predicted theoretically is the counter-intuitive magnetization reversal path for low dilutions. There, magnetization reversal is always by coherent rotation and upon decreasing external fields the ferromagnetic magnetization vector rotates away from its closest easy axis.

8 Outlook – Nanostructured exchange bias systems

In the past years, the increasing interest which exchange bias systems have been gaining has been mainly due to their importance which they play in the development of spin electronic devices. On the way to be able to deliberately tune the properties of such systems it is crucial to also understand the effects and underlying mechanisms which are connected to their ever decreasing dimensions when nanostructures come into play. Nanostructured in that sense means that for the exchange bias systems the dimensional parameters of either the ferromagnetic, the antiferromagnetic or even both are modified.

Various examples of the importance of nanostructured exchange bias systems have been given in Sec. 3.3, where the focus was put on the asymmetries connected to such systems. Despite numerous reports on nanostructured exchange bias systems [Sort et al., 2004; Eisenmenger et al., 2005; Nogués et al., 2000] a detailed understanding of the size-dependence of the exchange bias effect in nanostructures is still lacking. For instance, Baltz et al. [2005] have shown that under certain circumstances even the trends are unclear as to whether exchange bias increases or decreases with size reduction of the samples.

Another important aspect regarding the miniaturization within exchange bias systems has been addressed very recently by Malinowski et al. [2007] where structures have been investigated with dimensions within the region of the antiferromagnetic domain size. The authors have shown that within nanoscale spheres contained in self-assembled samples the lateral confinement of IrMn domains in $[Pt/Co]_3$/IrMn multilayers leads to an inverse proportionality of the exchange bias effect regarding the particle diameter.

This chapter will serve as a first step towards a systematic investigation of nanostructured ferromagnetic-antiferromagnetic multilayers and it is intended to be not more than a crude introduction to this vast topic.

8.1 Modeling and simulation

Again, the domain state model for exchange bias will serve as a starting point for the investigation of nanostructured systems. Generally, two different kind of nanostructured systems will be investigated. The first one consisting of a patterned ferromagnetic monolayer exchange coupled to several antiferromagnetic layers, both of them having finite lateral dimensions. In this case, only the lateral dimensions of the ferromagnetic layer will be varied systematically while the properties of antiferromagnet are left unchanged. In the second case, the lateral dimensions of both the ferromagnet and the antiferromagnet are change at the same time. In either case open boundary conditions are imposed and the underlying Hamilton function can be given in the following general expression

$$
\begin{aligned}
\mathcal{H} = & -\sum_{\langle i,j \rangle} J_{ij}\epsilon_i\epsilon_j \boldsymbol{S}_i \cdot \boldsymbol{S}_j && \text{Nearest neighbor exchange interaction} \\
& -\sum_{i,\theta} \epsilon_i D_i^\theta \left(S_i^\theta\right)^2 && \text{Anisotropies (in-plane, uniaxial)} \\
& -\omega\epsilon_i\epsilon_j \sum_{i<j} \frac{3(\boldsymbol{S}_i \cdot \boldsymbol{e}_{ij})(\boldsymbol{e}_{ij} \cdot \boldsymbol{S}_j) - \boldsymbol{S}_i \cdot \boldsymbol{S}_j}{r_{ij}^3} && \text{Dipolar interaction} \\
& -\epsilon_i \boldsymbol{B} \sum_i \boldsymbol{S}_i. && \text{Coupling to external field}
\end{aligned}
$$

Here, the system is completely modeled as Heisenberg system. The first line describes the nearest neighbor exchange interaction between adjacent spins on the lattice. Depending on the choice of the exchange constant the coupling is either ferromagnetic ($J_{ij} = J_{\mathrm{FM}}$) or antiferromagnetic ($J_{ij} = J_{\mathrm{AFM}}$). For the coupling across the interface, this constant is set to a value of $1/2 J_{\mathrm{FM}}$. The second line sums up any anisotropies describing either easy or hard axes, which is determined by the sign of the anisotropy constant

$$
D_i^\theta = \begin{cases} D_{\mathrm{FM}}^\theta & : \quad i \in \mathrm{FM} \\ D_{\mathrm{AFM}}^\theta & : \quad i \in \mathrm{AFM} \end{cases}
$$

θ denotes Cartesian coordinates x, y, z. Here, only uniaxial anisotropies will be considered which for both the ferromagnet ($D_{\mathrm{FM}} = 0.01 J_{\mathrm{FM}}$) and the antiferro-

magnet ($D_{\mathrm{AFM}} = 0.8 J_{\mathrm{FM}}$) are aligned with the z axis. It is important to note that surface anisotropies are not included. The third line describes the long-ranged dipolar interaction which will be efficiently evaluated using fast Fourier techniques. The strength of this interaction is given by the constant ω which is usually a few tenth of a percent of the strength of the nearest neighbor exchange coupling, in the present case $\omega = 0.004 J_{\mathrm{FM}}$. As a consequence of the inclusion of this long range coupling the reversal behavior for larger system sizes can be compared to that of continuous thin films, e. g., the magnetization of all ferromagnetic dots may rotate coherently. This would not necessarily be the case when only nearest neighbor exchange couplings were included.

Finally, the last term accounts for the coupling of the spins to an external field $\boldsymbol{B}$. The variable $\epsilon_i = 0, 1$ describes the usual site dilution of the antiferromagnet, i. e., whether site i carries a magnetic moment or not. Throughout the remainder of this work the parameters for dilution will be set to the following values $p_{\mathrm{vol}} = 0.6$ throughout the volume of the antiferromagnet and $p_{\mathrm{int}} = 0.5$ within the interface layer. Again, this way results for larger system sizes can be compared to the results obtained from previous simulations for continuous thin films.

For the Monte-Carlo simulation the heat-bath algorithm is used and in order to efficiently sample spin configurations the aforementioned threefold trial step is implemented (see Sec. 4.3.1). For the simulation procedure the usual field cooling process is performed, i. e., the system is cooled in an external field $B_{\mathrm{Cool}} = 0.1 J_{\mathrm{FM}}$ from $k_{\mathrm{B}}T = 1.0 J_{\mathrm{FM}}$ to $k_{\mathrm{B}}T = 0.1 J_{\mathrm{FM}}$. Then, the hysteresis loop is simulated from which quantities such as the exchange bias field or coercivities are calculated.

8.2 Variation of the lateral size of the ferromagnet

To explore the effects of a systematic variation of the lateral size of the ferromagnet the system displayed in Fig. 8.1 is investigated. It consists of a 3×3 array of ferromagnetic squares with variable lateral dimensions. Thus, nine ferromagnetic square dots are exchange coupled to an antiferromagnet with a lateral dimension of 128×128 and layer thickness $t_{\mathrm{AFM}} = 3$.

For the simulation the center of each of the ferromagnetic dot was kept at the same location, while varying the lateral dimension from 6×6 up to 18×18. For each system size a configurational average of ten different defect configurations

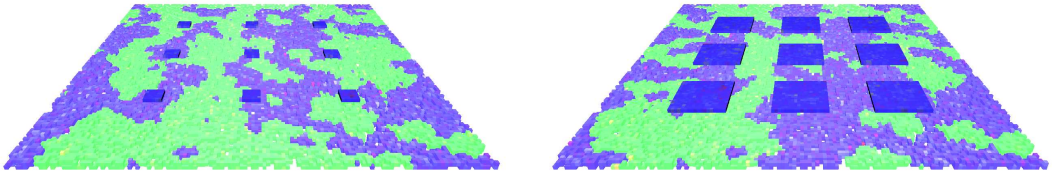

(a) Ferromagnetic dots with lateral dimensions of 8×8. Usually, each dot is lying within one antiferromagnetic domain.

(b) Ferromagnetic dots with lateral dimensions of 18×18. Generally, ferromagnetic dots extend across several antiferromagnetic domain wall boundaries.

Figure 8.1: Variable lateral dimensions in exchange bias systems. The snapshots display the spin configurations at a maximum external field.

of the antiferromagnet has been simulated. The increased number of defect realizations were needed to mitigate the effects of thermal fluctuations when approaching small system sizes.

The results of the simulations are shown in Fig. 8.2, where the dependence of both the coercivity and the exchange bias field[1] on the lateral dimension of the ferromagnet are displayed. For the coercive field a monotonic decrease is observed when the ferromagnetic system size is decreased. For the exchange bias field this is not the case. Rather, a more or less constant value is obtained for system sizes down to 8×8. Then, the exchange bias field suddenly drops significantly almost approaching zero.

A possible explanation for this breakdown can be given in terms of an average size of antiferromagnetic domains which can be deduced from the spin configuration given in Fig. 8.1. However, one has to be aware of the fact that these domains are of a fractal nature, thus there is no typical length scale. A more appropriate explanation for the vanishing exchange bias may be the fact that for these system sizes one is well within the region of the superparamagnetic limit, which is also supported by the fact that thermal fluctuations seem to grow considerably for the lateral size 6×6.

[1]The displayed quantities are obtained by monitoring the magnetization per spin for the ferromagnetic pattern as such, not on an individual basis for each dot.

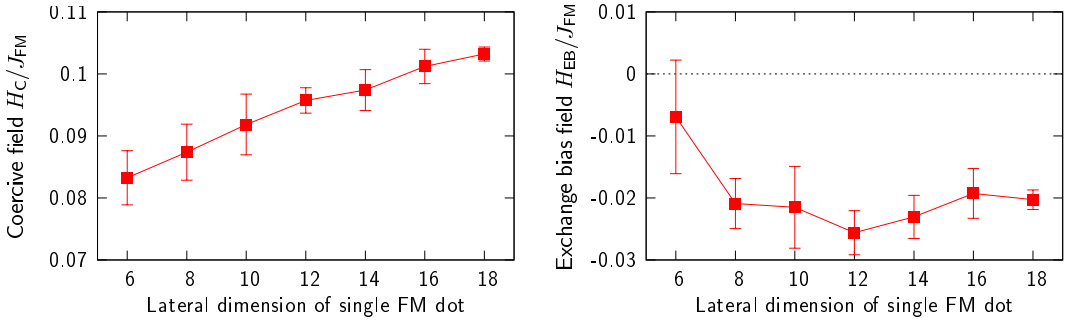

(a) Monotonic decrease of the coercive in dependence on decreasing lateral ferromagnetic systems sizes.

(b) Sudden breakdown of the exchange bias field for very small lateral dimensions. For larger system sizes the value of continuous thin film exchange bias systems is obtained.

Figure 8.2: Coercivity and exchange bias field in dependence on the lateral dimension of the ferromagnet.

Another interesting observation is that for larger system sizes on the one hand the coercivity is well below for what has been observed for continuous thin ferromagnetic films exchange coupled to an antiferromagnet [Misra et al., 2004]. There, for comparable system parameters a value of approximately $0.16J_{\mathrm{FM}}$ was obtained, while in the present case the largest system size roughly yields $0.1J_{\mathrm{FM}}$. This is even more surprising when taking into account that the exchange bias field is rather constant and gives almost the exact same value as for the continuous thin film, in both cases its value is $0.02J_{\mathrm{FM}}$ within a few percent error. This is especially true for increasing system sizes where the fluctuations of the results are decreasing.

The behavior of the exchange bias field can be explained when considering that for larger dimensions of the square dots the system approaches a thin film. Also, the dipole interaction leads to the fact that each dot is not only coupled indirectly to each other by means of the antiferromagnet but is also directly coupled by means of the long-ranged dipole interaction.

To explain the monotonic decrease of the coercivity when the lateral dimension

of the ferromagnetic square dots are reduced this approach no longer seems to work. In order to explore this behavior a detailed study investigating both the reversible and stable part of the interface magnetization of antiferromagnet may point into the right direction. One has to recall that the stable part of the interface magnetization leads to the exchange bias effect while the reversible part leads to an increased coercivity.

8.3 Variation of the lateral size of the magnetic mulitlayer

As mentioned in the previous section, there might be a relation between the size of the antiferromagnetic domains and quantities such as the exchange bias field. This will be looked at in more detail now when not only the ferromagnet but also the antiferromagnet will be subject to a variation of its lateral dimensions. Eventually, in such a confined system it will be energetically unfavorable to form domains within the antiferromagnet leading to a ferromagnet being exchange coupled to a single domain antiferromagnet.

In Fig. 8.3, two different system sizes are shown. Here, not square ferromagnetic-antiferromagnetic dots but rather exchange coupled disks are simulated. Thus, the dimensional parameter which is subject to change is the diameter of the dot. It is changed from 10 up to 48 with variable step size. The layer thickness of the antiferromagnet is set to six which is slightly larger than in previous simulations. This is done in order to obtain a stable domain structure even at low system sizes.

For obtaining results, a total of 24 different defect realizations of the antiferromagnet were considered owing to the rather small dimensions of the system which consequently led to considerable thermal fluctuations. The results for the exchange bias field are displayed in Fig. 8.4. There, this quantity is plotted versus the diameter of the ferromagnetic-antiferromagnetic disk for three different temperatures $k_{\mathrm{B}}T/J_{\mathrm{FM}} = 0.1, 0.3$ and 0.5.

Again, for large system sizes at low temperatures, $k_{\mathrm{B}T} = 0.1J_{\mathrm{FM}}$, the value for the exchange bias field approaches the one known from the usual continuous thin films with lateral dimensions of 128×128. This is not surprising because at a diameter of 50, the system is large enough to already display the typical domain structure. This remains true down to diameters of 20.

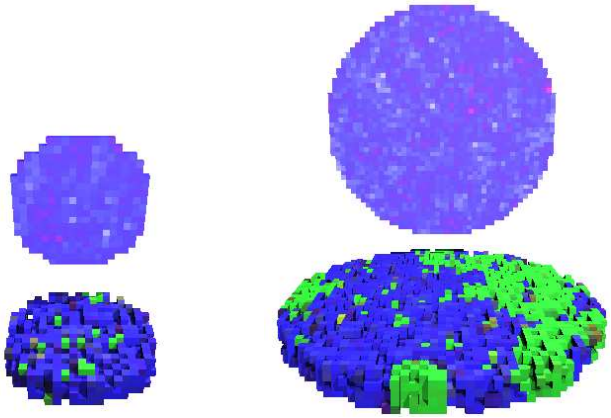

(a) Spin configuration with single domain antiferromagnet.

(b) Multi domain state for the antiferromagnet.

Figure 8.3: Spin configurations of exchange coupled disks. For a better view of the antiferromagnetic structure the ferromagnetic layer is displayed vertically. The snapshots show the spin configurations at saturation magnetization.

Here, two effects set in. On the one hand, thermal fluctuations are becoming larger, and on the other hand, the exchange bias field seems to be increased before it eventually drops to zero within the displayed error bars. Surprisingly enough, the region where the antiferromagnet starts to form a single domain as shown in Fig. 8.3a rather than displaying the usual multi domain state (Fig. 8.3b) is at a diameter of approximately 18.

One approach to answer this question whether the formation of a single domain state within a confined antiferromagnet leads to a temporary increase in the exchange bias would be to simulate systems where the change from a multi domain to a single domain state occurs at different diameters of the ferromagnetic-antiferromagnetic disk, preferentially at larger ones in order to move away from the superparamagnetic limit. Apparently, one way to do so would be to discard the open boundary conditions and impose periodic boundary conditions. Doing so would naturally shift the occurrence of a single domain

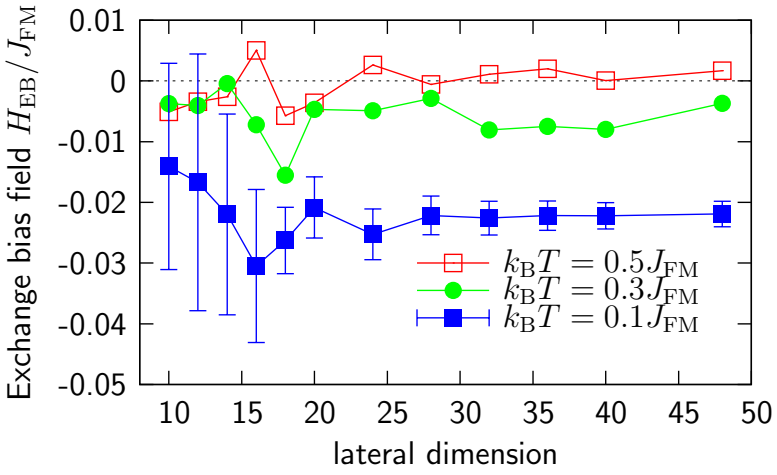

Figure 8.4: Exchange bias field in dependence on disk diameter for three different temperatures.

state to larger diameters.

This can easily be explained with the fact that the smaller the antiferromagnet is the more unlikely it is to lower the energy of the antiferromagnet by introducing a domain wall into the system for a given dilution p_{vol}. Therefore, when periodic boundary conditions are imposed, the system generally splits up into two domains but now usually with two domain walls. However, for the system which was considered here the long-ranged dipole interaction was used and thus results would not be easy to compare. To extend the simulations to systems with periodic boundary conditions or performing additional simulations where in both cases the dipole interaction was not taken into account was beyond the scope of this work.

Despite the remaining open questions, a taste was given as to how interesting the topic of nanostructured exchange bias system can be, and that many details of the underlying physics are still not understood. Therefore, to address these issues, there are demands for an increased effort, where solving the issue of thermal fluctuations along with the superparamagnetic limit probably is one of the most important ones.

9 Summary

The main subject of the presented work is the investigation of magnetization reversal of exchange coupled ferromagnetic-antiferromagnetic multilayers. Among the numerous features which such systems may display, in a first step, the experimentally observed asymmetry of the hysteresis loop is investigated within the framework of the domain state model. In agreement with corresponding experiments this model successfully explains many properties connected to exchange bias. In a second step the domain state model itself will be subject to investigations when turning from a site-diluted to a bond-diluted model. Comparing these two approaches will support the idea that the structural disorder is crucial for exchange bias to occur regardless of the type of disorder which is considered.

In order to explore the asymmetries, Monte-Carlo simulations are performed for two different kind of systems for both of which asymmetric reversal mechanism are obtained. These findings allow for a more complete picture of the theoretical understanding of the exchange bias effect as the experimentally observed asymmetries of the hysteresis can be explained within the domain state model.

The two systems which are under consideration for the investigation of the asymmetries are only differing concerning the structure of the antiferromagnet. In the first case this layer will be modeled as a diluted Ising antiferromagnet with a single easy axis. In the second case a twinned structure of the antiferromagnet will be assumed where two easy axis are perpendicular to each other within the film plane.

For the simulations of the system with uniaxial anisotropies the focus is put on the evaluation of the in-plane magnetization paths and the spin configurations of the ferromagnet during reversal. Together, they allow for a rather simple yet vivid characterization of the type of magnetization reversal of the hysteresis loop.

The examination of the exchange coupled multilayers shows that a systematic variation of the angle between the external field and the easy axis of the antiferromagnet reveals a rich variety of different reversal modes. Beginning with

symmetric reversal modes observed for small measuring angles magnetization reversal for either branch of the hysteresis loop is by coherent rotation where the net magnetic moment relaxes towards its closest easy axis before reversal eventually occurs. Then, for increasing measuring angels, reversal modes will display a maximum asymmetry characterized by a coherent rotation for the decreasing and a non-uniform mode for the increasing branch of the hysteresis loop. Upon further increasing the relevant angle, reversal will be symmetric again, i. e., on either side of the hysteresis loop a coherent rotation is displayed, however, in both cases the magnetization path is via the same side.

Apart from the fact that the measuring angle is identified as the main parameter on which the reversal mechanisms depend it is also explained why such an angular dependence actually occurs. Therefore, an expression for the effective field acting on the ferromagnet is given. It consists of contributions coming from the exchange field provided by the antiferromagnet, the anisotropy field of the ferromagnet and the external field. The relevant quantity is the angle which is spanned by the direction of this effective field and the axis of the applied field. In the case of large angles a well defined magnetization path for the ferromagnet is given leading to a coherent rotation. Consequently, for smaller angles this path is less well defined and a non-uniform reversal mechanism is likely to occur displaying only small perpendicular magnetization components with respect to the external field.

Despite the above view being followed in several works, e. g., by Paul et al. [2006] and Arenholz and Liu [2005], within this context systems only displaying a uniaxial anisotropy have not been investigated so far. Therefore, it is highly desirable to compare the results of corresponding experimental investigations where a systematic variation of the angle between the easy axis of the antiferromagnet and the external field is carried out. Beyond that, such experiments should reveal that asymmetric reversal modes do not only occur in systems displaying twinned or even more complex structures, e. g., see [Hoffmann, 2004], as it has been conjectured earlier by Fitzsimmons et al. [2002].

Furthermore the investigation of the training effect leads to surprising observations. When the measuring angle is small the behavior known from previous simulations within the domain state model is obtained. Repetitively cycling through hysteresis loops a sharp decrease of the exchange bias field from the first to the second hysteresis loop is observed. For the following cycles this quantity remains almost constant. However, for larger angles not a decrease

but rather an increase of the exchange bias field is observed. Unfortunately, an explanation can not readily be given. But it is certainly connected to the reversal mechanism which displays a maximum asymmetry within this range of angles.

That a consideration of more complex structures for the antiferromagnet is revealing and may lead to startlingly effects is shown as well. Motivated by recent experimental findings [Fitzsimmons et al., 2000; Tillmanns et al., 2005; Nogués et al., 1999; Pechan et al., 2002], the influence of the direction of the external field during field cooling and during hysteresis is explored for a system where the antiferromagnet displays a twinned structure.

Upon variation of these directions entirely different reversal modes are obtained, some of them are only identifiable via direct examination of the spin configurations during reversal. When cooling along one of the easy axes of the antiferromagnet then the reversal modes in dependence of the angle of measurement are in qualitative agreement with both the previously discussed simulations for systems with uniaxial anisotropies and recent experimental results [Tillmanns et al., 2005]. The same evolution of reversal modes is obtained ranging from symmetric with coherent rotation on either side of the hysteresis loop via asymmetric reversal with a nonuniform mode for one branch of the loop over to a symmetric reversal, again, displaying coherent rotation on either side of the loop with the magnetization rotating via the same side.

Contrary to this behavior an even more complex situation is encounter for cooling along the bisector of the twinned structure. Reversal modes can again be subdivided into being symmetric or asymmetric. However, for identifying coherent rotation a closer look at the actual spin configurations during reversal is necessary. It is shown that regardless of the angle of measurement on the decreasing branch of the hysteresis loop the twinned structure of the antiferromagnet is mapped onto the ferromagnet during reversal, leading to a coherent rotation on the length scale of the antiferromagnetic patches. This in mind, the results again comply with experimental findings [Fitzsimmons et al., 2000]. Asymmetric reversal modes are found for cooling in an external field and measuring along the bisector of the twinned structure, whereas symmetric reversal modes with coherent rotation are obtained when this procedure is being done along one of the easy axis of the antiferromagnet.

Beyond that it may be enlightening to further investigate the effects of nanostructured exchange bias systems since such systems play an important role in

the development of spin electronic devices. One aspect certainly is the behavior of nanostructured systems where the system parameters of either the ferromagnetic, the antiferromagnetic layer or even both are modified.

In a first attempt finite systems consisting of ferromagnetic square dots exchange coupled to an antiferromagnet are explored by means of numerical simulations. It is shown that for larger system sizes the results agree with those obtained for continuous thin films. For decreasing geometries the exchange bias field remains more or less constant before eventually at very low systems sizes for the ferromagnetic squares the exchange bias field breaks down to zero within the error bars. This behavior can be explained with the superparamagnetic behavior of the system.

In another simulation series both the ferromagnet and the antiferromagnet are subject to variation of the lateral size. Now disks consisting of a ferromagnet exchange coupled to an antiferromagnet are investigated. Preliminary results seem to imply that up to a certain limit exchange bias increases with decreasing system sizes before it drops to zero as the lateral dimension decreases even further. The maximum of the exchange bias field seems to fall into the region where the antiferromagnet is not in a multi domain state but rather displays a single domain.

The simulations are carried out for a system with open boundary conditions described entirely within a Heisenberg model which also includes the dipolar interaction – now system sizes are small enough to not have to deal with simulation times being excessively long. However, for system sizes such small both thermal fluctuations and the superparamagnetic limit interfere and possibly cover up the aforementioned behavior. Consequently, the investigation of nanostructured exchange bias systems demands for an increased effort in order to obtain a concise view of the matter.

Finally, to mitigate some of the common objections concerning the domain state model for exchange bias is revisited. It is shown that magnetic dilution as it is usually done in simulations is only one way to introduce a domain state in the antiferromagnet. Moreover, it is not important in which way it manifests itself in the antiferromagnet. Hence, exchange coupled multilayers have been investigated where structural disorder was introduced by means of bond dilution rather than site diluting the antiferromagnet. This is to address the concern that in experiments often times samples are not magnetically diluted. I. e., instead of randomly replacing magnetic ions by non-magnetic ones a fraction of the

antiferromagnetic exchange interactions is randomly set to zero.

From the results two main conclusions can be drawn. First of all, qualitative agreement between the site-diluted and the bond-diluted models is obtained, i. e., characteristic features such as dependence on the strength of dilution as well as the temperature dependence and the formation of a domain state agree with those observations made by Nowak et al. [2002b]. Secondly, it is shown that the maximum of the exchange bias field occurs at rather low dilutions which is the other major concern regarding the domain state model. A novel feature not observed so far is the in-plane magnetization path of the ferromagnet during reversal. For low dilutions the magnetization vector rotates away from its closest easy axis when the external field is decreased rather than relaxing towards it.

Also, it is important to stress the idea that it is structural disorder in general which causes exchange bias to occur. The type of disorder, site dilution or bond dilution in the present case, only plays a secondary role, and regardless of the type of disorder the same qualitative behavior should be observed in corresponding experiments. Regarding experiments, one might conjecture that impurities, dislocations, magnetic dilution, and grain boundaries – all of which can be considered as a certain type of disorder – lead to the same qualitative behavior as far as the phenomenon of exchange bias is concerned.

Very recently results on experiments have been presented where a ferromagnet was in contact with a spin glass [Ali et al., 2007]. It has been shown that such a system also exhibits all the key features such as coercivity enhancement, training effects, and exchange bias field shifts which are associated with conventional ferromagnetic-antiferromagnetic exchange coupled systems. From the bond-diluted domain state model it is only a small step towards a model incorporating a spin glass rather than a plain antiferromagnet. Therefore, a systematic study with simulations geared explicitly towards the investigation of a ferromagnet in contact with a spin-glass would allow for an even deeper insight into the physics of exchange bias.

Bibliography

M. Ali, P. Adie, C. H. Marrows, D. Greig, B. J. Hickey, and R. L. Stamps. *Exchange bias using a spin glass*. Nature Materials **6**, 70 (2007). → p. 86, 111

T. Ambrose and C. L. Chien. *Dependence of exchange field and coercivity on cooling field in NiFe/CoO bilyars*. J. Appl. Phys. **83**, 7222 (1998). → p. 19

E. Arenholz and K. Liu. *Angular dependence of the magnetization reversal in exchange-biased Fe/MnF_2*. Appl. Phys. Lett. **87**, 132501 (2005). → p. 108

V. Baltz, J. Sort, S. Landis, B. Rodmacq, and B. Dieny. *Tailoring Size Effects on the Exchange Bias in Ferromagnetic-Antiferromagnetic $<$ 100 nm Nanostructures*. Phys. Rev. Lett. **94**, 117201 (2005). → p. 99

X. Batlle and A. Labarta. *Finite-Size effects in fine particles: mangetic and transport properties*. J. Phys. D: Appl. Phys. **35**, R15 (2002). → p. 43

B. Beckmann, U. Nowak, and K. D. Usadel. *Asymmetric reversal modes in ferromagnetic/antiferromagnetic multilayers*. Phys. Rev. Lett. **91**, 187201 (2003). → p. 10, 41, 45, 46, 47, 51, 52, 85

B. Beckmann, U. Nowak, and K. D. Usadel. *Cooling field dependence of asymmetric reversal modes for ferromagnetic/antiferromagnetic multilayers*. Phys. Rev. B **74**, 054431 (2006). → p. 10, 20, 85

D. P. Belanger. In *Spin Glasses and Random Fields*, A. P. Young (ed.). World Scientific. Singapore (1998). → p. 31

D. V. Berkov, K. R. Ramstöck, and A. Hubert. *Solving micromagnetic problems*. Phys. stat. sol. (a) **137**, 207 (1993). → p. 29

G. Binasch, P. Grünberg, F. Saurenbach, and W. Zinn. *Enhanced magnetoresistance in layered magnetic structures with antiferromagnetic interlayer exchange*. Phys. Rev. B **39**, 4828 (1989). → p. 2

K. Binder and D. W. Heermann. In *Monte Carlo Simulation in Statistical Physics*, P. Fulde (ed.). Springer-Verlag. Berlin (1997). → p. 31, 32

C. Binek. *Training of the exchange-bias effect: A simple analytic approach*. Phys. Rev. B **70**, 014421 (2004). → p. 58

J. J. Binney, N. J. Dowrick, A. J. Fisher, and M. E. J. Newman. *The Theory of Critical Phenomena; An Introduction to the Renormalization Group*. Oxford. Clarendon Press (1992). → p. 33

S. Brems, D. Buntinx, K. Tmest, C. van Haesendonck, F. Radu, and H. Zabel. *Reversing the Training Effect in Exchange Bias CoO/Co Bilayers*. Phys. Rev. Lett. **95**, 157202 (2005). → p. 62

J. Camarero, J. Sort, A. Hoffmann, J. M. García-Martín, B. Dieny, R. Miranda, and J. Nogués. *Origin of the Asymmetric Magnetization Reversal Behavior in Exchange-Biased Systems: Competing Anisotropies*. Phys. Rev. Lett. **95**, 057204 (2005). → p. 22, 23, 74

R. W. Chantrell and K. O'Grady. *The magnetic properties of fine particles*. In *Applied Magnetism*, R. Gerber, C. D. Wright, and G. Asti (eds.). Kluwer Academic Publishers. Dordrecht (1994). → p. 2

D. T. Dekadjevi, A. Suvorova, S. Pogossian, D. Spenato, and J. B. Youssef. *Experimental evidence for the role of nonuniform modes in the asymmetric magnetization reversal of a Ni/NiO system*. Phys. Rev. B **74**, 100402(R) (2006). → p. 74

B. Dieny, V. Speriosu, S. Parkin, P. Baumgart, and D. Wilhoit. *Magnetotransport Properties of Magnetically Soft Spin-Valve Structure*. J. Appl. Phys. **69**, 4774 (1991). → p. 10

J. Eisenmenger, Z.-P. Li, W. A. A. Macedo, and I. K. Schuller. *Exchange Bias and Asymmetric Reversal in Nanostructured Dot Arrays*. Phys. Rev. Lett. **94**, 057203 (2005). → p. 24, 99

M. R. Fitzsimmons, C. Leighton, A. Hoffmann, K. Liu, C. F. Majkrzak, J. A. Dura, J. R. Groves, R. W. Springer, P. N. Arendt, V. Leiner, H. Lauter, and I. K. Schuller. *Influence of in-plane crystalline quality of an antiferromagnet*

on perpendicular exchange coupling and exchange bias. Phys. Rev. B **65**, 134436 (2002). → p. 22, 69, 108

M. R. Fitzsimmons, C. Leighton, A. Hoffmann, P. C. Yashar, J. Nogués, K. Liu, C. F. Majkrzak, J. A. Dura, H. Fritzsche, and I. K. Schuller. *Influence of interfacial disorder and temperature on magnetization reversal in exchange-coupled bilayers*. Phys. Rev. B **64**, 104415 (2001). → p. 70

M. R. Fitzsimmons, P. Yashar, C. Leighton, I. K. Schuller, J. Nogués, C. F. Majkrzak, and J. A. Dura. *Asymmetric Magnetization Reversal in Exchange-Biased Hysteresis Loops*. Phys. Rev. Lett. **84**, 3986 (2000). → p. 4, 19, 21, 69, 81, 109

E. Girgis, R. D. Portugal, H. Loosvelt, M. J. V. Bael, I. Gordon, M. Malfait, K. Temst, C. V. Haesendonck, L. H. A. Leunissen, and R. Jonckheere. *Enhanced Asymmetric Magnetization Reversal in Nanoscale Co/CoO Arrays: Competition between Exchange Bias and Magnetostatic Coupling*. Phys. Rev. Lett. **91**, 187202 (2003). → p. 24, 25

H. Dosch. *Evanescent absorption in kinematic surface Bragg diffraction*. Phys. Rev. B **35**, 2137 (1987). → p. 70

S.-J. Han, D. P. Belanger, W. Kleemann, and U. Nowak. *Relaxation of the excess magnetization of random-field-induced metastable domains in* $Fe_{0.47}Zn_{0.53}F_2$. Phys. Rev. B **45**, 9728 (1992). → p. 17

D. Heim, R. Fontana, C. Tsang, V. Speriosu, B. Gurney, and M. Williams. *Design and Operation of Spin Valve Sensors*. IEEE Trans. Magn. **30**, 316 (1994). → p. 10

A. Hochstrat, C. Binek, and W. Kleemann. *Training of the exchange-bias effect in NiO-Fe heterostructures*. Phys. Rev. B **66**, 092409 (2002). → p. 58

A. Hoffmann. *Symmetry Driven Irreversibilities at Ferromagnetic-Antiferromagnetic Interfaces*. Phys. Rev. Lett. **93**, 097203 (2004). → p. 69, 108

A. Hubert and R. Schäfer. *Magnetic Domains*. Berlin. Springer-Verlag (1998). → p. 29, 71

Y. Imry and S. Ma. *Random-Field Instability of the Ordered State of Continuous Symmetry*. Phys. Rev. Lett. **35**, 1399 (1975). → p. 16

J. Keller, P. Miltényi, B. Beschoten, G. Güntherodt, U. Nowak, and K. D. Usadel. *The domain state model for exchange bias II: Experiment*. Phys. Rev. B **66**, 14431 (2002). → p. 14, 15, 30, 58, 85, 91

W. Kleemann. *Random-field induced antiferromagnetic, ferroelectric and structural domain states*. Int. J. Mod. Phys. B **7**, 2469 (1993). → p. 31

N. C. Koon. *Calculations of Exchange Bias in Thin Films with Ferromagnetic/Antiferromagnetic Interfaces*. Phys. Rev. Lett. **78**, 4865 (1998). → p. 12, 13

K. Liu, M. Baker, M. Tuominen, T. P. Russell, and I. K. Schuller. *Tailoring exchange bias with magnetic nanostructures*. Phys. Rev. B **63**, 060403(R) (2001). → p. 70

P. Lyman and R. V. Hal. *How much information?*. Retrieved from www2.sims.berkeley.edu/research/projects/how-much-info-2003 (2003). → p. 1

G. Malinowski, M. Albrecht, I. L. Guhr, J. M. D. Coey, and S. van Dijken. *Size-dependent scaling of perpendicular exchange bias in magnetic nanostructures*. Phys. Rev. B **75**, 012413 (2007). → p. 99

A. P. Malozemoff. *Random-field model of exchange anisotropy at rough ferromagnetic-antiferromagnetic interfaces*. Phys. Rev. B **35**, 3679 (1987). → p. 4, 11

A. P. Malozemoff. J. Appl. Phys. **63**, 3874 (1988). → p. 4

A. P. Malozemoff and J. C. Slonczewski. *Magnetic Domain Walls in Bubble Materials*. New York. Academic Press (1979). → p. 71

W. H. Meiklejohn and C. P. Bean. *New Magnetic Anisotropy*. Phys. Rev. **102**, 1413 (1956). → p. 3, 7, 8

W. H. Meiklejohn and C. P. Bean. *New Magnetic Anisotropy*. Phys. Rev. **105**, 904 (1957). → p. 7

T. Mewes, R. Lopusnik, J. Fassbender, B. Hillebrands, M. Jung, D. Engel, A. Ehresmann, and H. Schmoranzer. *Suppression of exchange bias by ion irradiation*. Appl. Phys. Lett. **76**, 1057 (2000). → p. 4

R. P. Michel, A. Chaiken, and C. T. Wang. J. Appl. Phys. **81**, 5374 (1997). → p. 30

P. Miltényi, M. Gierlings, J. Keller, B. Beschoten, G. Güntherodt, U. Nowak, and K. D. Usadel. *Diluted Antiferromagnets in Exchange Bias: Proof of Domain State Model*. Phys. Rev. Lett. **84**, 4224 (2000). → p. 4, 10, 14, 30

A. Misra, U. Nowak, and K. D. Usadel. *Control of exchange bias by diluting the antiferromagnetic layer*. J. Appl. Phys. **93**, 6593 (2003). → p. 4

A. Misra, U. Nowak, and K. D. Usadel. *Structure of domains in an exchange bias model*. J. Appl. Phys. in Druck (2004). → p. 42, 90, 97, 103

J. S. Moodera, L. R. Kinder, T. M. Wong, and R. Meservey. *Large Magnetoresistance at Room Temperature in Ferromagnetic Thin Film Tunnel Junctions*. Phys. Rev. Lett. **74**, 3273 (1995). → p. 2

A. Mougin, T. Mewes, M. Jung, D. Engel, A. Ehresmann, H. Schmoranzer, J. Fassbender, and B. Hillebrands. *Local manipulation and reversal of the exchange bias field by ion irradiation in FeNi/FeMn double layers*. Phys. Rev. B **63**, 60409 (2001). → p. 4

J. Nogués, D. Lederman, T. J. Moran, and I. K. Schuller. *Positive Exchange Bias in FeF_2-Fe Bilayers*. Phys. Rev. Lett. **76**, 4624 (1996). → p. 45

J. Nogués, T. J. Moran, D. Lederman, I. K. Schuller, and K. V. Rao. *Role of interfacial structure on exchange-biased FeF_2-Fe*. Phys. Rev. B **59**, 6984 (1999). → p. 19, 69, 109

J. Nogués and I. K. Schuller. *Exchange Bias*. J. Magn. Magn. Mat. **192**, 203 (1999). → p. 7, 30

J. Nogués, J. Sort, V. Langlais, V. Skumryev, S. Suriñach, J. Muñoz, and M. Baró. *Correlation between antiferromagnetic interface coupling and positive exchange bias*. Phys. Rev. B **61**, 1315 (2000). → p. 99

F. Nolting, A. Scholl, J. Stöhr, J. W. Seo, J. Fompeyrine, H. Siegwart, J.-P. Locquet, S. Anders, J. Lüning, E. E. Fullerton, M. F. Toney, M. R. Scheinfein, and H. A. Padmore. *Direct observation of the alignment of ferromagnetic spins by antiferromagnetic spins*. Nature **405**, 767 (2000). → p. 4, 80

U. Nowak. *Thermally activated reversal in magnetic nanostructures*. In *Annual Reviews of Computational Physics IX*, D. Stauffer (ed.) page 105. World Scientific. Singapore (2001). → p. 33

U. Nowak, J. Esser, and K. D. Usadel. *Dynamics of domains in diluted antiferromagnets*. Physica A **232**, 40 (1996). → p. 17

U. Nowak, A. Misra, and K. D. Usadel. *Modelling exchange bias microscopically*. J. Magn. Magn. Mat. **240**, 243 (2002a). → p. 42

U. Nowak, K. D. Usadel, P. Miltényi, J. Keller, B. Beschoten, and G. Güntherodt. *The domain state model for exchange bias I: Theory*. Phys. Rev. B **66**, 14430 (2002b). → p. 4, 10, 14, 15, 16, 42, 43, 45, 53, 58, 85, 90, 91, 97, 111

R. C. O'Handley. *Principles and Applications*. New York. Wiley-Interscience (2000). → p. 2

H. Ohldag, A. Scholl, F. Nolting, S. Anders, F. U. Hillebrecht, and J. Stöhr. *Spin Reorientation at the Antiferromagnetic NiO(001) Surface in Response to an Adjacent Ferromagnet*. Phys. Rev. Lett. **86**, 2878 (2001). → p. 4, 80

A. Paul, E. Kentzinger, U. Rücker, and T. Brückel. *Symmetry and asymmetry during magnetization reversal in exchange biased multilayers and bilayers*. Phys. Rev. B **73**, 092410 (2006). → p. 108

M. J. Pechan, D. Bennett, N. Teng, C. Leighton, J. Nogués, and I. K. Schuller. *Induced anisotropy and positive exchange bias: A temperature, angular, and cooling field study by ferromagnetic resonance*. Phys. Rev. B **65**, 064410 (2002). → p. 69, 109

P. Pollak, W. Kleemann, and D. P. Belanger. *Metastability of the uniform magnetization in three-dimensional random-field Ising model systems. II. $Fe_{0.47}Zn_{0.53}F_2$*. Phys. Rev. B **38**, 4773 (1988). → p. 11

W. H. Press, B. P. Flannery, S. A. Teukolsky, and W. T. Vetterling. *Numerical Recipes*. Cambridge. Cambridge University Press (1990). → p. 29

F. Radu, M. Etzkorn, T. Schmitte, R. Siebrecht, A. Schreyer, K. Westerholt, and H. Zabel. *Asymmetric magnetization reversal on exchange biased CoO/Co bilayers*. prb **67**, 134409 (2003). → p. 4

F. Reif. *Fundamentals of statistical and thermal physics*. New York. McGraw-Hill Book Company (1965). → p. 32

A. Scholl, M. Liberati, E. Arenholz, H. Ohldag, and J. Stör. *Creation of an Antiferromagnetic Exchange Spring*. Phys. Rev. Lett. **92**, 247201 (2004). → p. 14

T. C. Schulthess and W. H. Butler. *Consequences of Spin-Flop Coupling in Exchange Biased Films*. Phys. Rev. Lett. **81**, 4516 (1998). → p. 14

H. T. Shi and D. Lederman. *Exchange bias flop in $Fe_xZn_{1-x}F_2$/Co bilayers*. Phys. Rev. B **66**, 094426 (2002). → p. 46, 74

H. T. Shi, D. Lederman, and E. E. C. Fullerton. *Exchange bias in $Fe_xZn_{1-x}F_2$/Co bilayers*. J. Appl. Phys. **91**, 7763 (2002). → p. 4

V. Skumryev, S. Stoyanov, Y. Zhang, G. Hadjipanayis, D. Givord, and J. Nogués. *Beating the superparamagnetic limit with exchange bias*. Nature **423**, 850 (2003). → p. 10, 24

J. Sort, B. Dieny, M. Fraune, C. Koenig, F. Lunnebach, B. Beschoten, and G. Guntherodt. *Perpendicular exchange bias in antiferromagnetic-ferromagnetic nanostructures*. Appl. Phys. Lett. **84**, 3696 (2004). → p. 99

J. Spray and U. Nowak. *Exchange bias in ferromagnetic/antiferromagnetic bilayers with imperfect interfaces*. J. Phys. D: Appl. Phys. **39**, 4536 (2006). → p. 85

M. Staats, U. Nowak, and K. D. Usadel. *Non-exponential relaxation in diluted antiferromagnets*. Phase Transitions **65**, 159 (1998). → p. 17

M. D. Stiles and R. D. McMichael. *Model for exchange bias in polycrystalline ferromagnet-antiferromagnet bilayers*. Phys. Rev. B **59**, 3722 (1999). → p. 14, 15

E. C. Stoner and E. P. Wohlfarth. *A mechanism of magnetic hysteresis in heterogeneous alloys*. Philos. Trans. R. Soc. London Ser. A **240**, 599 (1949). → p. 22

A. Tillmanns, S. Oertker, B. Beschoten, G. Güntherodt, J. Eisenmenger, and I. K. Schuller. *Asymmetric magnetization reversal in the exchange bias system Fe/FeF_2 studied by MOKE*. Unpublished. cond-mat/0509419 (2005). → p. 22, 69, 78, 79, 109

K. D. Usadel and U. Nowak. *Diluted antiferromagnets in a magnetic field: evidence for a spin-glass phase*. J. Magn. Magn. Mat. **104-107**, 179 (1992). → p. 64

B. E. Warren. *X-Ray Diffraction*. New York. Dover (1990). → p. 70

S. W. Yuan and H. N. Bertram. *Fast adaptive algorithm for micromagnetics*. IEEE Trans. Mag. **28**, 2031 (1992). → p. 29

Danksagung

An dieser Stelle möchte ich all denen meinen Dank aussprechen, die zum Gelingen dieser Arbeit beigetragen haben.

Zunächst möchte ich mich bei Herrn Prof. em. Dr. K. D. Usadel und insbesondere bei Herrn Prof. Dr. Ulrich Nowak für das sehr interessante Thema und die ausgezeichnete Betreuung dieser Arbeit bedanken. Die zahlreichen Einladungen an die *University of York* waren von besonderer Bedeutung für das Gelingen der vorliegenden Arbeit.

Für die Einladung an die *University of California, San Diego*, und die anregenden Diskussionen danke ich Herrn Prof. Dr. I. K. Schuller.

Den Mitarbeitern der Abteilung Theoretische Tieftemperaturphysik möchte ich meinen Dank aussprechen für die Hilfsbereitschaft und stets freundliche Atmosphäre in der Arbeitsgruppe.

Georg Rollmann, Magnus Kreth und Minoru Sugihara möchte ich für die vielen kleinen Tips und Hilfestellungen danken, auch für die Zeit, in denen nicht die Arbeit im Vordergrund stand.

Herrn Prof. em. Dr. Usadel, Herrn Prof. Dr. Nowak und Herrn Dip.-Math. Daniel Kilimann danke ich für das kritische Lesen des Manuskripts oder Teile dessen und die daraus entsprungenen zahlreichen Anregungen, welche bei der Erstellung der Arbeit vieles erleichtert haben.

Der Deutschen Forschungsgemeinschaft gilt mein Dank für die Förderung der Arbeit im Rahmen des Sonderforschungsbereiches 491.

Dem Ehepaar Klaus und Angelika Heiß möchte ich nicht zuletzt dafür danken, mich auf diesen Weg gebracht zu haben.

Für ihre Unterstützung danke ich meiner Familie, insbesondere meinen Eltern Heike und Heiner Beckmann.

Danken möchte ich ganz besonders meiner Frau Sabrina und meinem Sohn Neil, die mich über vieles haben hinwegsehen lassen, gerade auch wenn es einmal nicht wie gewünscht lief.